University of Illinois at Urbana-Champaign

ACRC

Air Conditioning and Refrigeration Center A National Science Foundation/University Cooperative Research Center

Investigation of Transient Two-Phase Flow during Refrigeration and Air Conditioning System Startup

M. J. Hedrick, E. W. Jassim, and T. A. Newell

ACRC TR-254 December 2006

For additional information:

Air Conditioning and Refrigeration Center
University of Illinois
Department of Mechanical Science & Engineering
1206 West Green Street
Urbana, IL 61801

(217) 333-3115

Prepared as part of ACRC Project #200
Investigation of Transient Two-Phase Flow during Refrigeration and Air Conditioning System Startup
T. A. Newell, and J. C. Chato, Principal Investigators

The Air Conditioning and Refrigeration Center was founded in 1988 with a grant from the estate of Richard W. Kritzer, the founder of Peerless of America Inc. A State of Illinois Technology Challenge Grant helped build the laboratory facilities. The ACRC receives continuing support from the Richard W. Kritzer Endowment and the National Science Foundation. The following organizations have also become sponsors of the Center.

Arçelik A. S.
Behr GmbH and Co.
Carrier Corporation
Cerro Flow Products, Inc.
Daikin Industries, Ltd.
Danfoss A/S
Delphi Thermal and Interior
Embraco S. A.
Emerson Climate Technologies, Inc.
General Motors Corporation
Hill PHOENIX
Honeywell, Inc.
Hydro Aluminum Precision Tubing
Ingersoll-Rand/Climate Control
Lennox International, Inc.
LG Electronics, Inc.
Manitowoc Ice, Inc.
Matsushita Electric Industrial Co., Ltd.
Modine Manufacturing Co.
Novelis Global Technology Centre
Parker Hannifin Corporation
Peerless of America, Inc.
Samsung Electronics Co., Ltd.
Sanden Corporation
Sanyo Electric Co., Ltd.
Tecumseh Products Company
Trane
Visteon Automotive Systems
Wieland-Werke, AG

For additional information:

Air Conditioning & Refrigeration Center
Mechanical & Industrial Engineering Dept.
University of Illinois
1206 West Green Street
Urbana, IL 61801

217 333 3115

Abstract

The purpose of this investigation is to develop models for transient slug flow under refrigeration system startup conditions. Slug flow is generated for two-phase air-water and R134a with pressure differences of 69-520 kPa; slug volumes of 40-400 ml; and 6.35, 10.2, and 13.4 mm tube diameters under high and low pressure side conditions. Flow visualization images are recorded with a high speed camera and digital web camera. A film thickness sensor design is described for use in the once through flow loop. The trends of the film thickness sensor output, pressure difference, slug location, and slug breakdown distance are discussed. Four separate models are generated to describe the slug acceleration and breakdown. The models are compared to experimental data and simplified further. The simplified model predicts the acceleration and breakdown of the slug with four inputs: fluid, applied pressure difference, slug volume, and tube diameter. The performance and uncertainty of the model are discussed. Models are also generated to determine the tube length required for slug breakdown.

Table of Contents

List of Figures

Page

List of Tables

Nomenclature

a	Acceleration [m/s^2]
A	Area [m^2]
dP	Pressure Difference [Pa]
D	Diameter [m]
f	Friction Factor [ ]
F	Force [N]
g	Gravity [m/s^2]
h	Height [mm]
L	Length [m]
m	Mass [kg]
P	Pressure [Pa]
R	Radius of Reflection [mm]
Re_D	Reynold's Number based on Diameter [ ]
S	Shear Perimeter [m]
t	Time [s]
v	Velocity [m/s]
V	Volume [m^3]
x	Location [m]
z	Elevation [m]

Greek Symbols

Γ	Viscous Pressure Drop [Pa/m]
ε	Liquid Holdup/Void Fraction [ ]
θ	Inclination Angle [rad]
μ	Dynamic Viscosity [kg/m-s]
ν	Kinematic Viscosity [m^2/s]
ρ	Density [kg/m^3]
τ	Shear Stress [Pa]

Subscripts and Superscripts

$+$	Dimensionless grouping
ave	Average
A	Applied
An	Annular
B	Breakdown
C,W-L	Critical, Tube Wall-Liquid Interface
C,L-V	Critical, Liquid-Vapor Interface
F	Film
g	Gas Component
G	Gas Phase
Gi	Gas-Liquid Interface – Acting on Gas
Gg	Gas Component in Gas Phase (Partial)
Gl	Liquid Component in Gas Phase (Partial)
Gw	Gas-Wall Interface
H20	Water

i	Current Section
i+1	Next Section
I	Phase Interface
l	Liquid Component
L	Liquid Phase
Li	Gas-Liquid Interface – Acting on Liquid
max	Maximum
M	Mixture
R134a	Refrigerant R134a
S	Slug
St	Stratified
Tot	Total
TS	Test Section
vis	Viscous
Wall	Wall
XC	Cross Section

Chapter 1. Introduction

The ability to predict the distribution of refrigeration charge under steady state conditions has been improving as more two-phase steady state research is being conducted. Substantial research on transient two-phase flow, specifically slug flow, has been conducted since the 1970s; however, much of this research is not practical for analyzing slug flow during vapor compression system startup. When a refrigeration system is shut down, the refrigerant vapor condenses and pools in either the high or low pressure side of the system. This liquid mass is accelerated from rest as a result of a pressure difference across the slug from compressor startup. Liquid slugs create undesirable effects such as damage to system components, undesirable noises, and delay in the establishment of steady state conditions. This investigation attempts to describe the motion of the liquid slug and the conditions during which slug dissipation or breakdown will occur. Once the refrigerant slug can be accurately modeled, steps can be taken to eliminate the damage to components and minimize or eliminate aforementioned undesirable effects.

The refrigerant slug motion is expected to behave differently on the high side versus the low side of a system. A slug on the high side would tend to remain as subcooled liquid due to the increase in high side pressure during startup. This mass would then be accelerated towards a receiver or an expansion device. On the low side, the pressure is reduced during startup, possibly below the refrigerant saturation pressure. This would cause nucleation of refrigerant vapor bubbles, which has an unknown effect on the acceleration and breakdown of the slug.

Transient slug flow testing using air-water and two-phase R134a is conducted for 69-520 kPa applied pressure differences across the slug; 40-400 ml initial slug volumes; and 6.35, 10.2, and 13.4 mm diameter tubes. Both fluids are tested under high side simulated conditions while R134a is also tested under low side conditions. High side testing is more extensive than low side testing because slug breakdown occurs upstream of the test section under most low side testing conditions. The upstream pressure, downstream pressure, and data from 11 film thickness sensors are collected during testing. Flow visualization images capture the motion of the slug and determine the slug breakdown location.

Models are generated to predict the acceleration and pipe length required for slug breakdown. The models assume quasi-equilibrium conditions and consider the contribution of viscosity and mass loss due to film deposition on the slug acceleration. Simple viscous tube flow relations are used. Since annular flow is observed immediately following the slug in air-water tests and stratified flow is observed in two-phase R134a tests, the film deposition is treated accordingly in the model. The model is further simplified to predict the film deposition, acceleration, and pipe length required for slug breakdown requiring inputs which characterize the flow (fluid, pressure difference, slug volume, and tube diameter).

A summary of existing transient two-phase flow research and optical film thickness sensor methods are presented in Chapter 2. Chapter 3 describes the construction of the experimental apparatus as well as an overview of test conditions and procedures. Experimental flow visualization images, pressure data, and film thickness data are presented in Chapter 4, as well as trends describing the effects of the independent variables on slug acceleration. The development of analytical models to predict slug acceleration and their accuracy are described in Chapter 5. The conclusions of the study and suggestions for future work are summarized in Chapter 6.

Chapter 2. Literature Review

This chapter summarizes the available transient two-phase flow literature pertaining to slug flow on a macroscopic level and the transient motion of a single liquid slug. In addition, optical methods commonly used to determine film thickness are discussed due to their importance in the current work.

2.1. Transient Two-Phase Flow Literature

Transient two-phase flow research was initiated by the nuclear industry in the 1970's to better understand LOCA (Loss Of Coolant Accidents) in steam-water pipe flow (Kohda et al. 1988). Nuclear analysis codes focus on two-phase flows with rapid transient events. The oil pipeline industry has also generated a substantial amount of work by modifying nuclear analysis codes to better represent pipeline flow conditions with slower transient events. Most of the research concerning slug flow, however, is focused on the description of the macroscopic properties of the flow. As an exception, Sakaguchi et al. (1987) describes the dynamic motion of a single slug and its effects on impact force. In almost every instance, the inlet liquid and gas flow rates and the outlet pressure are controlled as independent variables.

Several parameters have been used throughout the literature to describe two-phase flow. A variable representing the volumetric fraction of liquid or vapor to the total volume, commonly referred to as liquid fraction and void fraction, respectively, can be found in almost every model. Many different liquid/void fraction models are found in the transient two-phase literature. Tatiel et. al (1997) defines the liquid fraction according to Equation 2.1.

$$\varepsilon_L = \frac{m_L}{\rho_L V} \tag{2.1}$$

This definition is used in the slug flow model proposed by Minami and Shoham (1994). Sakaguchi et al. (1987) and Grolman and Fortuin (1996) define the liquid holdup as the height of a liquid layer collected in the bottom of a tube of circular cross section. Sharma et al. (1986) and Kohda et al. (1988) introduce the liquid holdup as the total volume fraction of liquid; similarly, the volumetric void fraction (gas volume fraction) is used by De Henau and Raithby (1995a), De Henau and Raithby (1995b), and Richter et al. (2001).

Two main approaches have been proposed for the analysis of transient two-phase flow, both of which rely on numerically solving a set of continuity, momentum, and/or energy conservation equations. The first method contains transient terms in each of the equations; the second method assumes that some of the transient terms may be neglected.

2.1.1. Slug Flow Modeling – Fully Transient

The following references propose a completely transient analysis: Sharma et al. (1986), Kohda et al. (1988), De Henau and Raithby (1995a), De Henau and Raithby (1995b), Grolman and Fortuin (1996), and Richter et al. (2001).

Sharma et al. (1986) and Kohda et al. (1998) both present models with separate, one-dimensional liquid and gas continuity equations and a mixture momentum equation. At the time of the research, mixture models provided comparable accuracy compared to two-fluid models due to lack of understanding of interaction between phases. The governing continuity and momentum equations are shown in Equations 2.2 and 2.3, respectively.

$$\frac{\partial}{\partial t}\left(\varepsilon_L \rho_L + (1-\varepsilon_L)\rho_{Gl}\right) + \frac{\partial}{\partial x}\left(\varepsilon_L \rho_L v_L + (1-\varepsilon_L)\rho_{Gl} v_G\right) = 0$$
$$\frac{\partial}{\partial t}\left((1-\varepsilon_L)\rho_{Gg}\right) + \frac{\partial}{\partial x}\left((1-\varepsilon_L)\rho_{Gg} v_G\right) = 0 \tag{2.2}$$

$$\frac{\partial}{\partial t}\left(\varepsilon_L \rho_L v_L + (1-\varepsilon_L)\rho_G v_G\right) + \frac{\partial}{\partial x}\left(\varepsilon_L \rho_L {v_L}^2 + (1-\varepsilon_L)\rho_G {v_G}^2\right) + \frac{\partial P}{\partial x} + \left(\varepsilon_L \rho_L + (1-\varepsilon_L)\rho_G\right) g \sin\theta + \Gamma = 0 \tag{2.3}$$

The liquid continuity equation accounts for liquid entrainment in the gas phase, but the presence of vapor in the liquid phase (saturated or bubbles) is neglected. Entrainment terms are not found in the momentum equation. Kohda et al. (1988) did not assume an isothermal flow, and therefore included a transient energy equation. Tests were conducted on a horizontal 105.3 mm diameter tube in which downstream pressure, inlet and outlet flow rate, and liquid holdup were measured for air-water flow. The air and water flow rates at the beginning of the test were specified; the flow rates of each fluid were varied in time.

The equations proposed by Sharma et al. (1986) differ slightly from Equations 2.2 and 2.3 because velocities are defined in terms of an overall mixture velocity. The model was validated by comparing the predicted outlet liquid flow rate to a previous experiment by Cunliffe (1978). The experiment consisted of increasing the inlet gas flow rate over time and observing fluctuations in the outlet liquid flow rate. No additional experimental work was conducted.

The remaining models which use a fully transient set instead consider the momentum equations of each phase separately. They also assume no liquid entrainment as opposed to Equations 2.2 and 2.3. Generalized continuity and momentum equations are presented by De Henau and Riaithby (1995a) and are shown in Equations 2.4 and 2.5.

$$A\frac{\partial}{\partial t}\left((1-\varepsilon_L)\rho_G\right) + \frac{\partial}{\partial x}\left(A(1-\varepsilon_L)\rho_G v_G\right) = 0$$
$$A\frac{\partial}{\partial t}\left(\varepsilon_L \rho_L\right) + \frac{\partial}{\partial x}\left(A\varepsilon_L \rho_L v_L\right) = 0 \tag{2.4}$$

$$A\frac{\partial}{\partial t}\left((1-\varepsilon_L)\rho_G v_G\right) + \frac{\partial}{\partial x}\left(A(1-\varepsilon_L)\rho_G {v_G}^2\right) + A(1-\varepsilon_L)\frac{\partial P}{\partial x} + A(1-\varepsilon_L)\rho_G g \sin\theta = \Gamma_{Gw} + \Gamma_{Gi}$$
$$A\frac{\partial}{\partial t}\left(\varepsilon_L \rho_G v_G\right) + \frac{\partial}{\partial x}\left(A\varepsilon_L \rho_G {v_G}^2\right) + A\varepsilon_L \frac{\partial P}{\partial x} + A\varepsilon_L \rho_G g \sin\theta = \Gamma_{Lw} + \Gamma_{Li} \tag{2.5}$$

Like Equations 2.2 and 2.3, these equations contain temporal, convective, pressure, gravitational, and viscous terms. De Henau and Raithby (1995a) also developed empirical equations to determine the interfacial viscous pressure drop specifically for slug flow using the Dukler and Hubbard (1975) description of a slug unit shown in Figure 2.1. Model validation consisted of comparing the predicted gas fraction, pressure, and liquid flow rate at the outlet to previous experiments by Kokal (1989). Steady and transient slug flow experiments with tube diameters ranging from 51.2 to 76.3 mm in horizontal and inclined tubes were conducted. Air-water and air-oil were tested.

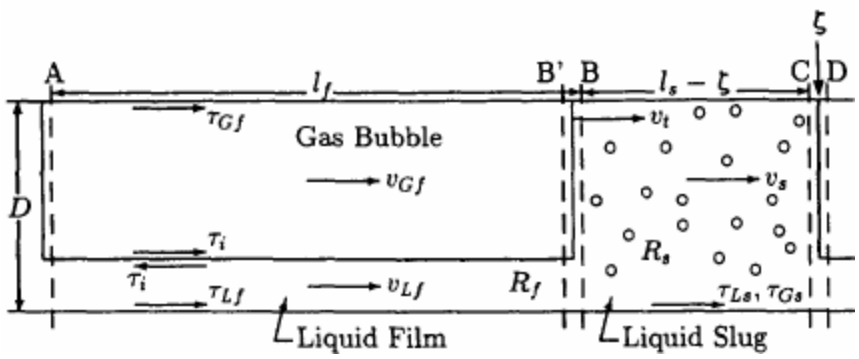

Figure 2.1. Slug Unit Diagram Used by Dukler and Hubbard (1975)

Richter et al. (2001) used similar assumptions to De Hanau and Raithby (1995a), but developed separate continuity and momentum equations for regions with only liquid and regions with two phases. The model was used to determine the bubble velocity of air-water flow in inclined tubes 5-10 mm in diameter.

Grolman and Fortuin (1996) modified the liquid momentum equation in Equation 2.5 to include a liquid phase velocity profile factor. This factor was implemented to decrease the stability of current wavy flow models by correcting for the Bernoulli Effect, drawing the wave toward the channel roof as a result of the higher gas velocity. The model also used generalized equations for the loss of momentum due to friction. The model was used to investigate transition from wavy annular to slug flow in inclined tubes using air-water and air-tetradecane. Tube diameters of 26 and 51 mm were tested and liquid holdup was measured as the experiment proceeded until a slug was formed.

2.1.2. Slug Flow Modeling – Quasi-Equilibrium Assumptions

Models solving a full set of transient solutions have only been considered thus far, however some analysis methods make quasi-equilibrium assumptions. One such model is proposed by Taitel and Barnea (1997). Their model divides the tube into small segments and assumes that there is a quasi-equilibrium force balance on each segment. The force balance substitutes for the transient momentum equations in separated (annular and stratified) flow in Equation 2.6 and dispersed flow in Equation 2.7.

$$\begin{aligned}\left(P_i - P_{i+1}\right)A_G - \tau_G S_G \Delta x - \tau_I S_I \Delta x - \rho_G g A_G \left(z_{i+1} - z_i\right) = 0 \\ \left(P_i - P_{i+1}\right)A_L - \tau_L S_L \Delta x + \tau_I S_I \Delta x - \rho_L g A_L \left(z_{i+1} - z_i\right) = 0\end{aligned} \tag{2.6}$$

$$\left(P_i - P_{i+1}\right)A = \frac{1}{2} f_M \rho_M v_M^2 \pi D \Delta x + \rho_G A \rho_M \left(z_{i+1} - z_i\right) \tag{2.7}$$

Pressure, viscosity at the interface, viscosity at the wall and gravitational terms are included. The flow parameters at each segment are determined by solving for liquid and gas velocities included in the shear stress terms (Equation 2.6) by using existing correlations for the friction factor in the separated flow case. For dispersed flow, individual fluid velocities are derived from a mixture velocity equation and volume fractions of each phase. The transient nature of liquid and gas masses are determined by multiplying the difference between the flow rate at the next time step and the current time step by a time increment and adding the product to the current mass. The appropriate equation set (Equation 2.6 or 2.7) is determined by using the Kelvin-Helmholtz transition criterion and liquid holdup information. The model was never compared to experimental data but was developed to generically model transient two-phase flow.

Minami and Shoham (1994) used similar modeling techniques to that of Taitel and Barnea (1997). They used a more complicated momentum equation for slug flow using relative lengths of the sections of the slug unit in Figure 2.1. They also implemented additional criterion for more accurate determination of the flow pattern. Unfortunately, the continuity equations were based on an original work by Taitel et al. (1989), where the gas flow rate was assumed to be constant. As Taitel and Barnea (1997) discuss in their later work, this assumption does not accurately represent the effect of accumulation of gas in the tube. Air-kerosene tests were conducted with a steady gas flow rate of 0.064 m^3/s and a constant liquid flow rate of 0.0018 m^3/s at the inlet. A pressure drop of approximately 90 kPa was applied over the 400 m long, 77.9 mm diameter test section. Slug flow developed shortly after the liquid flow rate was applied and the liquid front traveled an average of approximately 2 m/s.

Experimental work by Sakaguchi et al. (1987) reveals interesting trends related to the dynamics of individual slugs. The model used is composed of quasi-equilibrium continuity and momentum equations similar to those proposed by Taitel and Barnea (1997), but the momentum equations also contain an accelerational term. The purpose of their model was to try to predict the motion and impact force of individual slugs. The experiments were initiated under steady state wavy or stratified flow patterns with air-water. A stepwise increase in the inlet vapor flow rate was used to generate a single slug that traveled the entire length of the 8 m, 40 mm diameter tube. The motion of the slug front, motion of the slug tail, and pressure drop were recorded. Stratified flow was observed immediately following the slug and an average liquid holdup of 0.12 was not found to change significantly with diameter or flow rate. The pressure drop across the slug was approximately equal to the sum of the accelerational pressure and the viscous pressure. The mass of the slug changed across the length of the tube. Liquid from the stratified/wavy flow in front of the slug was absorbed and a film was deposited on the tube wall behind the slug. The net effect was an increase in mass due to a thicker film in front of the slug than behind. The liquid holdup at the end of the tube was smaller than the rest of the tube. As the slug approached this region, its acceleration increased rapidly due to a net reduction in the mass of the slug.

2.1.3. Contribution

Although it is apparent that extensive transient slug flow research has been conducted, few results, if any, are applicable to refrigeration and air conditioning startup. Most of the models and experimental work described are concerned with predicting transitions to slug flow from some initial, stable two-phase flow condition. Refrigeration system startup is completely different, it begins with the fluid at rest and flow is initialized due to a sudden increase in the pressure difference. Also, tube diameters tested in existing literature are typically larger (26-105.3 mm) than those seen in vapor compression systems. Refrigerant under saturation conditions also requires special consideration due to the temperature dependence on local pressure. This characteristic is not explored in the previous research, but is addressed in the current work.

With the exception of Sakaguchi et al. (1987), no work has addressed the physical processes that govern individual slug motion and breakdown. This is the fundamental focus of the present work.

2.2. Optical Film Thickness Sensor Literature

Previous transient two-phase flow research often used conductance or capacitance sensors in order to determine the liquid holdup or volumetric void fraction. These sensors could be used to determine the location of a slug mass; however, the current work seeks to provide some understanding of the nature of the film deposited by the

slug. Due to the importance of the direct measurement of the liquid film thickness in this paper, optical film thickness sensors are discussed briefly.

Yu et al. (1996) presents an optical film thickness sensor design for use in measuring the film thickness in annular two phase flow. The sensor uses a bundle of six receiving fiber optic lines clustered around a central emitting fiber connected to a laser light source as shown in Figure 2.2. The intensity of the light from the emitting fiber captured by the photodiodes on the receiving fibers can be correlated to the height of the liquid film. Numerical analyses predict a Gaussian distribution of the intensity with the radius from the center of the emitting fiber; experiments using a flat, reflective surface have verified the theoretical predictions. The results show a strong dependence of the reflected intensity with angle of the reflected surface at film thicknesses less than 4 millimeters, the range of the sensor.

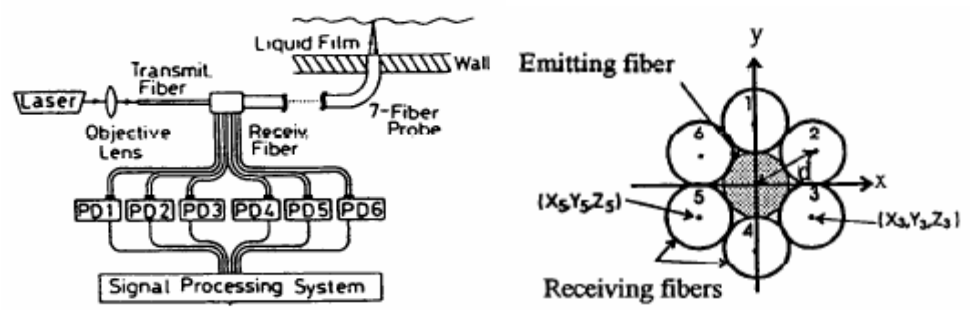

Figure 2.2. Fiber Optic Film Thickness Sensor Diagram Used by Yu et al. (1996)

Hurlburt and Newell (1996) present an optical film thickness sensor that operates on some of the same principles, but can be mounted on the outside of a transparent tube. This sensor utilizes the sharp increase in reflectivity at a critical angle associated with a liquid vapor interface that results from the difference of refraction indices of the fluids. A simple formula is presented that defines the distance of the reflected light interface in Equation 2.8.

$$R = 2h_{Wall}\tan\theta_{C,W-L} + 2h_F\tan\theta_{C,L-V} \tag{2.8}$$

This distance was measured by observing the radius of a light ring on ruled tube surface through automated software. The wave velocity was also measured by comparing voltage outputs on photodiodes from the reflected light of an LED instead of using a camera to observe the wave velocity directly. A diagram of the sensor apparatus is shown in Figure 2.3. A similar setup is used in the current study.

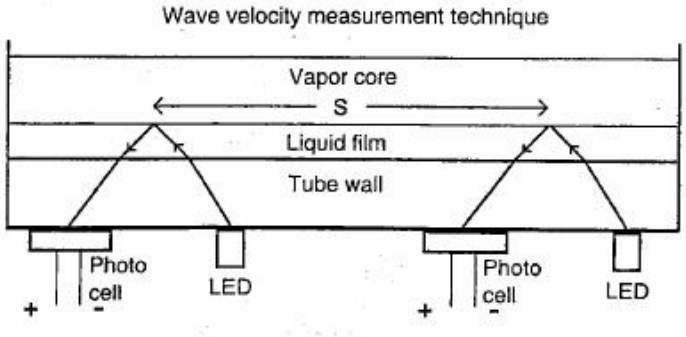

Figure 2.3. Wave Velocity Sensor Diagram Used by Hurlburt and Newell (1996)

Chapter 3. Experimental Setup and Test Matrix

This chapter describes the experimental test facilities, the test matrix, and test procedures used in the present study. The facility design, construction methods, instrumentation selection and development, instrumentation calibration and uncertainty, testing conditions, and once through flow loop operation are described in detail.

3.1. Flow Loop Description

The once through flow loop, depicted in Figure 3.1, is used for transient two-phase flow experiments in the present study. Vapor flows from a high pressure reservoir through a "u" shaped liquid trap used to generate liquid slugs. The slug then travels through a test section which contains film thickness sensors throughout its length and pressure transducers at the inlet and outlet. Finally, the slug travels to the low pressure reservoir.

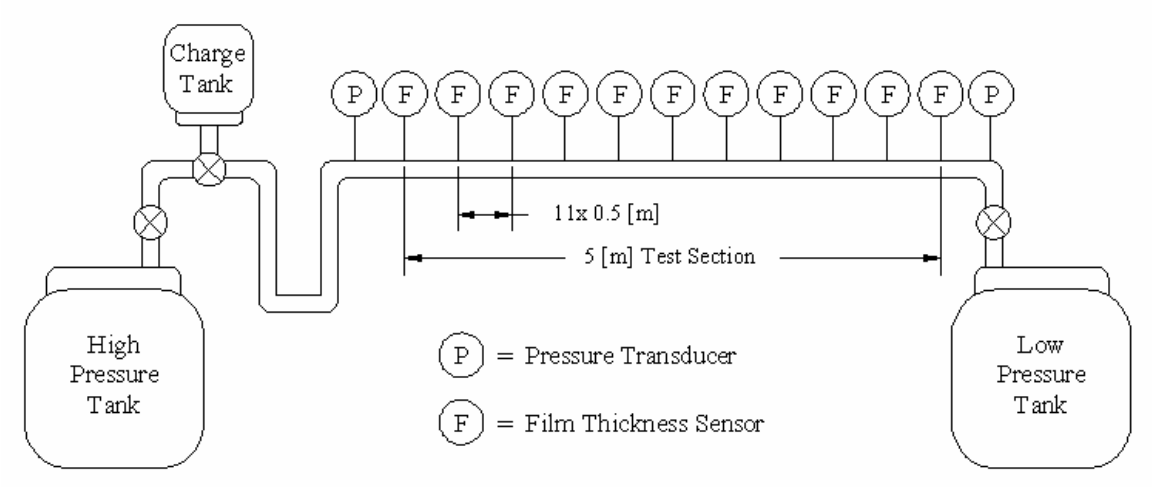

Figure 3.1. Experimental Flow Loop Schematic

During a test, a liquid charge is added to the system from the charging tank and collected in the u-shaped section. Once the liquid volume is stable, either the high pressure or the low pressure reservoir valves can be opened to generate a pressure difference across the slug. The slug then travels from its stable position in the liquid trap to the downstream reservoir, leaving a liquid film as the slug passes. The test apparatus consists of three main parts: the pressure reservoirs, the liquid trap, and the test section.

3.1.1 Pressure Reservoirs

The applied pressure difference in refrigerant tests is controlled by maintaining high and low temperatures on the high and low side tanks, respectively. Since the refrigerant is at saturation conditions in each tank, the pressure is directly related to the imposed temperatures. Two 27 kg refrigerant charge tanks are used as pressure reservoirs. The high pressure tank contains approximately 11 kg of charge and the low pressure tank contains 2 kg of charge at the beginning of testing. Although a relatively small amount of refrigerant is required in each tank for the testing, a larger amount is added to provide a larger thermal mass. The increased thermal mass attempts to maintain a constant pressure in each tank during testing; in addition, it increases the number of experiments that can be run before switching tanks. The charge tanks are connected to the liquid trap through 5.56 mm diameter rubber

refrigerant charge hoses. Valves are positioned at the inlets and exits of the pressure reservoirs for both air-water and two-phase refrigerant systems to provide a variety of flow conditions.

For air-water testing, the high side tank is replaced by a dry compressed air supply. A pressure regulator (Wilkerson R18-04-F0G0, 0-2.07 MPa) controls the pressure difference applied across the liquid slug. The low pressure reservoir is replaced by a drain tube open to the atmosphere. This setup not only provides simple control of the applied pressure difference over a range of approximately 0-7000 kPa, but also allows for an estimate of the applied pressure difference for comparison with pressure transducer data. The regulator is connected to the liquid trap through 15.5 mm diameter PVC tube.

3.1.2 Liquid Trap

A metered amount of liquid is added into the liquid trap prior to testing to determine the effect of slug volume on the acceleration and breakdown of the slug. A 500 ml graduated cylinder is connected to the liquid trap by a valve in order to measure the amount of liquid added during air-water tests; this graduated cylinder replaces the charge tank shown in Figure 3.1. A 2 kg refrigerant charge tank controlled by a valve is used to insert refrigerant into the liquid trap. The volume of liquid refrigerant is measured by observing the liquid height in the liquid trap indicated by markings made on the u-shaped section tubing.

The liquid trap consists of a 9.53 mm flexible PVC tube 3.50 m in length. The tube has a u-shape, with a 0.10 m radius 180º bend at the bottom. The shape allows the liquid mass to collect in a stable location and fill the entire cross section of the tube with a small amount of liquid. The collection section will ensure slug flow at the start of the transient event when the pressure is applied. The pooling of refrigerant liquid in this manner is also conducted to mimic the collection of refrigerant in vapor compression cycles when the system is shut off and returns to ambient temperature. The length of the liquid trap is such that it can accommodate liquid slugs from 0-400 ml.

3.1.3 Test Section

The test section consists of a 5 m long horizontal PVC tube of constant circular cross section connected between the liquid trap and the downstream pressure reservoir. The test section is constructed with PVC union fittings at the ends in order to facilitate the removal and replacement of test sections. Eleven film thickness sensors are placed every 0.5 meters along the test section as indicated in Figure 3.1. Pressure taps, dimensioned in Figure 3.2, are located at the inlet and exit of the test section in order to minimize the flow interruption caused by the transducers.

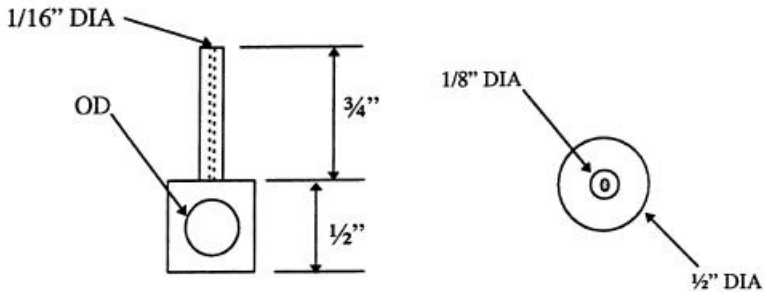

Figure 3.2. Pressure Tap Dimensions

3.2. Instrumentation

A variety of rapid response sensors are used to collect pressure difference, film thickness, slug position, time, and flow visualization data. Sensor selection, design, and uncertainty are described herein.

3.2.1. Instrumentation Selection and Design

The transient nature of the experiment requires high speed data acquisition capabilities. The NI 6220-PCI DAQ with a SCB-68 signal conditioning block allows 16 analog input channels at over 1000 samples per second.

Two absolute pressure transducers located at each end of the test section are used rather than a single differential pressure transducer in order to measure saturation pressures near the reservoir tanks and maintain a short response time. Honeywell SPTmV0300PG5W02 pressure transducers are used with a 0.5 %FS accuracy, and a 0.1 ms response time.

Optical film thickness sensors are not commercially available and had to be fabricated. The film thickness sensor design is derived from the work of Hurlburt and Newell (1996). The sensors consist of an LED and a photodiode and operate on the principle of variation of surface reflectivity due to the difference in the index of refraction of two fluids. The principle is shown graphically in Figure 3.3. There is a critical angle, determined by the refraction indices of the fluids at the liquid-vapor interface, above which the light is reflected back toward the outer surface of the tube (where the photodiode is located). As the reflected radius grows, more light reaches the photodiode surface, increasing the output voltage of the photodiode. The voltage output from the photodiode can be related directly to the height of the film thickness if the properties of the fluid are known. The time at which the slug front passes the photodiode can also be determined through analysis of the photodiode output as described in Chapter 4.

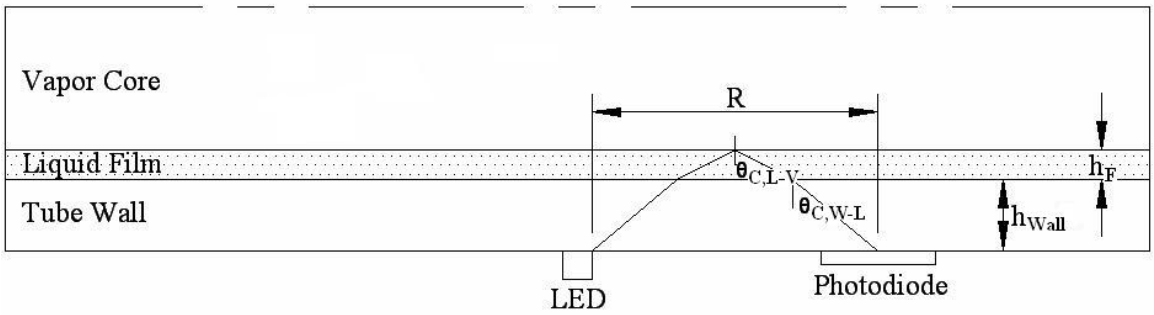

Figure 3.3. Schematic of the Film Thickness Sensor Experimental Setup

The tube wall contribution to the reflected radius is calculated according to the geometrical relation in Equation 2.8 by setting the film height to zero and assuming a PVC-liquid interface. Table 3.1 displays the index of refraction values used in calculations for the photodiode placement. The refractive index for PVC is obtained through manufacturer's information; Chae et al. (1990) provides refractive indices for R134a liquid and vapor; and the refractive indices for liquid water and air are from Hurlburt and Newell (1996).

Table 3.1. Refractive Indices

Substance	Refractive Index
PVC	1.54
Water – Liquid	1.33
Air	1.00
R134a – Liquid	1.23
R134a - Vapor	1.00

The reflected radius is calculated for application to two different tubes and both air-water and two-phase refrigerant systems. The results are shown in table 3.2.

Table 3.2. Reflected Radii for Photodiode Placement

Tube Diameter [mm]	Working Fluid	Reflected Radius [mm]
10.2	Air-water	11.9
10.2	R134a	9.2
13.4	Air-water	13.6
13.4	R134a	10.5

The photodiodes are placed on the bottom of the tube at a distance of 9.2 mm and 10.5 mm from the LED for the 10.2 mm diameter tube and the 13.4 mm diameter tube, respectively. The shortest reflected radius in table 3.2 is chosen to ensure the sensors will perform well regardless of the working fluid; locating them on the bottom of the tube allows for film measurement in either an annular or stratified flow case.

PerkinElmer VTS3085 photodiodes are used with an active surface area of 21 mm^2 and response time of 1 ms. The large surface area allows a maximum measurable film thickness of 4.5 mm for air-water and 3.6 mm for two-phase R134a and allows room for small errors in the placement relative to the LEDs. A circuit is connected to the photodiode in order to amplify the voltage signal for improved resolution in DAQ measurement. Figure 3.4 shows the photodiode circuitry. An opaque, black coating is applied on the outside surface of the tube 19 mm upstream and 36 mm downstream of the photodiode in order to minimize the sensor sensitivity to changes in the ambient lighting conditions.

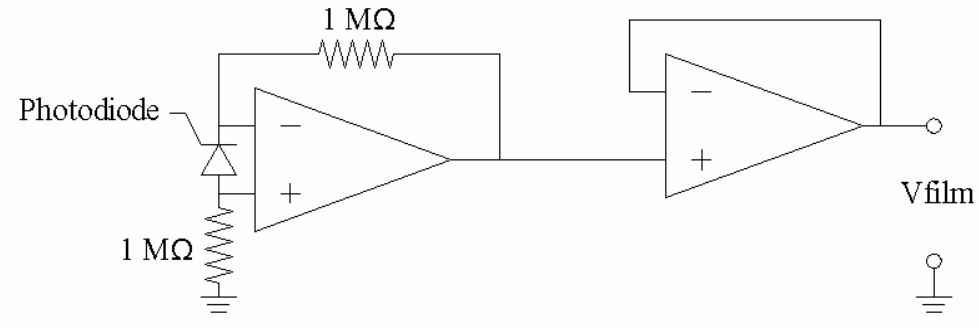

Figure 3.4. Diagram of the Photodiode Amplification Circuit

Two different video recording apparatuses are used to capture flow visualization images of the transient slug flow. A schematic of the flow visualization setup is shown in Figure 3.5. The first consists of a digital web

camera and a stroboscope. The web camera setup provides good quality images by illuminating the test section with the stroboscope at 30 frames/second, the same frame rate as the camera. Unfortunately, this visualization method does not have a high enough frame rate to capture all of the transient phenomena. To determine the distance traveled by the liquid slug before breakdown, a FASTCAM Ultima-1024 is used to capture video at 125 frames/second. This frame rate is sufficient to capture all of the transient phenomena, but has poorer image quality than that recorded by the web camera setup. For each camera, an alternating black and white vertically striped pattern is used as a background to enhance the appearance of the vapor-liquid interfaces. This optical technique was developed by Jassim (2006).

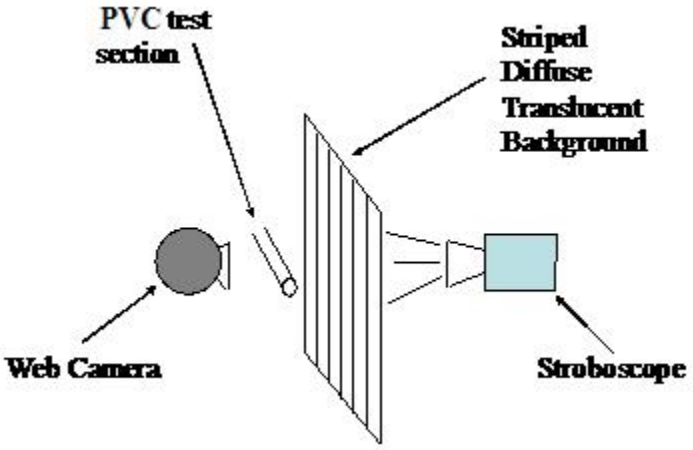

Figure 3.5. Flow Visualization Schematic for the Web Camera and High Speed Camera

3.2.2 Instrument Calibration

The pressure transducers are calibrated using a Pressure Instruments DTG-2K digital test gage over a range of 0-1400 kPa in increments of 70 kPa. The transducer voltage variation with pressure over the calibrated range is highly linear with a linear regression value of 1.0000 for each transducer, showing very strong linearity. The uncertainty in the calibration is ±1 kPa; however, a significant amount of noise found in experimental measurements results in an uncertainty of approximately ±20 kPa.

The film thickness sensors are calibrated for air-water by adding a measured amount of water corresponding to a liquid thickness into the horizontally level tube. The sensors are calibrated from 0-3.0 mm in increments of 0.5 mm. The change in observed voltage between 2.5 and 3.0 mm is very small, indicating that the sensors can only measure liquid films up to 2.5 mm thick. The uncertainty in the film thickness measurement is approximately ±0.5 mm due to the difficulty in obtaining a uniform film thickness across the entire tube during calibration and the resolution of the calibration measurements.

The film thickness sensors are also calibrated for two-phase R134a by using the air-water calibration and a relationship between the indices of refraction of the fluids. Table 3.3 shows the film thicknesses measured during calibration for the air-water system and equivalent film thicknesses for the two-phase R134a system. R134a film thicknesses less than 2.00 mm (the minimum in table 3.3) are obtained by extrapolating a calibration curve through the data points shown in table 3.3.

Table 3.3. Water to R134a Film Thickness Correlation

$h_{L,H20}$ [mm]	$h_{L,R134a}$ [mm]
0.0	2.00
0.5	2.41
1.0	2.82
1.5	3.23
2.0	3.64
2.5	4.05
3.0	4.45

The R134a film thicknesses shown in table 3.3 are the film heights required to obtain an equivalent reflected radius for the air-water film thickness shown on the left. The equivalent R134a film thickness corresponding to a liquid height of 0.0 mm is calculated assuming a PVC-liquid interface at the wall of zero liquid thickness. Calculation using a PVC-vapor interface for the 0.0 mm case causes a discontinuity due to the difference in the indices of refraction of the interfaces. The sensor output for the 0.0 mm film is not used in calibration because of this discontinuity. The voltages recorded during air-water testing corresponding to the water film thickness should be equal to the voltages observed when the corresponding R134a film thickness in table 3.3 is present. The uncertainty in the film thickness measurement for R134a is, again, approximately ±0.5 mm.

There is a ±10 mm uncertainty in the location of the film thickness sensors on the tube. There is also an uncertainty in the time at which the liquid slug passes each film thickness sensor. This time is determined through analysis of the photodiode output as described in Chapter 4. The estimated uncertainty in time at which the slug passes each sensor is ±0.01 s.

There is an uncertainty in the initial slug volume of ±5 ml for air-water tests. Height markings were placed on the liquid trap tube corresponding to 10 ml increments for measurement of the initial slug volume for R134a tests. During R134a testing, only a small part of the tube in the liquid trap is cooled by an ice bath and higher pressure vapor between the liquid and the high side valve constantly bubbles through the slug. The bubbles and uncertainty in liquid height markings contribute to an uncertainty in initial slug volume of ±10 ml for R134a.

The uncertainty in the measured tube length required for slug breakdown, x_B, determined in flow visualization experiments is estimated to be ±0.12 m.

The uncertainties of all of the measured variables are summarized in tabular form in table 3.4.

Table 3.4. Summary of Measurement Uncertainties

Variable	Uncertainty
P_U	±20 kPa
P_D	±20 kPa
h_F	±0.5 mm
x	±10 mm
t	±0.01 s
V_{H2O}	±5 ml
V_{R134a}	±10 ml
x_B	±0.12 m

3.3 Testing

This section presents the testing conditions and the tested range of independent variables explored in the experiments. A detailed description of the operation of the experimental apparatus is also provided.

3.3.1. Test Matrix

The two-phase fluid, applied pressure difference, tube diameter, and slug volume are varied in the present study in order to investigate the acceleration and breakdown of slugs over a range of conditions commonly found in vapor compression systems.

Two different two-phase fluids are investigated in the present study: air-water, and R134a. Though water and air are of little practical use as refrigerants, these fluids are chosen to simplify the initial experimental setup since the tests can be conducted at atmospheric conditions and provide low vapor to liquid density ratio data for model validation. R134a is also tested due to its extensive use in the refrigeration and air conditioning industry. Unlike air-water, refrigerant slugs have the ability to change phase if the pressure is decreased below saturation forming vapor bubbles which may affect the slug motion and breakdown.

Air-water tests are conducted with applied pressure differences across the slug of 69, 138, 207, and 276 kPa. The transient pressure difference follows a step profile, starting at 0 kPa and increasing to the desired value almost immediately after the opening of a valve. The applied pressure difference for R134a is more difficult to control. Due to evaporative cooling of the high pressure side refrigerant reservoir, the transient pressure profile often deviates from a step profile. The pressure difference is generated by heating the upstream pressure tank prior to testing and placing the downstream tank in an ice bath or dry ice-acetone bath. Pressure differences ranging from 70-520 kPa are generated.

Three different tube diameters are used throughout testing. 10.2 and 13.4 mm diameter PVC test sections can be interchanged while the rest of the testing apparatus remains. These tubes are outfitted with all 11 film thickness sensors. A 6.35 mm diameter reinforced flexible PVC tube is constrained horizontally to provide the third tested diameter. Unfortunately, the reinforcing fibers interfere with the LED light sources so the tube is only outfitted with photodiodes. The tube can therefore only measure the time at which the slug front passes the sensors and not the film thickness present after the slug.

The initial volume of the slug is also treated as an independent variable. Refrigerant charges of 200-400 ml are common in air conditioning and refrigeration systems. In air-water tests, initial slug volumes of 100, 200, 300, and 400 ml are tested. Due to pressure distributions along the test section and the size of the liquid trap, refrigerant slugs from 50 to only 200 ml can be tested. The slug volumes are difficult to repeat as a result of bubbles passing through the liquid volume resulting from temperature variation between sections of the test apparatus.

In actual air conditioning and refrigeration systems refrigerant masses in the high pressure side of a vapor compression system are pushed toward an expansion device as a result of a sudden increase in pressure on the high pressure side of the compressor. Conversely, refrigerant masses in the low side of the system are drawn toward the low pressure side of the compressor as a result of the sudden decrease in pressure as the compressor is turned on. In the present tests both air-water and two-phase R134a systems are tested under simulated high side pressure conditions. Because of the implications of saturation pressure and boiling effects, R134a is also tested under low side conditions.

Due to results explained in Chapter 4, a limited amount of testing is conducted in simulated low side conditions. Flow visualization video, pressure, and film thickness sensor data are collected for applied pressures ranging from 40-290 kPa and slug volumes ranging from 40-193 ml in all three tube sizes under low side conditions.

3.3.2. Testing Procedure

Air-water and two-phase R134a tests are conducted in a slightly different manner. Prior to all testing, all instrumentation (DAQ, cameras, LEDs, photodiode circuits, pressure transducers) are enabled. Due to the interference of the light flashes of the stroboscope with the photodiode sensors, flow visualization video and data are collected separately by repeating tests.

Prior to air-water testing, the upstream and downstream valves of the test section are opened and dry air is allowed to flow through the test section in order to set the pressure regulator to the desired pressure; once the pressure is set, the upstream valve is closed. A metered amount of liquid is added to the collection section. Once the liquid is settled in the bottom of the collection section and stable, the DAQ or video recorder is initialized immediately followed by opening the upstream valve. Data is recorded until the slug passes the end of the test section and the deposited film dissipates. The upstream valve is again closed and the process is repeated for each subsequent test condition.

R134a testing requires additional steps. For tests simulating the high side of a vapor compression system, the upstream valve is initially closed and the downstream valve is initially open. The high pressure reservoir is heated in order to achieve a higher saturation pressure and the low pressure reservoir is placed in an ice bath. Liquid R134a at ambient temperature is added by opening the valve connecting the charge tank and liquid trap. Care must be taken during this step in order to avoid boiling over of liquid into the horizontal test section. The bottom of the liquid trap is placed in an ice bath in order to attempt to achieve a relatively constant pressure distribution in the test section. The system is then allowed to stabilize until the liquid in the liquid trap stops boiling. The liquid volume is then measured. Next, the DAQ or video recording equipment is initialized and data is recorded until only refrigerant vapor is present in the test section. The upstream valve is then closed.

Testing under low side simulated conditions is slightly different; the upstream valve is initially open and the downstream valve is initially closed. Both the high pressure reservoir and charge tanks are at approximately ambient temperature. The low side tank is placed in a dry ice-acetone bath in order to provide a large enough pressure difference to accelerate the slug. A liquid charge of measured volume is again added as previously described under high side conditions, except an ice bath is not applied to the liquid trap. Once the liquid in the liquid trap is stable, the test is initialized and the low side valve is opened. The test is continued until all liquid refrigerant travels into the low side pressure tank.

Chapter 4. Test Results

The results of the tests detailed in Chapter 3 are provided herein. Flow visualization images provide insights about slug speeds, flow patterns, and slug breakdown. Pressure difference and film thickness sensor data describe the relevant forces, flow patterns, film properties, and slug motion.

4.1. Flow Visualization

Video from the web camera and high speed camera is used to estimate the slug velocity. The web camera visualization setup described in Chapter 3 is mainly used to determine what flow regimes are present and define the regions of the slug. The high speed camera is used to determine the location of slug breakdown. The images depict flow traveling from left to right.

4.1.1. Slug Velocity

The slug velocity can be estimated by observing the difference in position of the slug front between consecutive images at a given frame rate. The maximum frame rate of the digital web camera is 30 frames/second and the largest viewable horizontal dimension in the cameras frame of view is 95 mm. A slug must travel less than 2.88 m/s at the camera location for the digital web camera to capture the slug front in two consecutive frames. However, the majority of the slugs have a velocity above 2.88m/s, so the slug fronts are not easily observed.

The adjustable frame rate on the high speed camera allows for the capture of multiple images of the slug front as it passes by. However, the slug front is not easily defined due to mixing at the liquid-vapor interface. The mixing causes a cloudy interface, making it difficult to define and track between consecutive images. Liquid slugs above 200 ml travel at speeds approaching 10 m/s. Smaller slug volumes (less than 200 ml) have velocities in a range of 15-25 m/s. These velocity estimates are compared to the actual slug motion recorded by the film thickness sensors.

4.1.2. Slug Regions

Distinct regions are observed in the present transient slug flow experiments. Though the relative sizes of the regions vary widely through the variation of the test parameters, the following regions are always observed: slug front, slug mass, and trailing liquid film.

A series of photographs shown in Figure 4.1 depicts the passing of a 200 ml R134a slug front in a 13.4 mm diameter tube captured with the high speed camera. The camera is located 3.80 m downstream from the test section entrance and the images are captured 4 ms apart. The mixing between the liquid and vapor phases of the interface, particularly in high pressure and small volume tests, make the interface difficult to distinguish. Figure 4.1 shows a long slug front region where a stratified liquid layer begins filling the bottom of the tube and gradually increases in thickness until it fills the tube. This suggests that gravity can play a significant role in the formation of the slug front. Testing conditions causing a larger acceleration show an increasingly negative (approaching vertical) slope of the slug profile as inertial forces begin to dominate over gravitational forces.

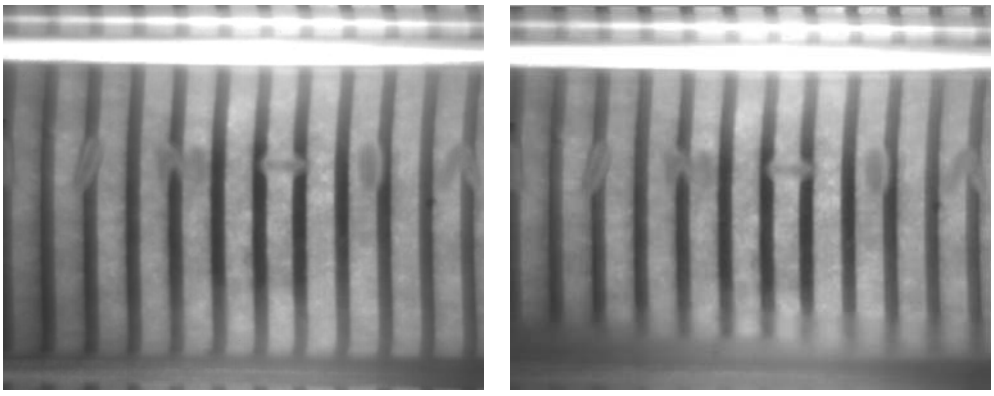

A B

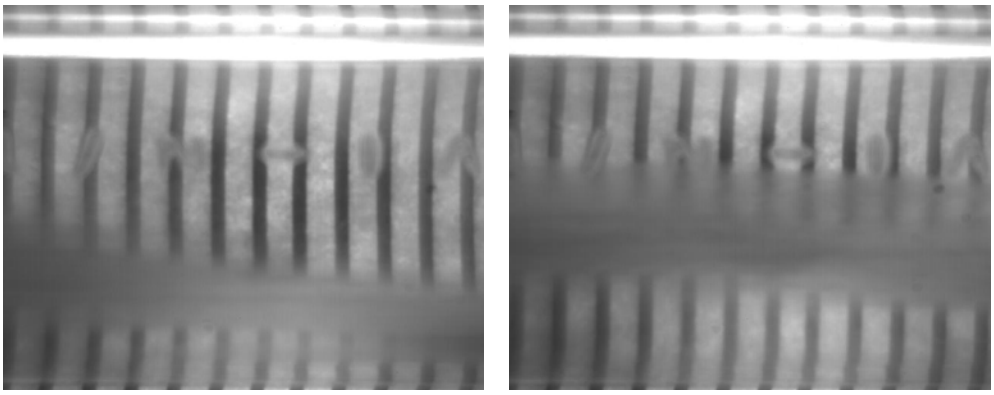

C D

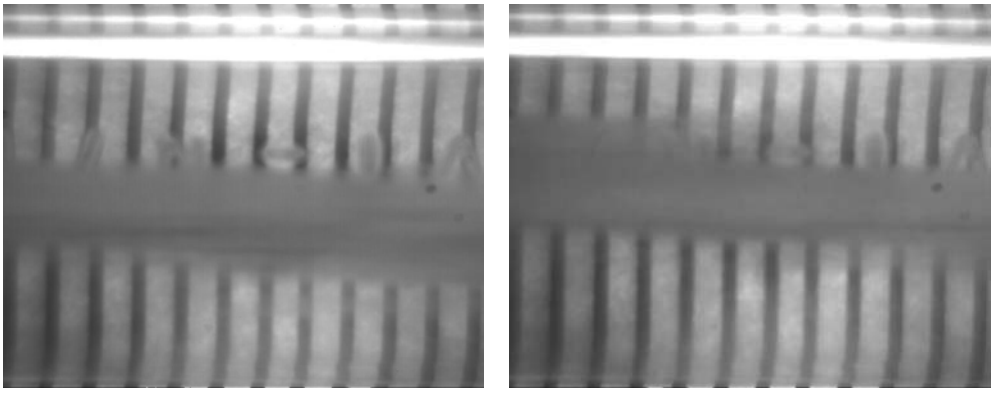

E F

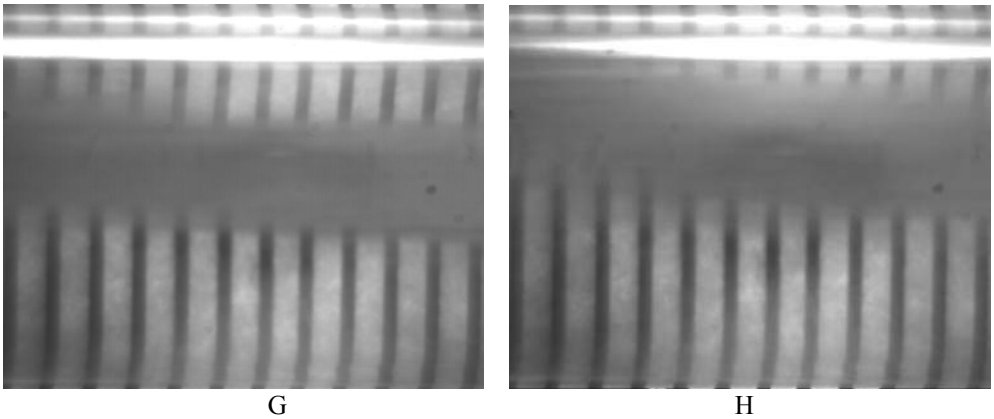

G H

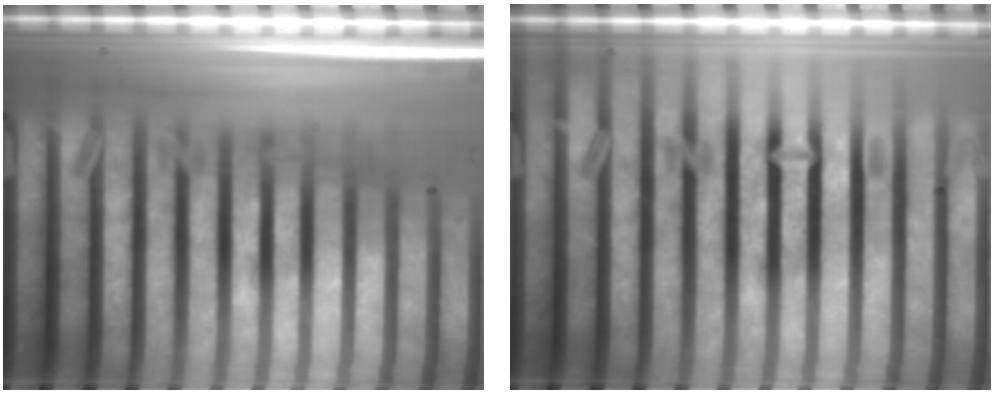

I J

Figure 4.1. Images of a Slug Front for a 30 kPa Pressure Difference, 200 ml Initial Slug Volume, in 13.4 mm Diameter Tube, R134a Test, Using a 125 Frame per Second High Speed Camera 3.80 m Downstream from the Test Section Entrance

Liquid droplets are occasionally deposited on the tube wall in the beginning of the test section before the liquid slug is observed. This effect is shown in Figure 4.2 for air-water in a 10.2 mm diameter tube, but is also observed for R134a and in the 13.4 mm diameter tube. The cause of this behavior is unknown, but likely attributed to test section construction. One possible cause is illustrated in Figure 4.3. There are small discontinuities in the tube wall as a result of tube fittings between the liquid trap and the entrance section and the high side pressure tap. Some liquid from previous tests remains in these discontinuities. As the slug accelerates, it pushes the vapor ahead of it and shears off some of the liquid in the discontinuity, which is deposited on the wall downstream of the discontinuity. Another possible explanation is that the reductions/expansions in the tube diameter, required to connect the liquid trap and test section, cause local flow disturbances. These disturbances may cause a small front portion of the slug to break off, disperse into droplets, and accelerate ahead of the main slug volume.

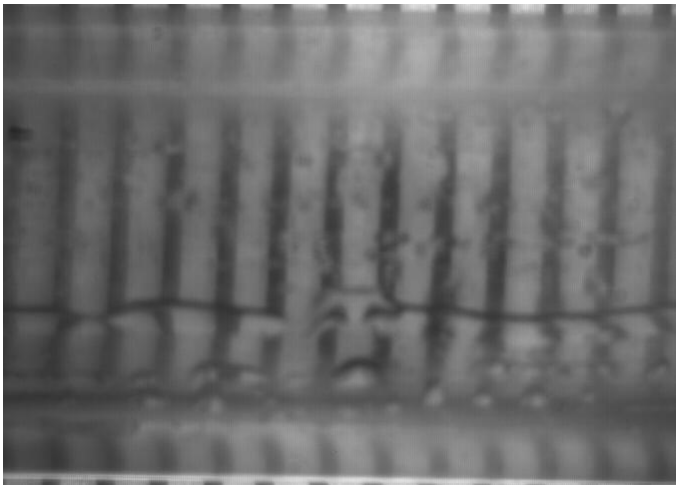

Figure 4.2. Image of Droplets Deposited on Tube Wall Prior to Slug Passage for a 207 kPa Pressure Difference, 150 ml Initial Slug Volume, in 10.2 mm Diameter Tube, Air-water Test, Using a 125 Frame Per Second High Speed Camera 0.32 m Downstream from the Test Section Entrance

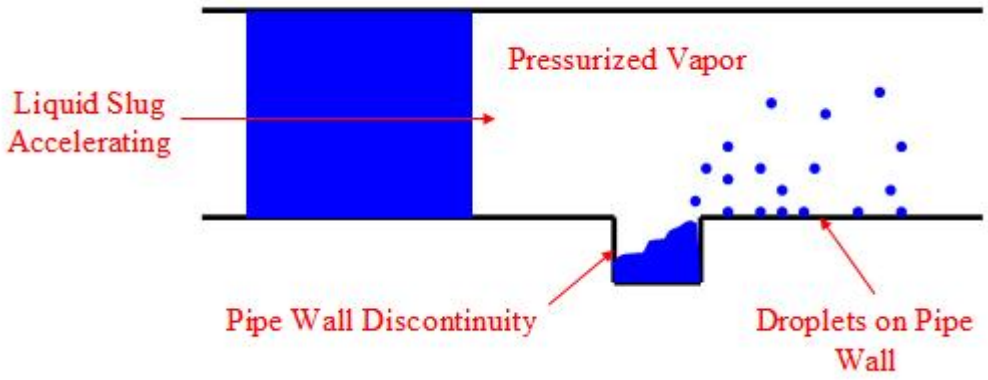

Figure 4.3. Illustration of Droplets Deposited on Tube Wall Ahead of Slug

Figure 4.4 shows another series of images for an air-water test in a 10.2 mm diameter tube captured by the digital web camera at a location of 0.67 m downstream of the test section entrance. A graphical representation of the observed slug regions is presented in Figure 4.5. The letters indicating distinct slug regions in Figure 4.5 correspond to flow visualization images with the same letters in Figure 4.4. The first section of the slug, image Figure 4.4A, is characterized by a dense mixture of liquid and vapor resulting from the highly turbulent flow and the entrainment of vapor near the slug front. The image looks slightly lighter near the bottom of the tube because more liquid is at the bottom surface of the tube. Bubble flow is observed behind the slug front as less vapor is able to penetrate deeper into the slug, as shown in Figure 4.4B. Occasionally an intermittent flow pattern of large, elongated bubbles is also observed following the cloudy mixture. As the bubbles become smaller and less numerous, the liquid eventually fills the entire cross section as shown in image Figure 4.4C. The small marks on this image are scratches on the outer surface of the tube, not bubbles. The liquid slug is immediately followed by a turbulent wavy annular, for air-water tests, or stratified flow, for R134a tests, film region shown in image Figure 4.4D. The liquid film in the slug tail is sheared thinner by the high velocity vapor as the slug travels further away from a given location. Eventually a thin film is left behind by the slug on the tube wall as shown in image Figure 4.4E. This film does not appear to decrease in thickness significantly until the entire film is sheared off the wall by the vapor. Typically the film shears off of the top and sides of the tube before shearing the film off of the bottom.

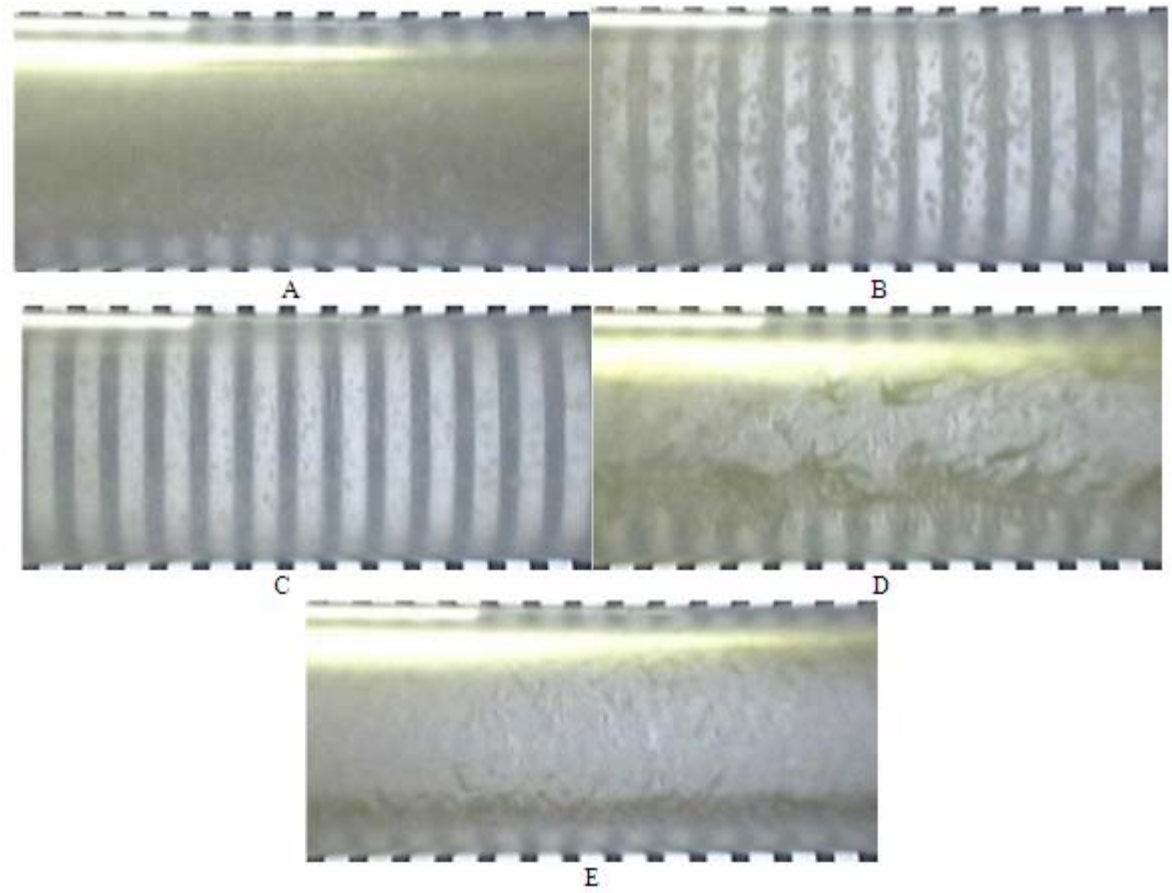

Figure 4.4. Slug Region Images for a 207 kPa Pressure Difference, 300 ml Initial Slug Volume, in 10.2 mm Diameter Tube, Air-water Test, taken with a 30 Frame per Second Web Camera 0.67 m Downstream of the Test Section Entrance

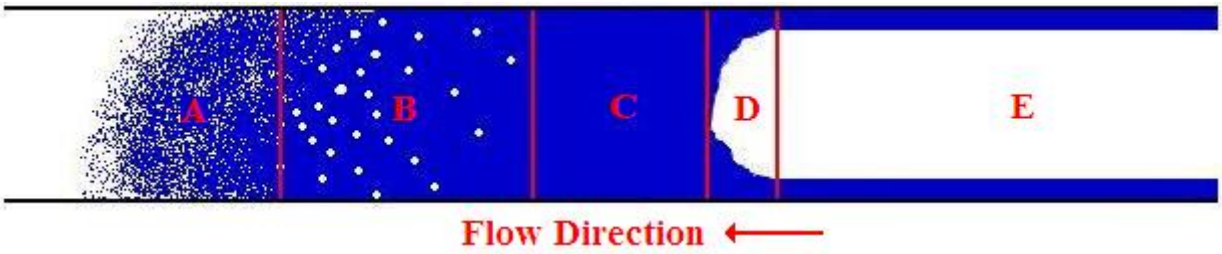

Figure 4.5. Graphical Representation of Observed Slug Regions

There are both similarities and differences between the observed slug regions in Figure 4.4 and the slug unit proposed by Dukler and Hubbard (1975) in Figure 2.1. The profile of the observed slug front is angled and irregular, unlike the Dukler and Hubbard (1975) model. However, Sakaguchi et al. (1987) has shown that the pressure drop across the slug front is insignificant regardless of the profile of the slug front. The model does not consider the cloudy liquid-vapor mixture shown Figure 4.4A. In addition, the Dukler and Hubbard (1975) model does not consider the presence of annular flow after the slug observed during the present air-water testing. The uniform liquid film height following the slug tail and vapor entrainment in the slug are all observed, matching the Dukler and Hubbard (1975) model.

4.1.3. Slug Breakdown

The slug breakdown distance is an important parameter in the current study. The videos show that, regardless of pressure, liquid slugs over 200 ml do not breakdown within the 5 meter test section for air-water tests using a 10.2 mm diameter tube. However, slugs breakdown prior to reaching the test section entrance for initial volumes less than 150 ml in the 13.4 mm diameter tube. A summary of the slug breakdown distance results for air-water tests obtained from the present study is shown in table 4.1.

Table 4.1. Slug Breakdown Distances – Air-water

Applied Pressure Difference [kPa]	Initial Slug Volume [ml]	Tube Diameter [mm]	Slug Breakdown Distance [m]
69	100	10.2	2.7
138	100	10.2	2.7
207	100	10.2	2.6
276	100	10.2	2.7
69	150	10.2	4.1
138	150	10.2	4.3
207	150	10.2	4.1
207	150	13.4	2.8
207	200	13.4	3.9

The breakdown distance shown in the table is the actual distance traveled by the slug before it breaks down. This includes the distance between the initial slug front (in the liquid trap) and the test section entrance as well as the distance traveled within the test section. It can be seen from table 4.1 that the breakdown distance does not depend on pressure significantly, shown graphically in Figure 4.6. Slugs with larger initial volumes at a given tube diameter should travel further because there is more liquid available for film deposition; this is supported in table 4.1. Comparing tests of 150 ml at different tube diameters indicates that slugs travel further before breaking down in smaller tubes.

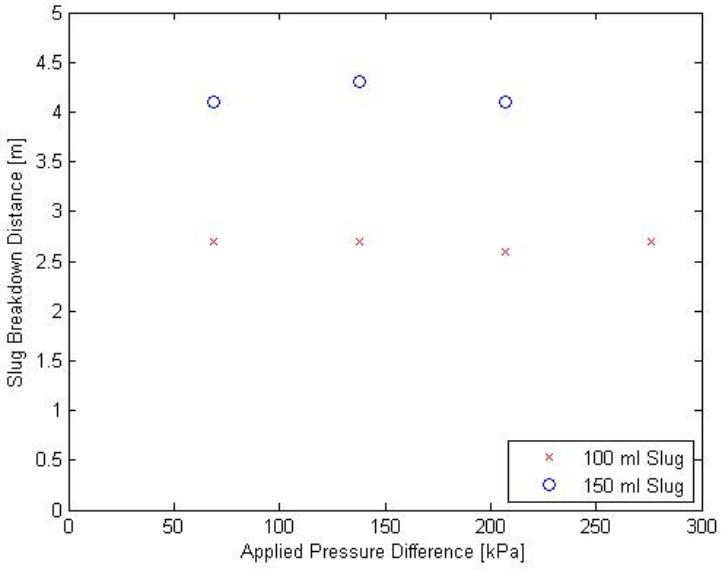

Figure 4.6. Air-water Slug Breakdown Distance Dependence on Pressure for High Side Tests in a 10.2 mm Diameter Tube

Table 4.2 shows slug breakdown distances for R134a tests. All of the tests in table 4.2 are under high side conditions.

Table 4.2. Slug Breakdown Distances – R134a

Applied Pressure Difference [kPa]	Initial Slug Volume [ml]	Tube Diameter [mm]	Slug Breakdown Distance [m]
197	35	10.2	2.7
197	45	10.2	4.4
197	60	10.2	6.9
197	85	13.4	7.2

R134a slugs of 35 ml travel approximately the same distance as air-water slugs of 100 ml at the same tube diameter. This suggests that an air-water slug deposits more liquid in the trailing film than for R134a as shown in the Film Thickness Sensor Response section of this chapter. Similar breakdown trends with slug volume and tube diameter observed for air-water are also manifest in R134a. Larger initial slug volumes for a given tube diameter travel further than smaller slug volumes. Also, slugs travel further in smaller tube diameters, which is discussed in more detail in the Slug Motion and Trends section of this chapter.

R134a slugs break down before the test section entrance for all tested slug volumes (35-200 ml) in the 10.2 and 13.4 mm diameter tubes under low side conditions. The pressure difference across the slug in the larger tubes quickly reduces to zero, as described in the following section, indicating slug breakdown. However, slugs are observed in the test section for tests using the 6.35 mm diameter tube. The difference in observed behavior between the larger tubes and the 6.35 mm diameter tube is likely due to the mass flux. The mass flux is sufficiently high in the 6.35 mm diameter tube to rapidly accelerate the liquid slug. In this case, the inertial and surface tension forces dominate over the gravitational forces on the liquid slug, preventing the slug from falling to the bottom of the tube.

4.2. Slug Flow Data

The applied pressure difference across the slug, film thickness, and slug location are measured in the present study as described in Chapter 3. Results from a representative test: 207 kPa applied pressure difference, 300 ml initial slug volume, 10.2 mm diameter, air-water, under high side conditions are presented in the current section.

4.2.1. Pressure Difference

The test conditions attempt to simulate system startup by applying a step increase of pressure difference. This situation is easier to generate in an air-water system than the R134a system because the flow is choked due to a small orifice at the exit of the refrigerant tank supplying the vapor. Figure 4.7 shows the pressure difference measured across the upstream and downstream pressure transducers for the representative test. The pressure difference between the high and low pressure reservoirs remains at zero until the liquid slug completely passes the upstream pressure transducer. After the slug passes, the pressure spikes due to the increased pressure observed by the upstream transducer at 0.8 seconds. Small variations in either pressure are present in R134a tests because of the difficulty in maintaining constant pressure in the reservoirs during the experiment. The applied pressure difference remains approximately constant until the slug front passes the downstream pressure transducer at 1.2 seconds. The measured pressure difference returns to zero after the slug passes the downstream transducer. The characteristics shown in Figure 4.7 are observed for air-water and R134a high side tests, and R134a low side tests in the 6.35 mm diameter tube.

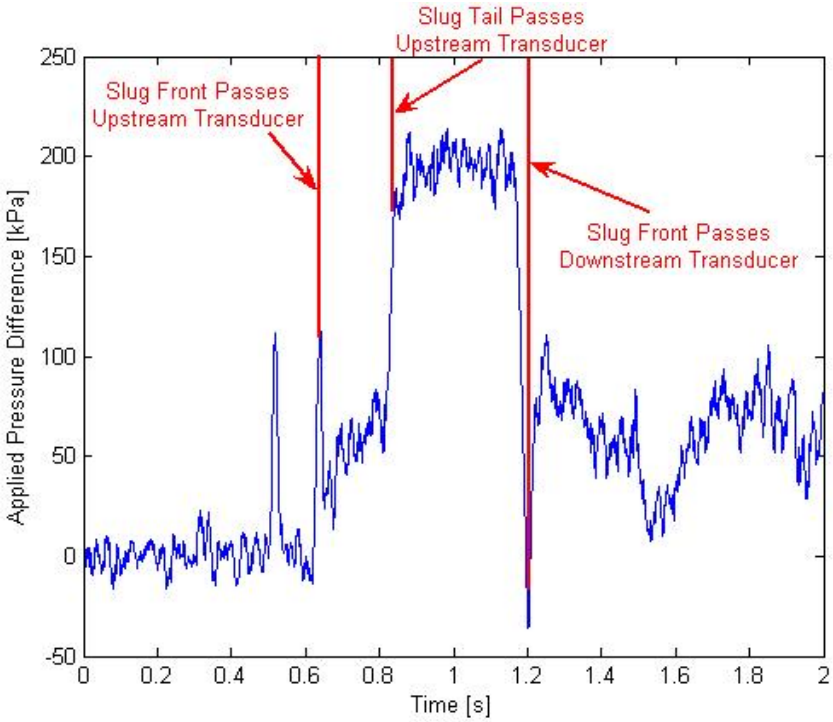

Figure 4.7. Pressure Profile for a 207 kPa Pressure Difference, 300 ml Initial Slug Volume, in 10.2 mm Diameter Tube, Air-water High Side Test

The pressure difference time trace for a low side test is much different. Figure 4.8 shows the time trace of the high and low side pressure transducers separately. The transducer outputs are almost identical, which suggests that the slug is broken up immediately when the low side valve is opened. The pressure indicated by the high and low side transducers decreases over time once all of the liquid is drawn from the test section. This is due to a drop in temperature, and therefore pressure, in the high side tank as both pressure reservoirs equilibrate. This result is typical of 10.2 and 13.4 mm diameter tubes; the pressure profile is similar to Figure 4.7 for low side tests in 6.35 mm diameter tube. The higher mass flux in the smaller tube allows the slug to remain as a coherent mass because the inertial forces dominate over the gravitational forces. As the mass flux decreases, the gravitational forces dominate over inertial and surface tension forces and the liquid falls to the bottom of the tube (stratified flow). Once there is a clear path, unobstructed by liquid, for the vapor to flow at the top of the tube, the pressure difference across the slug rapidly dissipates, breaking down the slug. As the tube diameter decreases the surface tension forces increase with respect to gravitational forces, consequently the slug breakdown distance increases. In addition, longer slugs will require more time to breakdown. In the limit as the slug velocity approaches zero, the viscous and surface tension forces on the slug are greater for a longer slug, which makes it more difficult for the liquid to fall to the bottom of the tube.

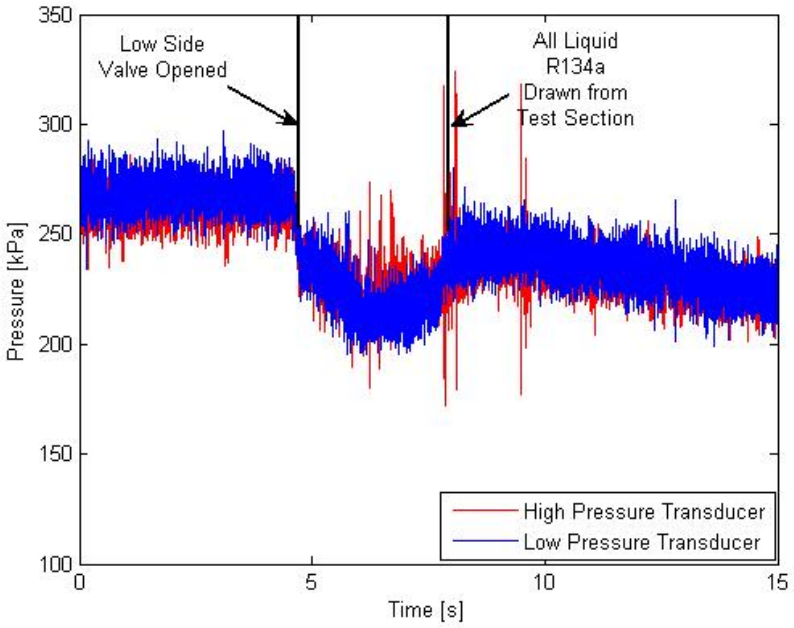

Figure 4.8. Pressure Profile for a 125 kPa Pressure Difference, 150 ml Initial Slug Volume, in 10.2 mm Diameter Tube, R134a Low Side Test

4.2.2. Film Thickness Sensor Response

As the slug passes each film thickness sensor, the voltage output of the sensor can be related to observed regions of the slug. These response characteristics are observed in all sensors if the slug is still intact at the location of the particular film thickness sensor. A graph of the voltage output from a film thickness sensor at 1.0 m for the representative test is shown in Figure 4.9. The voltage stays constant before region A at approximately 1.5 V because the slug has not yet reached the sensor. The film thickness increases with time as the angled slug front passes over the film thickness sensor, shown in region A of Figure 4.9. The sharp decrease in the voltage at the beginning of region B & C is due to the lack of a large reflecting surface. This decrease in voltage indicates the beginning of the liquid slug. When the entire tube cross section is filled with liquid, there is no interface to reflect the LED light back to the photodiode, and therefore the voltage drops to a minimum value (approximately 0.75 V in this case). No distinction can be made between the sensor output observed between the bubble region and the actual liquid slug because both flow conditions lack a large reflecting surface. The tail of the slug is captured at the end of region B & C; a sharp increase in the observed voltage indicates the presence of a liquid film. The voltage output of region D of Figure 4.9 is characteristic of the highly turbulent wavy film shown in Figure 4.4D. The voltage is higher, indicating a thicker film, and has a large amount of scatter compared to the signal in region E of Figure 4.9. The scatter in region D suggests the film thickness is changing rapidly, showing another similarity to the turbulent, thick film immediately following the slug observed in flow visualization. The signal scatter is reduced significantly and the output voltage remains constant throughout region E. This can be correlated to the thinner film with small waves shown in Figure 4.4E. The sensor shows agreement with the flow visualization video, which suggests that the film thickness remains relatively constant until the film is completely sheared off the tube wall. The film is sheared off of the wall at the beginning of region F in Figure 4.9. There is a sharp increase in the observed voltage as the film is sheared off due to a sudden change in the interface. Only a PVC-vapor interface is left after the film is

sheared off. Since PVC has a different index of refraction than the liquid, the distance that the LED light is reflected increases as does the observed voltage. This discontinuity arises because the PVC-vapor interface has a larger critical angle than the liquid-vapor interface, allowing more light to reach the photodiode when there is no film.

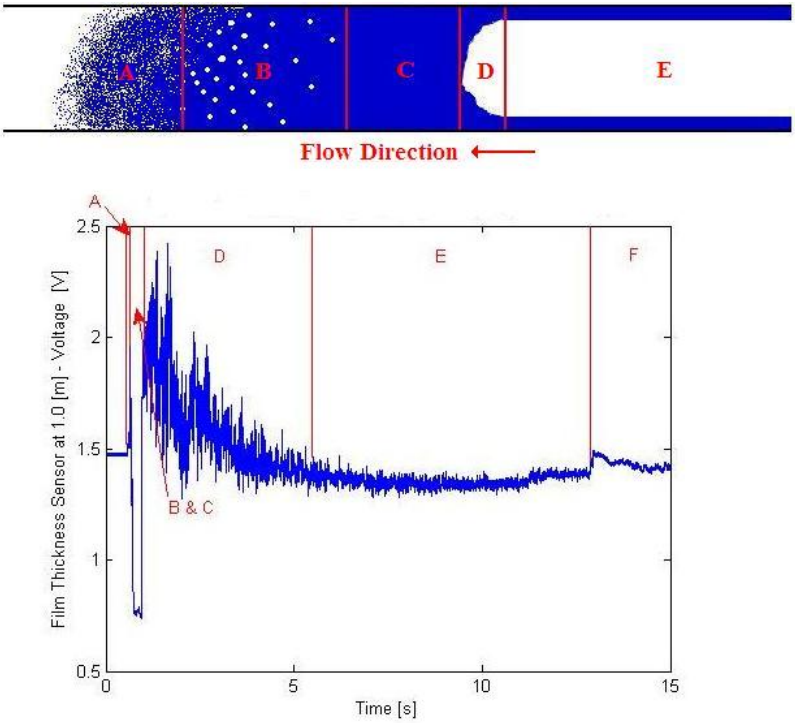

Figure 4.9. Film Thickness Sensor at 1.0 m Response for a 207 kPa Pressure Difference, 300 ml Initial Slug Volume, in 10.2 mm Diameter Tube, Air-water High Side Test

The only relevant film thickness measurements occur in regions D and E of Figure 4.9, where a liquid film is observed on the tube wall. The sensor output in the remaining regions only provides understanding about how the film thickness sensors work and indicates when a slug is present. Figure 4.10 shows the height of the observed film in mm after the voltage output in regions D and E of Figure 4.9 have been calibrated. The film is thickest (approximately 2.0 mm) immediately after the slug. The film thickness decreases slowly until it remains steady at 0.7 mm. This thickness remains constant until it is sheared off of the wall. Only the liquid film in region D affects the slug motion since the slug passes through the test section long before the thinner film in region E develops, as shown in the following section. The behavior of the thin film is discussed only to provide further information on the behavior of the film following slug flow.

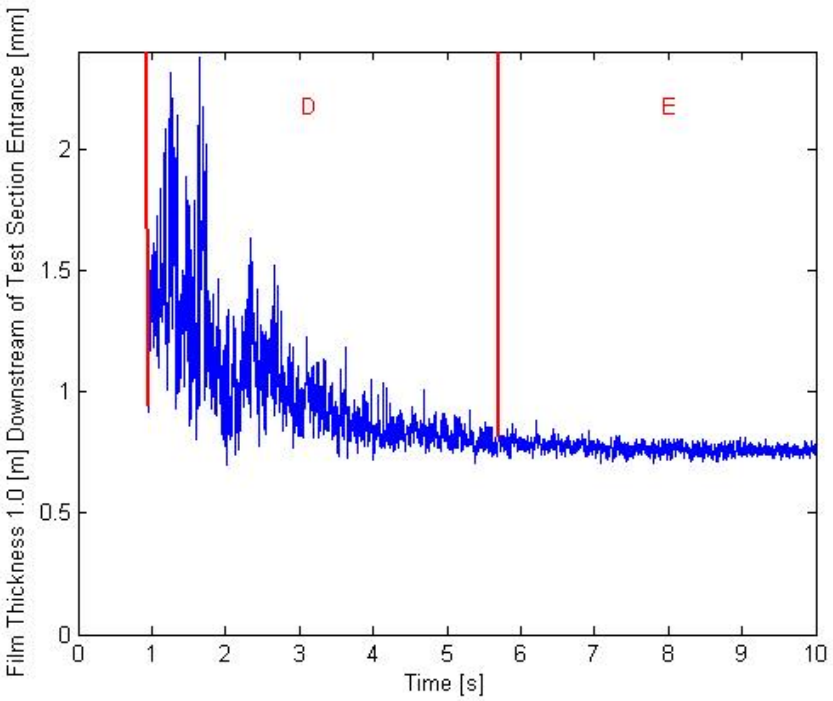

Figure 4.10. Film Thickness at 1.0 m for a 207 kPa Pressure Difference, 300 ml Initial Slug Volume, in 10.2 mm Diameter Tube, Air-water High Side Test

The average film thickness at an instant in time is calculated according to Equation 4.1 where $h_{F,n}$ is the average film height at sensor n at an instant.

$$h_{F,ave} = \frac{\sum_{n=1}^{11} h_{F,n}}{11} \tag{4.1}$$

The averaged film thickness provides information regarding the liquid volume that has been deposited on the wall, and therefore lost by the slug. Figure 4.11 shows the average film thickness profile for the representative test. The average film thickness is initially zero until the first film thickness sensor indicates the presence of a film. As the slug moves past more film thickness sensors, the average film thickness increases because more sensors measure a film at that instant (more nonzero terms in the summation in Equation 4.1). The film height measured by a film thickness sensor remains zero until the slug passes. This explains the steep increase in the average film thickness from 0.8-1.4 s in Figure 4.11. The average film thickness slowly decreases until the thin film (region E of Figure 4.10) develops across the entire test section.

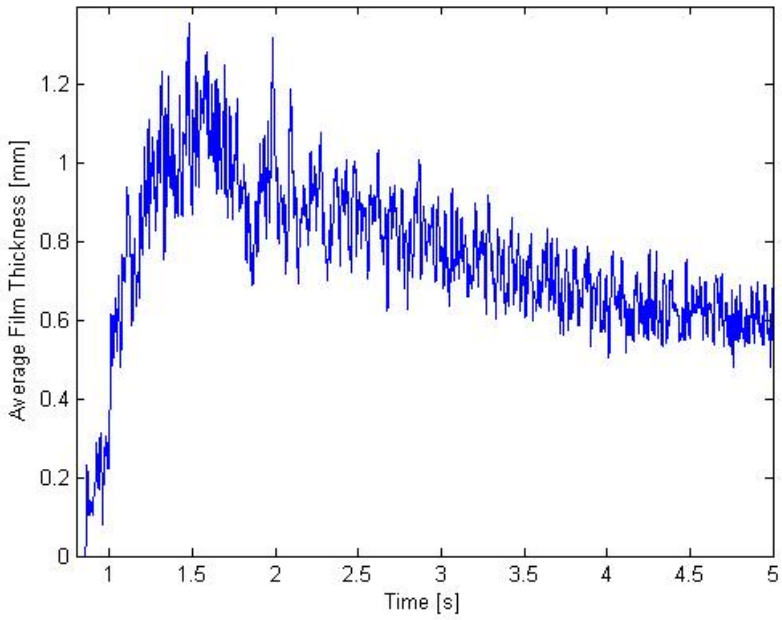

Figure 4.11. Average Film Thickness for a 207 kPa Pressure Difference, 300 ml Initial Slug Volume, in 10.2 mm Diameter Tube, Air-water High Side Test

In the representative test shown in Figure 4.11, the maximum average film thickness is approximately 1.2 mm while the height of the thin film is 0.6 mm. The maximum average film thickness varies from 1.0-1.4 mm for air-water tests and does not depend on tube diameter. The maximum film thickness is seen to slightly increase with slug volume, but the applied pressure does not appear to have any effect on the maximum film thickness. The thin annular film thickness is constant around 0.6 mm for air-water tests in the 10.2 mm diameter tube, but drops to a constant value of 0.3 mm in the 13.4 mm diameter tube. The maximum averaged thickness for the R134a tests is greater than the air-water tests with a maximum thickness varying from 1.3-1.7 mm. The same maximum film thickness trends are observed for the R134a tests for variation in slug volume and pressure. The thin stratified film thickness is found to be constant at approximately 0.7 mm for the R134a tests in the 10.2 mm diameter tube and 1.1 mm in the 13.4 mm diameter tube. The increase in the thin film height with tube diameter is opposite of the air-water tests. This is the result of R134a slug breakdown before the test section in the 13.4 mm diameter tube, leaving all of the slug volume deposited on the bottom of the tube wall. The R134a leaves a thicker film on the wall because it transitions to stratified flow immediately following the slug passage, while an annular flow pattern is observed in air-water tests.

The deposited film can also be approximated by measuring the film thickness present immediately after the slug passes each sensor. The thinning of the average film thickness shown after approximately 1.7 seconds in Figure 4.11 is not relevant to the slug acceleration. This thinning occurs after the slug has passed due to shearing imposed by the vapor core. This is discussed in more detail in Chapter 5.

4.2.3. Slug Motion and Trends

The time that the slug front passes each individual film thickness sensor is determined by noting the time at the beginning of region B in Figure 4.9. These times are plotted against the known locations of the sensors as shown

for the representative test in Figure 4.12. The film thickness sensor at 4.0 m is missing in the figure. The film thickness sensors are very fragile, and some have been broken throughout the testing; all working sensors are shown.

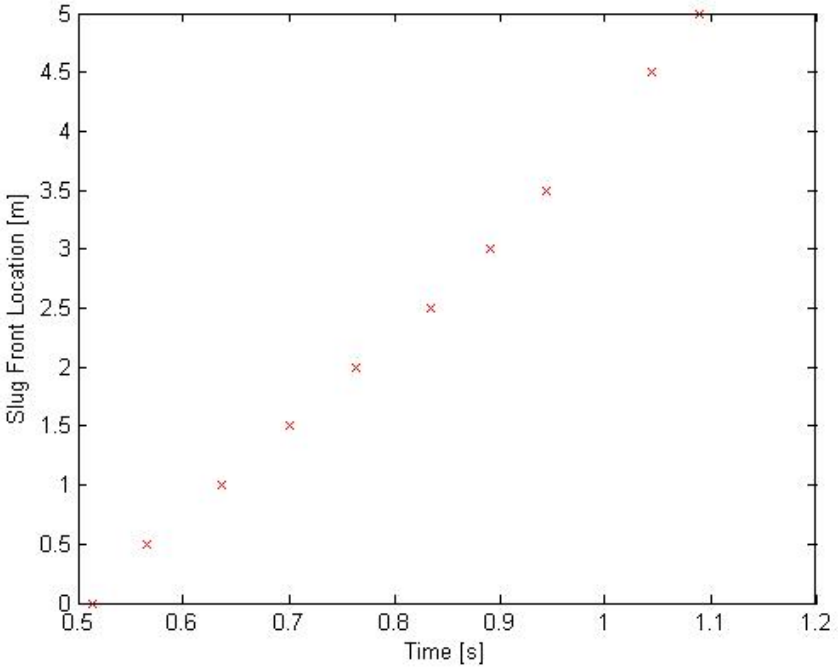

Figure 4.12. Measured Slug Front Location for a 207 kPa Pressure Difference, 300 ml Initial Slug Volume, in 10.2 mm Diameter Tube, Air-water High Side Test

The slug location versus time for the representative test is nearly linear in Figure 4.12 indicating that the acceleration of the slug occurred mostly upstream of the test section. For the test shown in Figure 4.12, the initial position of the slug front is 1.00 m upstream of the first film thickness sensor and the majority of the acceleration occurs within this distance. However, the plot shows a slight upward concavity which is more noticeable as the slug approaches the end of the test section (5.0 m). For the test shown in Figure 4.12, the average velocity of the slug front through the test section is approximately 9.1 m/s. This velocity agrees well with the 10 m/s slug velocity measured in the Flow Visualization section of this chapter. It also confirms that the digital web camera would not be able to capture multiple images of the slug front as it passed.

Figures 4.13 and 4.14 show how changing both the fluid and the applied pressure difference affect the slug location and slug velocity, respectively. The slug acceleration is shown by the slope of the slug velocity profile in time in Figure 4.14. Liquid R134a slugs tend to accelerate more slowly than water slugs under the same conditions. Water has a lower liquid density than R134a under similar test conditions, which may partially explain why R134a has a smaller acceleration. Air-water slugs deposit a much larger proportion of their liquid on the tube wall per unit length because the film is present around the entire diameter of the tube in annular flow. Though R134a slugs leave behind a thicker film than water, it is only marginally thicker (around 0.3 mm). R134a has a significantly lower viscosity than water which may explain why less liquid is sheared from the slug than in the air-water tests. The increase in acceleration is caused by the proportionally larger loss of mass in the water slug. This also explains the larger slope in the velocity versus time curve in Figure 4.14 observed near the end of the test section for air-water, which represents a greater acceleration.

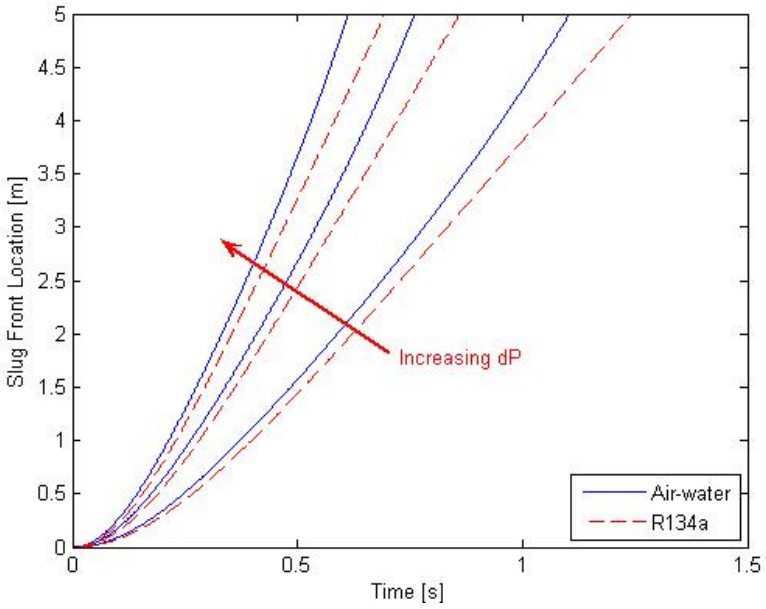

Figure 4.13. General Slug Location Trends Resulting from Increasing Applied Pressure Difference and Changing Fluid for a Given Tube Diameter and Initial Slug Volume

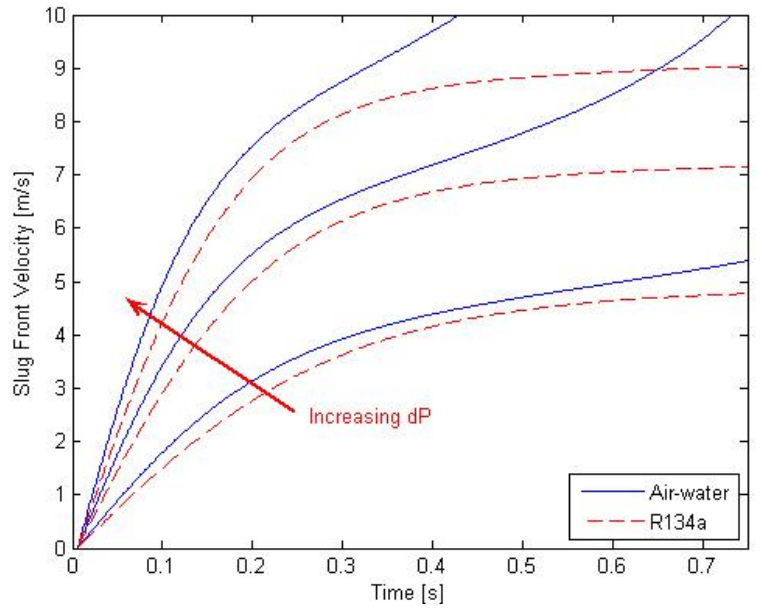

Figure 4.14. General Slug Velocity Trends Resulting from Increasing Applied Pressure Difference and Changing Fluid for a Given Tube Diameter and Initial Slug Volume

The effect of changing the tube diameter, for a given slug volume and pressure difference, on slug location and velocity is shown in Figures 4.15 and 4.16, respectively. The slug acceleration is shown by the slope of the slug velocity profile in time in Figure 4.16. For a given pressure difference and slug volume, the slug experiences a larger acceleration in larger tubes because the pressure is applied over a larger area for a given slug volume. The viscous drag will also decrease with increasing tube diameter for a given slug velocity and volume because the Reynolds number will increase resulting in a lower friction factor. Also for a fixed slug volume if the diameter is increased the slug length will decrease resulting in a lower viscous pressure drop.

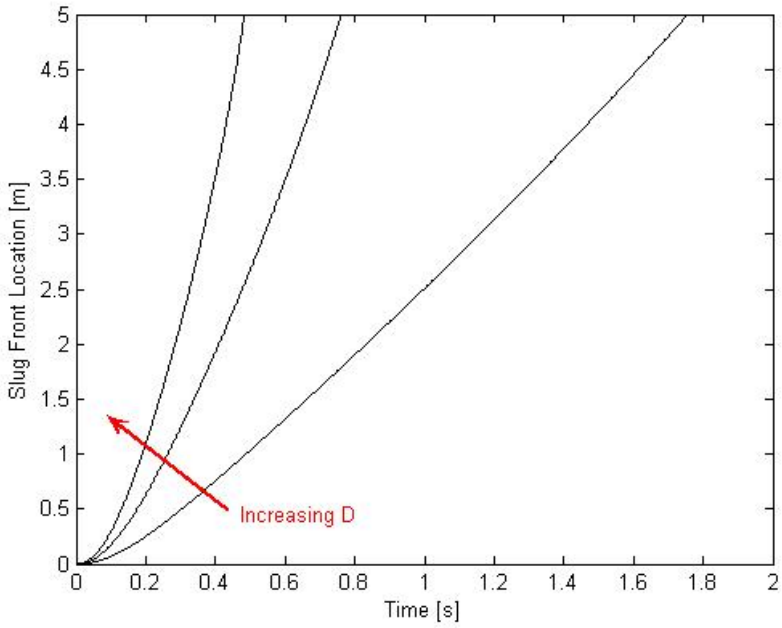

Figure 4.15. General Slug Location Trends Resulting from Increasing Tube Diameter for a Given Applied Pressure Difference and Initial Slug Volume

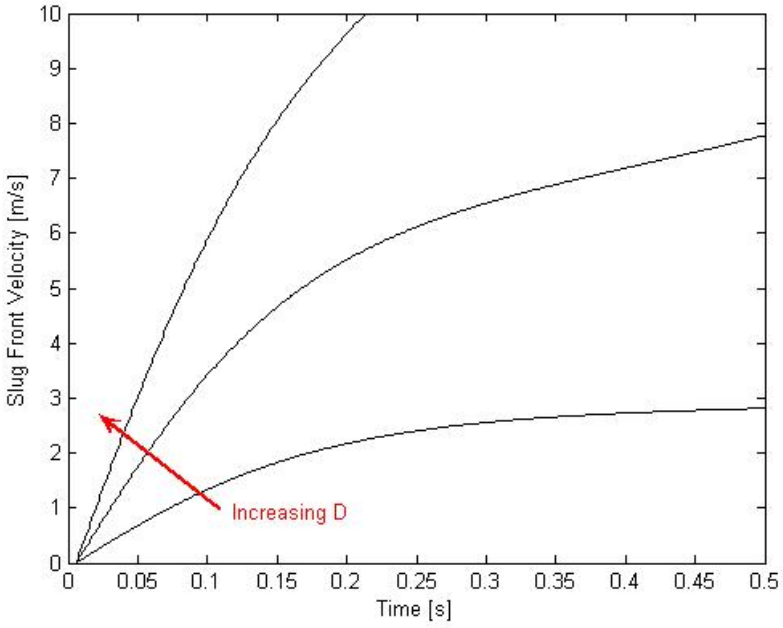

Figure 4.16. General Slug Velocity Trends Resulting from Increasing Tube Diameter for a Given Applied Pressure Difference and Initial Slug Volume

Slugs of larger volume have more mass and should accelerate more slowly for a given tube diameter and pressure difference; in addition, their velocity should be smaller because the shear forces increase as the slug length increases. Figures 4.17 and 4.18 show how decreasing the initial slug volume affects the slug position and velocity, respectively, for a given tube diameter and applied pressure difference. The slug acceleration is shown by the slope of the slug velocity profile in time in Figure 4.18. The assertion that larger slugs accelerate more slowly for a given tube diameter and applied pressure difference is confirmed in Figure 4.18. Another characteristic of the tests is the

larger acceleration near the end of the test section as the slug volume decreases. The film thickness sensors show that a fairly uniform film thickness is deposited on the wall only a minor decrease in film thickness can be observed with increasing mass flux and tube diameter. This implies a relatively constant amount of mass is deposited on the tube per unit length. Since the mass left on the tube wall is volumetrically proportionally larger in tests with small initial slug volumes, the accelerational effects are more pronounced with small slug volumes.

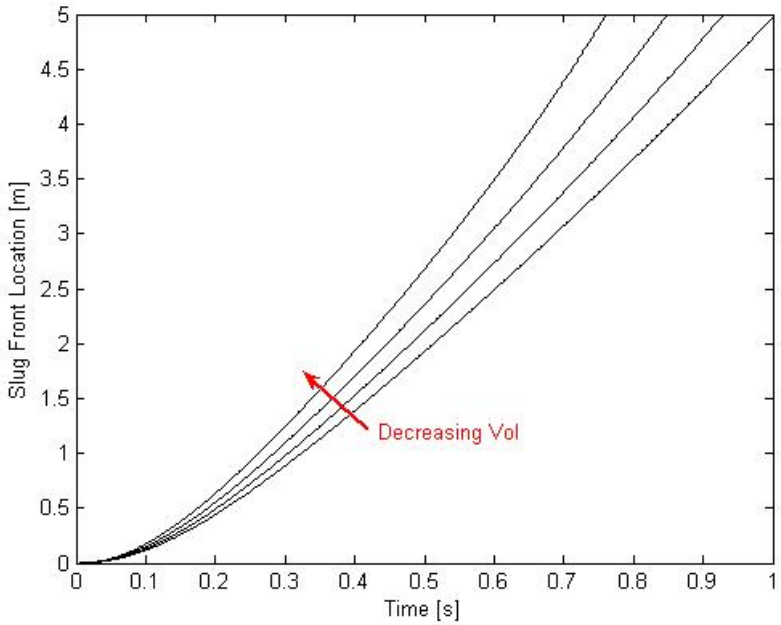

Figure 4.17. General Slug Location Trends Resulting from Decreasing Initial Slug Volume for a Given Tube Diameter and Applied Pressure Difference

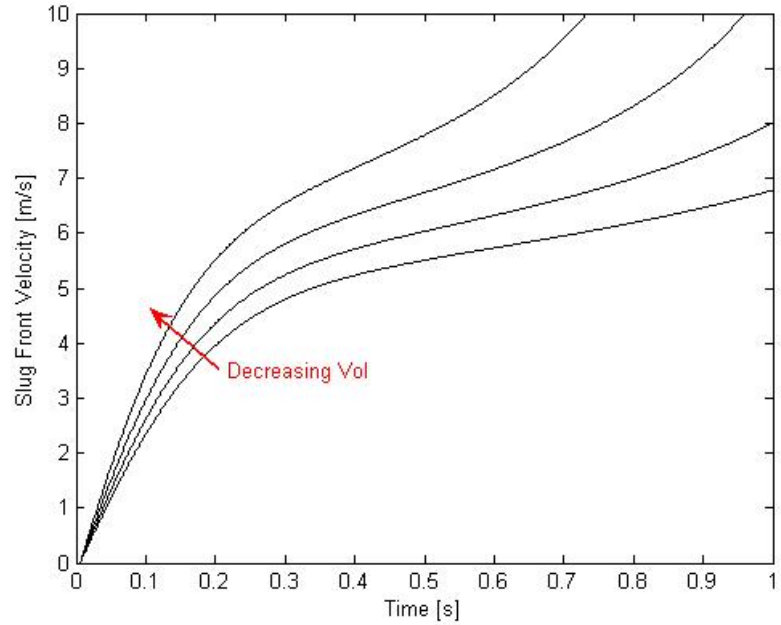

Figure 4.18. General Slug Velocity Trends Resulting from Decreasing Initial Slug Volume for a Given Tube Diameter and Applied Pressure Difference

Chapter 5. Modeling and Analysis

The current chapter describes assumptions and equations used to predict the acceleration and breakdown of the slug. The accuracy of the models is determined by comparing the models to the data obtained in Chapter 4.

5.1. Assumptions and Approach

Separate mass and momentum conservation equations are used for each fluid, which is consistent with most of the literature. The modeling approach, however, is distinctly different than the works cited in Chapter 2.

5.1.1. Assumptions

The assumptions presented herein are consistent with the observed physical processes in Chapter 4 and previous analysis methods discussed in Chapter 2. The flow is assumed to be adiabatic. Gravitational effects in the axial direction are ignored since the tube is oriented horizontally. A quasi-equilibrium liquid momentum equation is proposed similar to that of Taitel & Barnea (1997) but with an accelerational term.

Constant liquid density and viscosity are assumed during each test and are an average of the liquid properties at the high and low side tank conditions. The densities of both fluids vary less than 5% over the entire tested pressure range. The viscosity of water changes less than 1% but the viscosity of R134a can change up to 30%.

The model assumes that viscous pressure drop is only significant in the liquid slug region, regions B and C of Figure 4.5. The pressure drop of the vapor in front of the slug, slug front interface (region A of Figure 4.5), slug tail (region D of Figure 4.5), and the annular or stratified region following the slug (region E of Figure 4.5) are found to be negligible, as seen by previous literature and experimentation in the current work. Sakaguchi et al. (1987) found that the pressure difference is only significant in the liquid slug region through transient slug flow experiments using air-water in 30-40 mm diameter tubes. Figure 4.8 shows the high and low side pressures for a low-side experiment in which the slug breaks down immediately when the low side valve is opened. The high and low pressure transducers show the same pressure when the slug breaks down, indicating that the pressure drop across the film region is not significant. De Henau & Raithby (1995a) also note in their theoretical study that the pressure drop across the slug front is negligible unless the front is very long. They define the slug front as interface C-D of the slug unit shown in Figure 2.1 in agreement with the present study. Pressure drops due to diameter change and bends are less than 1 kpa for air-water tests and 6 kpa for R134a tests and are, therefore, neglected.

The model neglects liquid entrainment in the vapor or vapor penetration into the slug, although they are observed in flow visualization from Chapter 4. Evaporation and condensation at the slug front and tail are also neglected. A slug unit is assumed, like De Henau & Raithby (1995a) in Figure 2.1, without bubbles. The liquid slug is assumed to be impenetrable until it reaches a specified length at which breakdown occurs.

5.1.2. Approach

The current study considers the acceleration of a slug from a stationary state, unlike any of the literature investigated. In the present analysis, the sole contribution of the vapor phase is the application of a known pressure difference across the slug. Mass and momentum conservation equations are applied to the liquid slug. A simple force balance is obtained after modification of Equation 2.6 to include an accelerational term as given in Equation 5.1.

$$A_S\left(dP_A - dP_{vis}\right) = \rho_L V_S a \tag{5.1}$$

Equation 5.1 states that the pressure force applied on the slug by the vapor minus the viscous drag force is equal to the mass of the slug multiplied by the acceleration of the slug. The slug volume in Equation 5.1 varies with the location of the slug. Assuming constant density, the conservation of mass statement simplifies to a conservation of liquid volume expression.

$$V_{Tot} = V_S + V_F \tag{5.2}$$

The sum of the slug volume and the deposited film volume at any instant must equal the total initial slug volume. The model developed by Equations 5.1 and 5.2 is valid until the slug reaches the end of the test section. When the slug front passes the end of the test section, part of the liquid is located outside of the control volume and Equation 5.2 is no longer valid.

The slug velocity and position at the current time step is calculated from previous values of acceleration, velocity, and position. The force balance in Equation 5.1 is then used to determine the acceleration of the slug at the current time. The applied pressure difference at the current time is obtained directly from experimental measurement or is approximated as described in section 5.4. The viscous pressure drop is predicted using Equation 5.10. The volume of the slug changes due to film deposition on the tube walls which is either measured directly from experimentation or approximated as described in section 5.4. The slug velocity and location at the next time step can then be predicted since the acceleration, velocity, and position at the current time step are known. The process repeats as time is stepped forward in 0.001 s increments.

5.2. Proposed Models

Four models are developed to describe the slug acceleration. Simple rigid body motion and viscous pipe flow principles are applied and the mass loss due to film deposition is considered.

5.2.1. Rigid Body Model

The first model considers only rigid body motion of the slug; it neglects liquid viscosity and loss of slug mass due to film deposition. Figure 5.1a shows a schematic of the applied pressures and slug geometry used in the rigid body model. Equation 5.3 predicts the slug acceleration assuming that pressure difference driving the slug is acting over the entire tube cross sectional area.

$$a = \frac{dPA_{xs}}{\rho_L V_{Tot}} \tag{5.3}$$

The model of the slug acceleration in Equation 5.3 can be compared to experimental data from Chapter 4 by using experimental values for each of the terms in Equation 5.3. In this case, the cross sectional area and initial slug volume are controlled experimental variables. When comparing the model to experimental results, the applied pressure difference variation in time is determined experimentally by the difference between the upstream and downstream pressure transducers. This is the simplest model and serves as a baseline with which to compare viscous and trailing film effects. Equation 5.3 provides a framework for the derivation of the other models; the terms of the equation are modified to account for viscous effects and the trailing film.

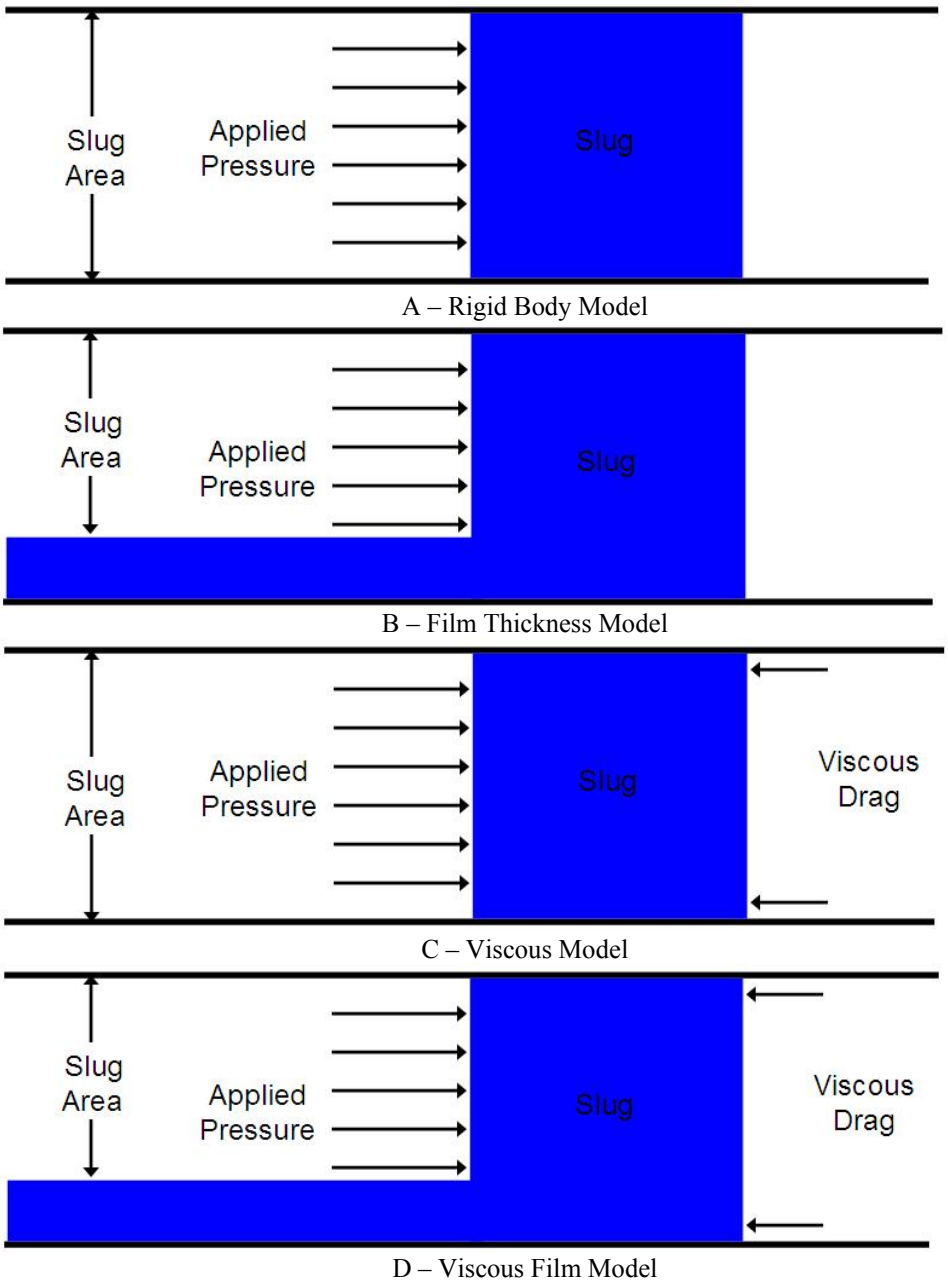

Figure 5.1. Schematic of Slug Geometry and Applied Pressures Used for Calculation of Slug Acceleration for Rigid Body (A), Film Thickness (B), Viscous (C), and Viscous Film (D) Models

5.2.2. Film Thickness Model

The film thickness model considers the liquid mass deposited on the wall but does not consider viscous pressure drop. Figure 5.1b shows a schematic of the applied pressures and slug geometry used in the film thickness model. The slug acceleration is defined according to Equation 5.4.

$$a = \frac{dPA_S}{\rho_L V_S} \tag{5.4}$$

The slug area to which the pressure difference is applied and slug volume are reduced by the presence of a liquid film. Experimental results from Chapter 4 show that annular flow exists in the air-water tests and stratified flow exists in the two-phase R134a tests in the slug tail region (regions D and E in Figure 4.5) as shown in Figure 4.4D and 4.4E. The slug area and volume for annular flow are calculated according to Equations 5.5 and 5.6, respectively. The average film thickness across the entire tube length at an instant, $h_{F,ave}$, is presented in Equation 4.1 and is used in Equation 5.5. Figure 5.2 shows a diagram of the slug area for stratified and annular flows.

$$A_{S,An} = \frac{\pi}{4}\left(D - 2h_{F,ave}\right)^2 \tag{5.5}$$

$$V_S = V_{Tot} - V_F$$

$$V_F = \left(\frac{\pi}{4}D^2 - A_S\right)L_{TS} \tag{5.6}$$

In stratified flow, the liquid collects in the bottom of the tube as shown in Figure 5.2. The slug area and volume are different than in the annular flow case. The slug area is calculated according to Equation 5.7; the slug volume can again be calculated by Equation 5.6.

$$A_{S,St} = \frac{D^2}{4}\left\{\pi - \left[\cos^{-1}\left(1 - \frac{2h_{F,ave}}{D}\right) - \left(1 - \frac{2h_{F,ave}}{D}\right)\sin\left(\cos^{-1}\left(1 - \frac{2h_{F,ave}}{D}\right)\right)\right]\right\} \tag{5.7}$$

The film thickness model can be used to predict the slug location, velocity, and acceleration for the experiments described in Chapter 4. Applied pressure difference and average film thickness time traces are measured experimentally and can be used in Equations 5.4-5.7.

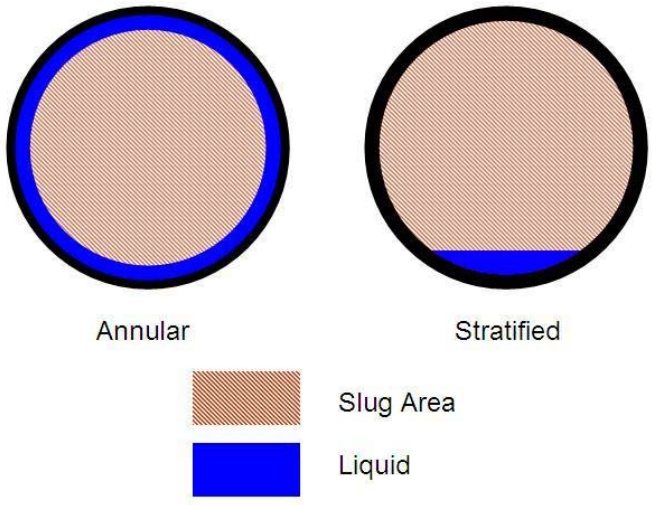

Figure 5.2. Diagram of Slug Area Geometry Used for Air-Water (Annular) and R134a (Stratified) Tests

5.2.3. Viscous Model

The viscous model accounts for the viscous pressure drop across the liquid slug but neglects the presence of a deposited film. Figure 5.1c shows a schematic of the applied pressures and slug geometry used in the viscous model. The slug acceleration is calculated according to Equation 5.8.

$$a = \frac{dP_A A_{XC}}{\rho_L V_{Tot}} \tag{5.8}$$

The only difference between Equations 5.8 and 5.3 is the pressure difference term. When considering viscosity, the applied pressure difference is reduced according to Equation 5.9.

$$dP_A = dP - dP_{vis} \tag{5.9}$$

The equation for viscous pressure drop in fully developed pipe flow is shown in Equation 5.10.

$$dP_{vis} = f \frac{L_S}{D} \frac{\rho_L v^2}{2} \tag{5.10}$$

The slug length is equal to the volume of the slug divided by the cross sectional area of the tube. The friction factor is determined by the Colebrook (1939) equation if the flow is turbulent ($Re_D \geq 2300$), as shown in Equation 5.11, and is given by Equation 5.12 if the flow is laminar ($Re_D < 2300$).

$$1/\sqrt{f} = -2.0 \log\left(\frac{2.51}{\mathrm{Re}_D \sqrt{f}} \right) \tag{5.11}$$

$$f = \frac{64}{Re_D} \tag{5.12}$$

Laminar flow is never observed for tests in the current study; Equation 5.12 was implemented in the model to conform to standard pipe flow friction factor calculation methods. The Reynold's Number, given in Equation 5.13, is used because only the viscous pressure drop across the liquid slug is considered.

$$Re_D = \frac{\rho_L v D}{\mu_L} \tag{5.13}$$

Pressure drop associated with the two-phase interactions is assumed to be negligible. Use of the Colebrook formula presents an obstacle in generating an analytical solution because of its implicit solution for *f*.

5.2.4. Viscous-Film Model

The viscous-film model considers the pressure drop due to viscosity and the film deposition on the tube wall. Figure 5.1d shows a schematic of the applied pressures and slug geometry used in the viscous-film model. Equation 5.14 describes the acceleration of the slug for the viscous-film model.

$$a = \frac{dP_A A_S}{\rho_L V_S} \tag{5.14}$$

Equations 5.5-5.7 and 5.9-5.13 are used in conjunction with Equation 5.14 to calculate slug acceleration with the viscous-film model. This model is the most detailed of the models developed and uses the least number of assumptions.

5.3. Performance of Models

The four models developed in the previous section are compared to experimental data. Their performance is compared and a model is selected for further refinement.

5.3.1. Model Comparison

Plots of the experimentally observed slug front location and model predictions are presented for all high side and low side tests in Appendix A and B, respectively. The film thickness and viscous-film models are not plotted for tests using the 6.35 mm diameter tube because the film thickness is not measured as discussed in Chapter 3.

Figure 5.3 shows the experimentally measured slug location and the slug location predicted by the models for the representative test used throughout Chapter 4 (207 kPa applied pressure difference, 300 ml initial slug volume, 10.2 mm diameter, air-water, under high side conditions). The viscous-film model fits the data best. The viscous-film model and the viscous model do not deviate significantly until approximately 1.5 m. The mass loss due to a deposited film is proportionally small compared to the total slug mass until the slug has traveled 1.5 m. The slope of the viscous-film model matches that of the measured location more accurately near the end of the test section. The calculated slug velocity and acceleration for the representative test are shown in Figures 5.4 and 5.5, respectively. The film thickness and rigid body models over predict the velocity and acceleration of the slug significantly. The net effect of considering film deposition is an increase in the slug acceleration. This is because the film thickness decreases the slug volume more than the slug area.

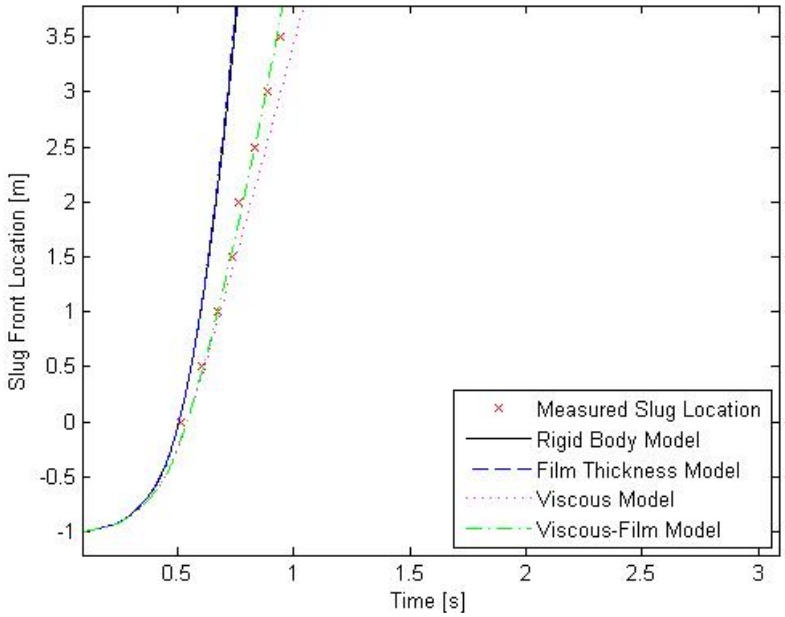

Figure 5.3. Slug Location vs. Time for a 207 kPa Pressure Difference, 300 ml Initial Slug Volume, in 10.2 mm Diameter Tube, Air-water High Side Test Using Rigid Body, Film Thickness, Viscous, and Viscous-Film Models

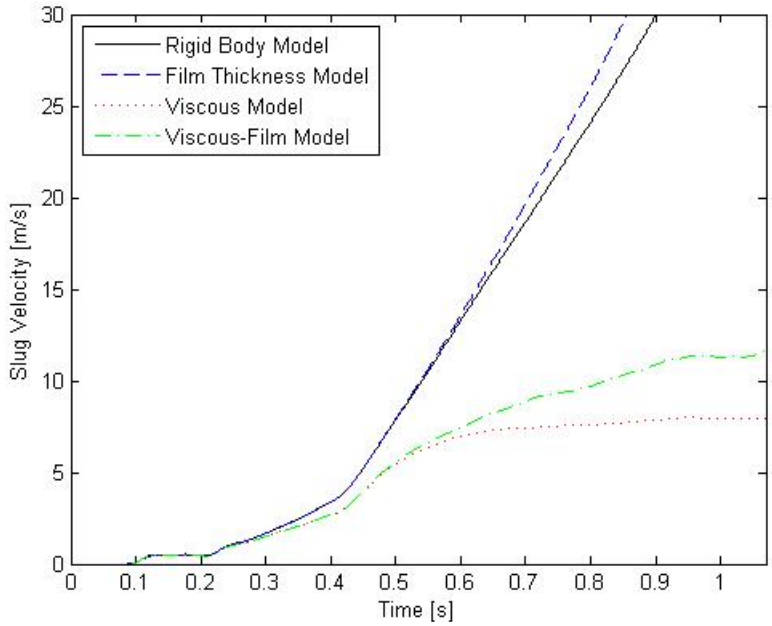

Figure 5.4. Slug Velocity vs. Time for a 207 kPa Pressure Difference, 300 ml Initial Slug Volume, in 10.2 mm Diameter Tube, Air-water High Side Test Using Rigid Body, Film Thickness, Viscous, and Viscous-Film Models

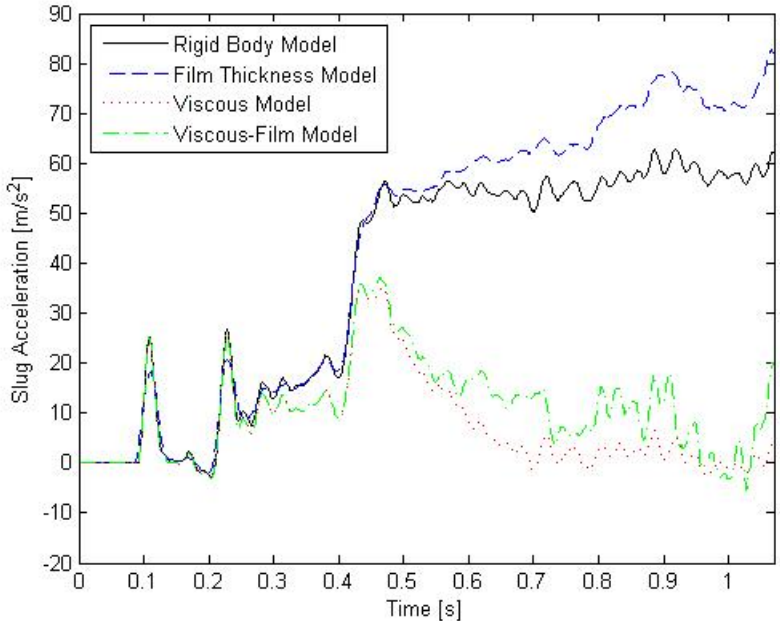

Figure 5.5. Slug Acceleration vs. Time for a 207 kPa Pressure Difference, 300 ml Initial Slug Volume, in 10.2 mm Diameter Tube, Air-water High Side Test Using Rigid Body, Film Thickness, Viscous, and Viscous-Film Models

The viscous and viscous-film models deviate significantly under certain conditions. Figures A.17-A.20 show a series of high side air-water tests with a 138 kpa applied pressure difference in a 10.2 mm diameter tube with varying initial slug volume. The difference between the viscous and viscous-film models is greater in experiments with a lower initial slug volume. The viscous-film model provides the best general fit to the data in Appendix A. It

is clear that the rigid body and viscosity models do not accurately represent the slug location in the 6.35 mm diameter tube. The film thickness and viscous-film models can not be applied to tests in the 6.35 mm diameter tube (A.1-12, A.45-48, B.1-4) because the film thickness is not be measured in the 6.35 mm diameter tube, as described in Chapter 3. Results in the 6.35 mm diameter tube are expected to compare better with the viscous-film model; the viscous model under predicts the slug location, the rigid body model over predicts the slug location, and the viscous-film model predicts slug location between the viscous and rigid body models.

5.3.2. Validation of Viscous-Film Model

Chapter 4 indicates that most of the slug acceleration occurs prior to the beginning of the test section. The viscous-film model shows a large acceleration before the test section (prior to 0.0 m) that decreases significantly once the slug reaches the test section in most of the tests (A.13-A.44, A.49-A.68). The slug reaches a quasi-terminal velocity, where the viscous pressure drop counteracts the applied pressure difference. The small acceleration of the slug is a result of the mass loss due to film deposition.

It is noted in Chapter 4 that a decrease in applied pressure, a decrease in tube diameter, and an increase in slug volume result in smaller velocities and accelerations at a given location. The slug velocity at a given location and acceleration are also smaller for R134a than air-water. All of these trends are captured by the viscous-film model for the experiments in Appendix A.

5.3.3. Viscous-Film Model Limitations

The viscous-film model is derived from equations that assume slug flow. Once slug breakdown occurs, the assumptions used in deriving the model are no longer accurate. This explains the deviation between the slug location predicted by the model and the observed location in tests with slug volumes less than 100 ml for both air-water and two-phase R134a in 13.4 mm diameter tubes (Figures A.29, A.64-68). Flow visualization video from Chapter 4 shows that slugs break down prior to reaching the end of the 5.0 m test section for air-water slugs less than 200 ml and R134a slugs less than 85 ml in the 13.4 mm diameter tube. This confirms that slug breakdown occurs in the tests shown in Figures A.29 and A.64-68, verifying that slug breakdown is likely the cause of the inaccuracy of the model.

Figures A.29, A.33, A.37, and A.41 show the experimental and predicted slug position versus time for a series of high side air-water tests with an increasing applied pressure difference (69, 138, 207, 276 kPa, respectively) in a 13.4 mm diameter tube with an initial slug volume of 100 ml. Although the slug breaks down within the test section in these tests as indicated by results from table 4.1 for air-water slugs, the model accurately predicts the slug position for all of the tests except for the 69 kPa applied pressure differences. There is significant deviation between the model and the observed slug position in Figure A.29, a test with a lower applied pressure difference (69 kPa) with the same initial volume, tube diameter, and fluid. The flow may behave like a slug even after breakdown with the large applied pressure difference because the dense two-phase mixture resulting from slug breakdown may still act as a barrier between the high and low pressure. The liquid is forced to the bottom of the tube more easily when the applied pressure difference is lower because gravity forces become more significant when compared to the inertial forces. This may explain why the model fits the data well for Figures A.33, A.37, and A.41 even when slug breakdown is observed in Chapter 4.

Figure 5.6 plots the estimated time that the slug front passes each film thickness sensor predicted by the viscous-film model against the experimentally observed time at which the slug passes each sensor for all

experiments. Data points after slug breakdown occurs are not included since the assumptions used in the model no longer apply. Figure 5.6 shows good agreement between the observed time and the predicted time of slug passage by the viscous-film model with a 1.7% mean absolute deviation. Most of the data points in Figure 5.6 are within the ±0.02 s error in the experimentally observed slug passage time. The data points that are out of the error bounds are mostly recorded at 0.0 m, where wall discontinuities or changes in the tube diameter between the liquid trap and test section cause local flow disturbances. Section 4.1.2 provides more detail about local flow disturbances near the test section entrance.

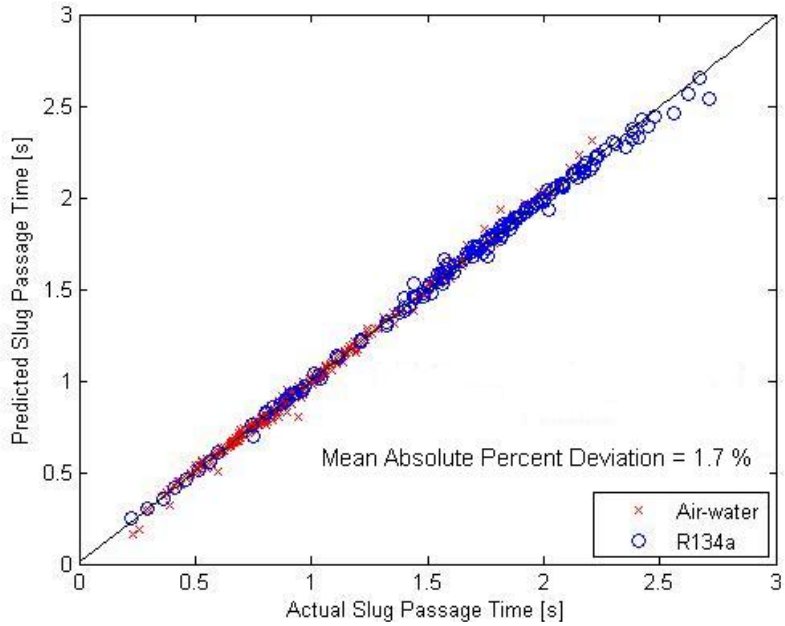

Figure 5.6. Time of Slug Passage Predicted by Viscous-Film Model vs. Time of Observed Slug Passage for All Tests in 10.2 and 13.4 mm Diameter Tubes

5.4. Viscous-Film Model Simplification

The viscous-film model is further simplified in an attempt to generate an analytical model. Additional assumptions are made and justified for the applied pressure difference and film thickness profile. The relationship between slug volume and slug breakdown distance is presented and a model for slug breakdown location is created.

5.4.1. Applied Pressure and Film Thickness Approximation

The viscous-film model requires experimental measurement of pressure difference and average film thickness in time to calculate the slug position. Figure 4.7 shows the applied pressure difference for the representative test from Chapter 4 (207 kPa applied pressure difference, 300 ml initial slug volume, 10.2 mm diameter, air-water, under high side conditions). The pressure difference is approximately a step increase while the slug is between the pressure transducers. Therefore a step increase in the pressure difference is assumed in the simplified model. The magnitude of the step is the average of the experimental pressure difference across the slug while the slug is between the upstream and downstream pressure transducers.

The slug area and volume of the film can be approximated using film thickness measurements recorded immediately after the slug passes each sensor. Although the film thickness decreases over time at a given location

as shown in the average film thickness profile in Figure 4.11, the thinning behavior is not relevant to the volume loss of the slug.

Figure 5.7 shows the maximum film thickness, which occurs immediately after the slug passes, recorded for each sensor, plotted against the sensor location. The figure agrees with observations in Chapter 4 that R134a deposits a thicker film than air-water. The maximum film thickness is seen to slightly decrease further down the test section for both fluids. The velocity of the slug increases further down the tube, as shown in the slug location vs. time plot for the representative test in Figure 5.4, which shears a thinner liquid layer. Chapter 3 states an uncertainty in the film thickness measurements of ±0.5 mm. Only 20 of the 272 air-water and 157 R134a data points shown in Figure 5.7 lie outside of the measurement error of the average maximum film thickness shown for each fluid. The R134a maximum film thicknesses under 1 mm at the 3.5 and 4.5 m locations in Figure 5.7 are observed for tests where slug breakdown is predicted upstream of the sensors according to observations in Chapter 4.

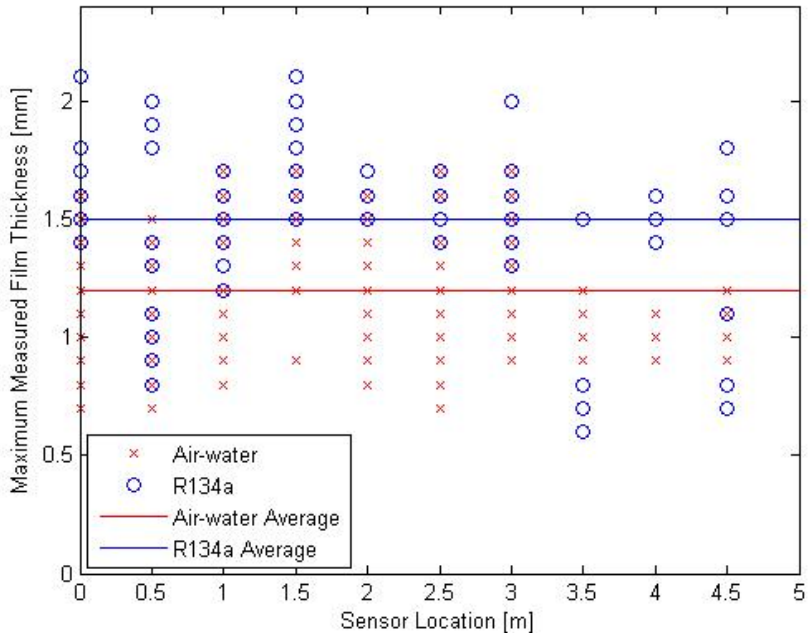

Figure 5.7. Maximum Measured Film Thickness at Each Sensor for Air-Water and R134a Tests in 10.2 and 13.4 mm Diameter Tubes

Lower maximum film thicknesses are observed for test with larger applied pressure differences. An example of this trend is shown in Figure 5.8 for a series of air-water tests in a 10.2 mm diameter tube with a constant initial slug volume of 100 ml. For tests with larger applied pressures the maximum film thickness at each location is lower due to the increased imparted on the liquid film. The maximum film thickness increases slightly for tests with larger initial slug volumes because these tests have lower velocity slugs.

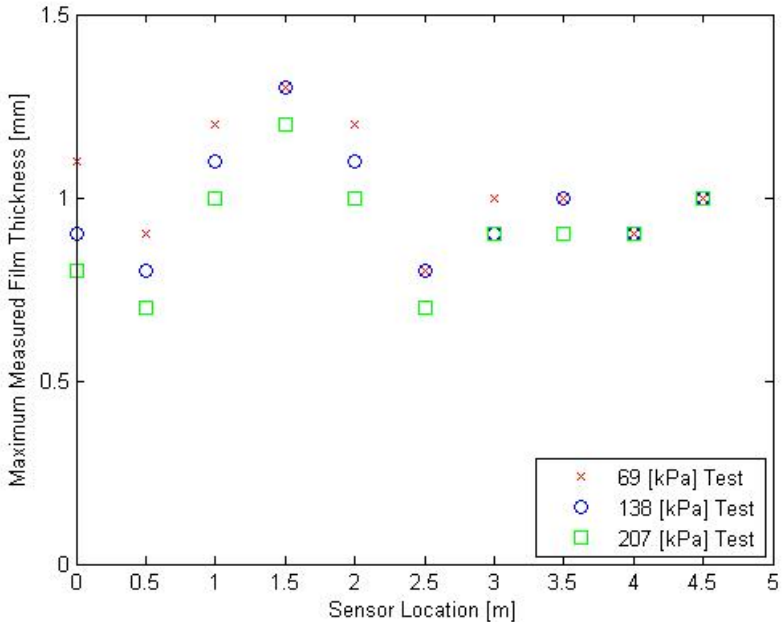

Figure 5.8. Maximum Film Thickness vs. Sensor Location for a Series of Air-Water Tests with Varying Applied Pressure Difference in a 10.2 mm Diameter Tube Using 100 ml Initial Slug Volume

Though there are noticeable trends in the maximum film thickness with the slug location, applied pressure difference, initial slug volume, and tube diameter; their variation is small compared to the measurement uncertainty. Therefore, the average film thickness is assumed to be constant for a given fluid according to Equation 5.15.

$$h_{F,ave} = h_{F,max} \tag{5.15}$$

$h_{F,max}$ is equal to the average maximum film thickness shown in Figure 5.7 for each fluid: 1.2 mm for air-water and 1.5 mm for R134a. The slug volume in Equation 5.6 is generalized to accommodate tube lengths other than the test section length used in the present study using Equation 5.16.

$$\begin{aligned} V_S &= V_{Tot} - V_F \\ V_F &= \left(\frac{\pi}{4} D^2 - A_S \right) x \end{aligned} \tag{5.16}$$

5.4.2. Dimensionless Film Thickness

Hurlburt and Newell (1997) define a nondimensional film thickness that utilizes relevant flow physics in steady two-phase flow to predict viscous pressure drop and heat transfer. This nondimensional film thickness is shown in Equation 5.17.

$$h^+ = \frac{h_F v^*}{\upsilon_L} \tag{5.17}$$

The height of the viscous sublayer corresponds to an h^+ is found by Hurlburt and Newell (1997) to be less than 5. The nondimensional film thickness is calculated in the current study using the relation shown in Equation 5.18 for v^*, where the interfacial shear force is balanced by the applied pressure.

$$v^* = \sqrt{\frac{\tau_i}{\rho_L}} \tag{5.18}$$

A slug Reynolds Number is also defined according to Equation 5.19 in order to compare the nondimensional film thickness.

$$Re_S = \frac{vL_S}{\upsilon_L} \tag{5.19}$$

Figure 5.9 shows the nondimensional film thickness variation with slug Reynolds Number for all tests using air-water and R134a in 10.2 and 13.4 mm diameter tubes. The experimentally determined nondimensional film thickness for both fluids varies from 152-1600 for air-water and 648-6640 for R134a, much higher than the viscous sublayer limit (5). The cause of this behavior is not known; there is some mechanism responsible for the increased thickness of the deposited film. Though there is no tube diameter dependence, R134a has a larger dimensionless film thickness than air-water. The dimensionless film thickness varies from 152-1600 for air-water and 648-6640 for R134a. There are no significant trends identified relating the slug Reynolds Number to the dimensionless film thickness.

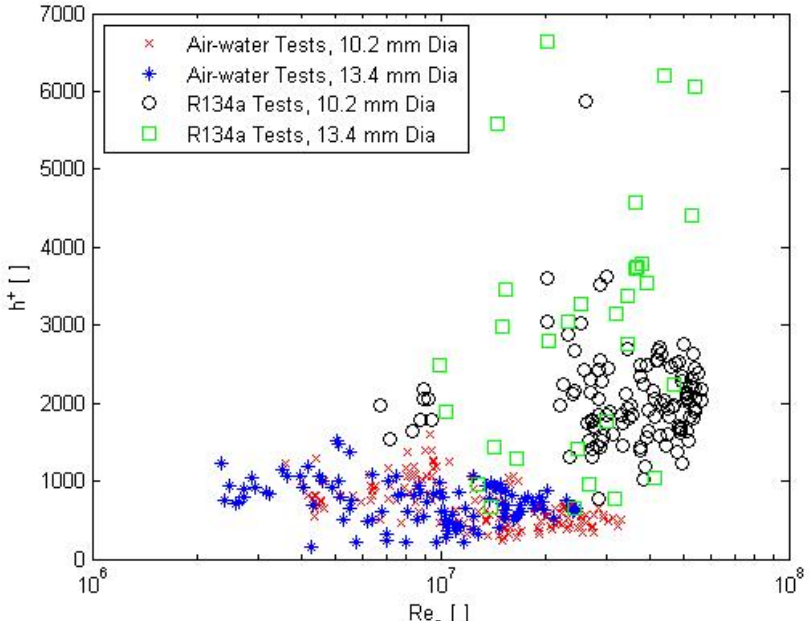

Figure 5.9. Dimensionless Slug Tail Film Thickness vs. Slug Reynolds Number for different Tube Diameters and Refrigerants

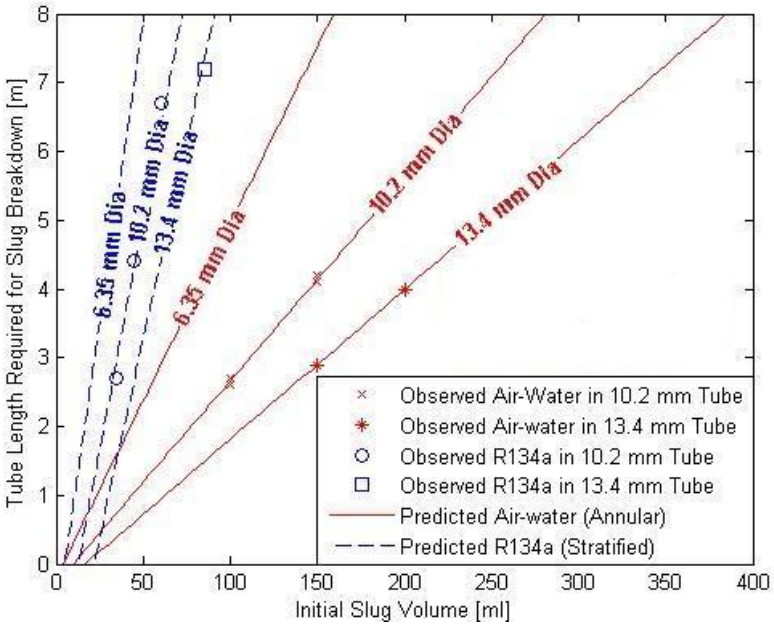

Figure 5.10. Tube Length Required for Slug Breakdown as a Function of Initial Slug Volume, Tube Diameter, and Fluid Compared to Observed Slug Breakdown Location

5.4.3. Slug Breakdown Model

The observations made in the previous section provide information necessary to predict slug breakdown. The assumption of a constant film thickness per unit length can be used to estimate the volume of the film, and therefore the remaining volume of the slug at the breakdown location. The volume and length of air-water slugs at breakdown are shown in table 5.1, assuming an annular flow regime following the slug.

Table 5.1. Slug Breakdown Calculations – Air-water

Applied Pressure [kPa]	Tube Diameter [mm]	Initial Volume [ml]	Breakdown Distance [m]	Breakdown Volume [ml]	Breakdown Length [mm]
69	10.2	100	2.7	9.0	111
138	10.2	100	2.7	10.1	123
207	10.2	100	2.6	11.1	136
276	10.2	100	2.7	8.4	103
69	10.2	150	4.2	8.9	108
138	10.2	150	4.2	8.5	104
207	10.2	150	4.1	9.5	117
207	13.4	150	2.9	17.1	121
207	13.4	200	4.0	17.9	127

The slug volume at breakdown is approximately constant for tests with the same tube diameter regardless of initial volume, but is significantly different between the 10.2 and 13.4 mm tubes. The length of the slug at breakdown varies less than 30 mm. The results in table 5.1 suggest that air-water slugs breakdown consistently when the liquid slug is approximately 117 mm in length, the average breakdown length shown in the table.

The constant slug breakdown length and uniform deposited film thickness observations imply that the slug breakdown length is only a function of the initial slug volume, tube diameter, and fluid. These independent variables are all constant for a given test, so the tube length required for slug breakdown can be solved analytically. The tube length required for slug breakdown for air-water can be determined using Equation 5.20.

$$x_{B,An} = \frac{\frac{4V_{Tot}}{\pi D^2} - L_B}{\left[1 - \left(1 - \frac{h_{F,\max}}{500D}\right)^2\right]} \tag{5.20}$$

The breakdown length is 0.117 m for air-water and the value of $h_{F,max}$ is 1.2 mm.

Similar observations regarding the slug breakdown length can be made for R134a. Table 5.2 contains the slug volume and the predicted slug length at breakdown using the constant applied film thickness observation from Equation 5.15 and assuming stratified flow following the slug.

Table 5.2. Slug Breakdown Calculations – R134a

Applied Pressure [kPa]	Tube Diameter [mm]	Initial Volume [ml]	Breakdown Distance [m]	Breakdown Volume [ml]	Breakdown Length [mm]
197	10.2	35	2.7	14.8	182
197	10.2	45	4.4	12.1	149
197	10.2	60	6.7	10.0	122
197	13.4	85	7.2	22.7	161

The slug breakdown volume is similar for tests of the same tube diameter. The length of the slug at breakdown varies 60 mm, which corresponds to a volume difference of less than 5 ml. Though the slug breakdown length is smaller for R134a tests with larger initial slug volumes, additional tests must be conducted in the future to determine whether this trend is significant. Consequently, the slug breakdown length is assumed constant and modeled by an average slug breakdown length to follow the same analysis as air-water. The average slug breakdown length for R134a is 153 mm. The slug breakdown length is greater for R134a than air-water. This can be expected considering R134a slugs have lower velocity, R134a is more dense, and R134a has a lower surface tension as described in Chapter 4. This causes gravity forces to dominate and breakdown slugs more easily.

An analytical solution of tube length required for slug breakdown of R134a is shown in Equation 5.21 as a function of initial volume, tube diameter, and fluid type.

$$x_{B,St} = \frac{\frac{4V_{Tot}}{D^2} - \pi L_B}{\cos^{-1}\left(1 - \frac{h_{F,\max}}{500D}\right) - \left(1 - \frac{h_{F,\max}}{500D}\right)\sin\left(\cos^{-1}\left(1 - \frac{h_{F,\max}}{500D}\right)\right)} \tag{5.21}$$

The slug breakdown length is 0.153 m and the value of $h_{F,max}$ is 1.5 mm.

Figure 5.10 depicts the tube length required for slug breakdown versus initial slug volume for different tube diameters and for both air-water and R134a. Equations 5.20 and 5.21 are used to generate the curves of constant tube diameter shown in Figure 5.10. The observed data points indicated on the plot are the experimentally observed

slug breakdown distances and corresponding initial slug volumes from tables 5.1 and 5.2. The slug breakdown distances from flow visualization observations confirm the validity of Equations 5.20 and 5.21. Figure 5.11 shows the tube length for slug breakdown predicted by Equations 5.20 and 5.21 plotted against the observed slug breakdown location in tables 5.1 and 5.2. The mean absolute percent deviation is 2.3%, showing that the slug breakdown model predicts the tube length required for slug breakdown well.

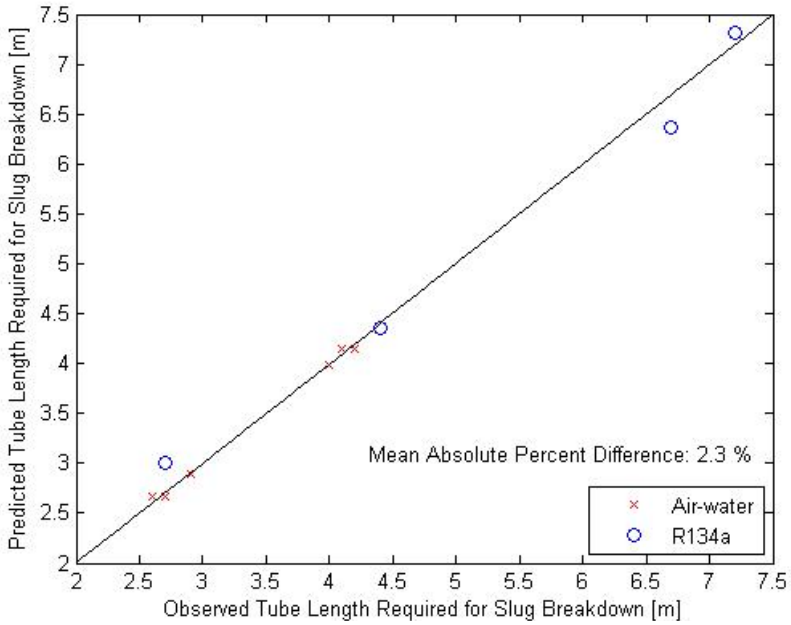

Figure 5.11. Tube Length Required for Slug Breakdown Predicted by Uniform Film Assumption in Simplified Viscous-Film Model vs. Observed Tube Length Required for Slug Breakdown

5.4.4. Analytical Slug Location Solution

An attempt is made to generate an analytical solution for the slug location using the approximation of the applied pressure difference and average film thickness made in the Pressure and Film Models section. The friction factor relationship in Equation 5.11 still presents an obstacle in generating an analytical solution. The friction factor varies from 0.013 and 0.024. The friction factor is approximated as a constant, the average friction factor for each test, as shown in Equation 5.22.

$$f = 0.015 \tag{5.22}$$

A nonlinear second-order homogeneous differential equation results from the solution of Equations 5.5, 5.9, 5.10, 5.13, 5.14, 5.15, 5.16, and 5.22 for air-water slug flow with an annular film region as shown in Equation 5.23. An initial position and velocity of zero specify the initial conditions.

$$(\alpha_{An}x-\beta_{An})\left(\frac{d^2x}{dt^2}\right)+(\gamma_{An}x-\delta_{An})\left(\frac{dx}{dt}\right)^2+\varepsilon_{An}x=0$$

$$\alpha_{An}=\rho_L\left[1-\left(1-\frac{h_{F,\max}}{500D}\right)^2\right],\beta_{An}=\frac{4\rho_L V_{Tot}}{\pi D^2},\gamma_{An}=\alpha_{An}\left(\frac{f}{2D}\right)\left(1-\frac{h_{F,\max}}{500D}\right)^2, \quad (5.23)$$

$$\delta_{An}=\beta_{An}\left(\frac{f}{2D}\right)\left(1-\frac{h_{F,\max}}{500D}\right)^2,\varepsilon_{An}=dP\left(1-\frac{h_{F,\max}}{500D}\right)^2$$

The lowercase Greek letters in Equation 5.23 are all constants that depend on the independent variables. No closed form solution for Equation 5.23 currently exists. The same complications arise when attempting to derive an analytical solution for R134a with a stratified film region using Equations 5.7, 5.9, 5.10, 5.13, 5.14, 5.15, 5.16, and 5.22 as shown in Equation 5.24. The same initial conditions apply.

$$(\alpha_{St}x-\beta_{St})\left(\frac{d^2x}{dt^2}\right)+(\gamma_{St}x-\delta_{St})\left(\frac{dx}{dt}\right)^2+\varepsilon_{St}=0$$

$$\alpha_{St}=\rho_L A,\beta_{St}=\frac{4\rho_L V_{Tot}}{D^2},\gamma_{St}=\alpha_{St}\left(\frac{f}{2D}\right)\left(1-\frac{A}{\pi}\right),\delta_{St}=\beta_{St}\left(\frac{f}{2D}\right)\left(1-\frac{A}{\pi}\right), \quad (5.24)$$

$$\varepsilon_{St}=dP(\pi-A)$$

The variable A introduced in Equation 5.24 is a constant defined by Equation 5.25.

$$A=\cos^{-1}\left(1-\frac{h_{F,\max}}{500D}\right)-\left(1-\frac{h_{F,\max}}{500D}\right)\sin\left(\cos^{-1}\left(1-\frac{h_{F,\max}}{500D}\right)\right) \quad (5.25)$$

Again, a closed form solution for Equation 5.24 is not currently available due to the nonlinear terms. A numerical solution technique is still required to solve for the slug location even after assumptions are made to approximate the applied pressure difference and average film thickness, regardless of flow morphology.

5.5. Simplified Viscous-Film Model Performance

The validity of the applied pressure and film thickness assumptions made in the previous section (excluding section 5.4.4) are tested by comparing slug location prediction of the simplified viscous-film model with the measured location for a variety of experiments. An uncertainty analysis is also presented. The simplified viscous-film model, developed in Matlab, is presented in Appendix C.

5.5.1. Simplified Viscous-Film Model Validation

Figure 5.12 shows the slug location predicted by the simplified viscous-film model compared to the measured location for the representative test (207 kPa applied pressure difference, 300 ml initial slug volume, 10.2 mm diameter, air-water, under high side conditions). The model has an average percent deviation of 1.8% and has a very similar profile to the original viscous-film model in Figure 5.3. The model does not predict slug breakdown within the 5.0 m test section length for the representative test, which agrees with flow visualization images from Chapter 4. The satisfactory model performance indicates that the assumptions of a uniform film deposition and a step profile for the applied pressure difference are reasonable.

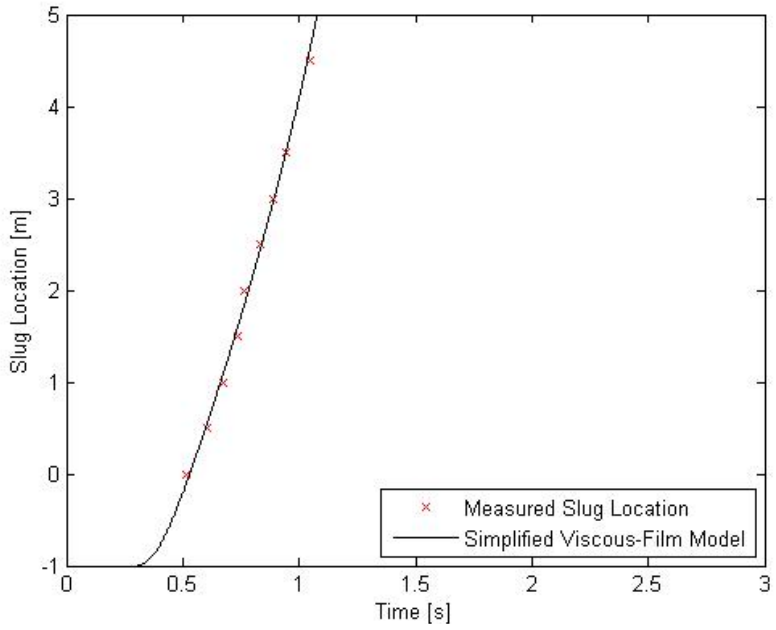

Figure 5.12. Slug Location vs. Time for a 207 kPa Pressure Difference, 300 ml Initial Slug Volume, in 10.2 mm Diameter Tube, Air-water High Side Test Using the Simplified Viscous-Film Model

Figure 5.13 shows the simplified model performance for a high side air-water test in a 13.4 mm diameter tube with a 276 kpa applied pressure difference and 200 ml initial slug volume to have an average percent deviation of 1.4%. Since the model performs well for both 10.2 and 13.4 mm diameter tubes, the constant film thickness coefficient assumption is reasonable.

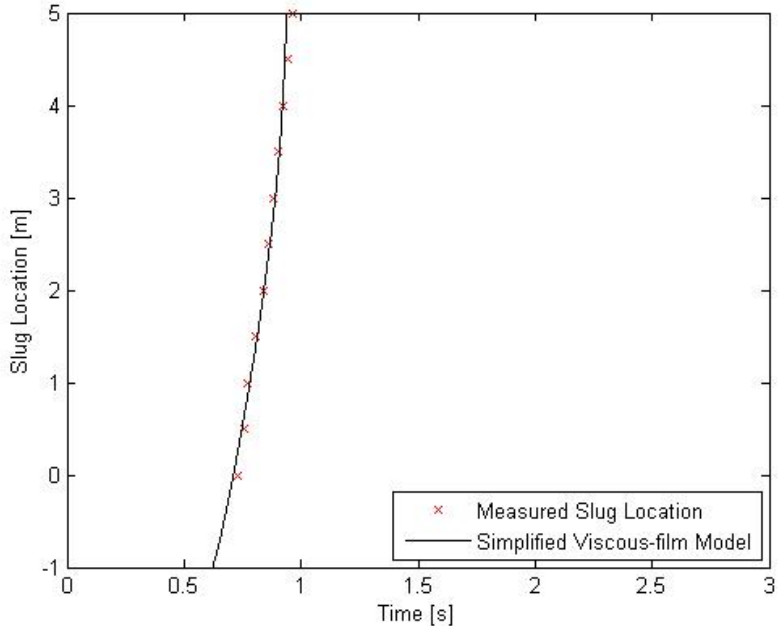

Figure 5.13. Slug Location vs. Time for a 276 kPa Pressure Difference, 200 ml Initial Slug Volume, in 13.4 mm Diameter Tube, Air-water High Side Test Using the Simplified Viscous-Film Model

The original viscous-film model can not be applied to tests with the 6.35 mm diameter tube because the film thickness is not measured directly during these tests. The simplified model, however, can be applied because it

estimates the film thickness. Figure 5.14 shows the simplified model location prediction for a high side air-water test in a 6.35 mm tube with a 137 kpa applied pressure difference and 100 ml initial slug volume. The model predicts the slug location with an average percent deviation of 2.4% until breakdown occurs near 4 m. The deviation between the model and experimental results at 0.0 m may be the result of local flow disturbances due to tube diameter changes between the test section and the liquid trap as discussed in Chapter 4. Figure 5.14 shows that the viscous-film model is effective for predicting slug location in the 6.35 mm diameter tube and again suggests the constant film thickness coefficient assumption is valid.

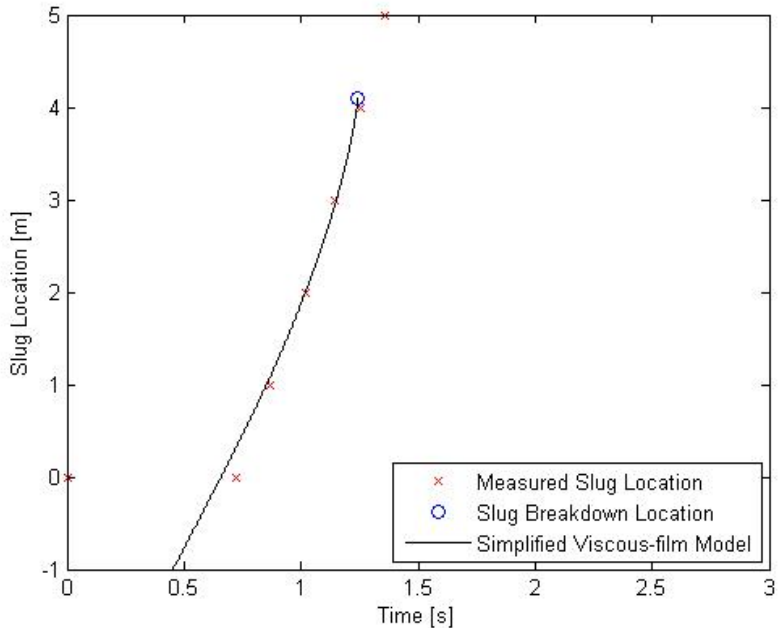

Figure 5.14. Slug Location and Breakdown Location vs. Time for a 137 kPa Pressure Difference, 100 ml Initial Slug Volume, in 6.35 mm Diameter Tube, Air-water High Side Test Using the Simplified Viscous Film Model

Figures 5.15 and 5.16 show the simplified model performance for high side and low side R134a tests, respectively. The model has an average percent deviation of 0.89% in Figure 5.15, and 0.26% in Figure 5.16. Figure 5.15 shows a high side test with a 260 kpa applied pressure difference, 165 ml initial slug volume, in a 10.2 mm diameter tube. Figure 5.16 shows a low side test in a 6.35 mm diameter tube with a 180 kpa applied pressure difference and 115 ml initial slug volume. The original viscous-film model can not be used in Figure 5.16 due to a lack of film thickness information. The figure shows that the viscous-film model can be used to predict slug location in low side tests as well. The constant film thickness coefficient assumption for R134a is supported by the results shown in Figures 5.15 and 5.16.

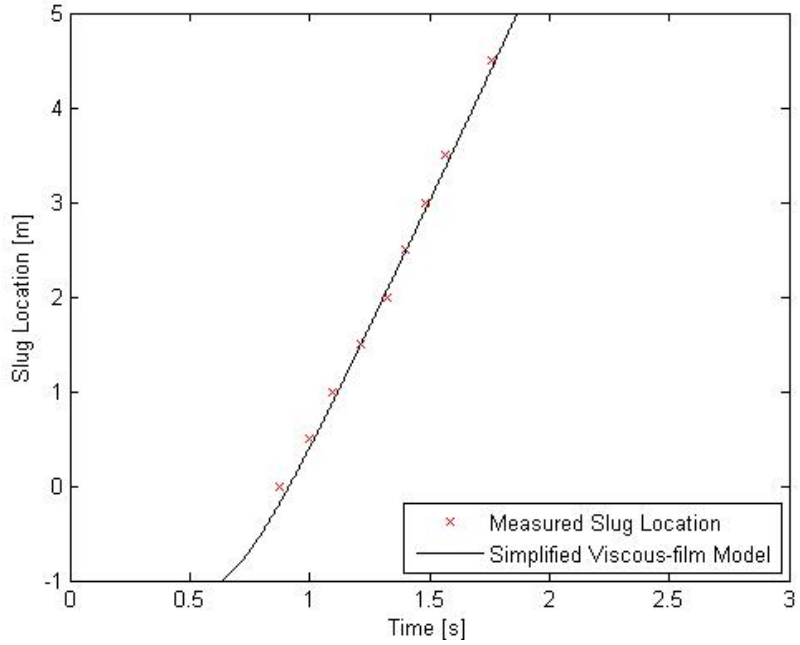

Figure 5.15. Slug Location vs. Time for a 260 kPa Pressure Difference, 165 ml Initial Slug Volume, in 10.2 mm Diameter Tube, R134a High Side Test Using the Simplified Viscous-Film Model

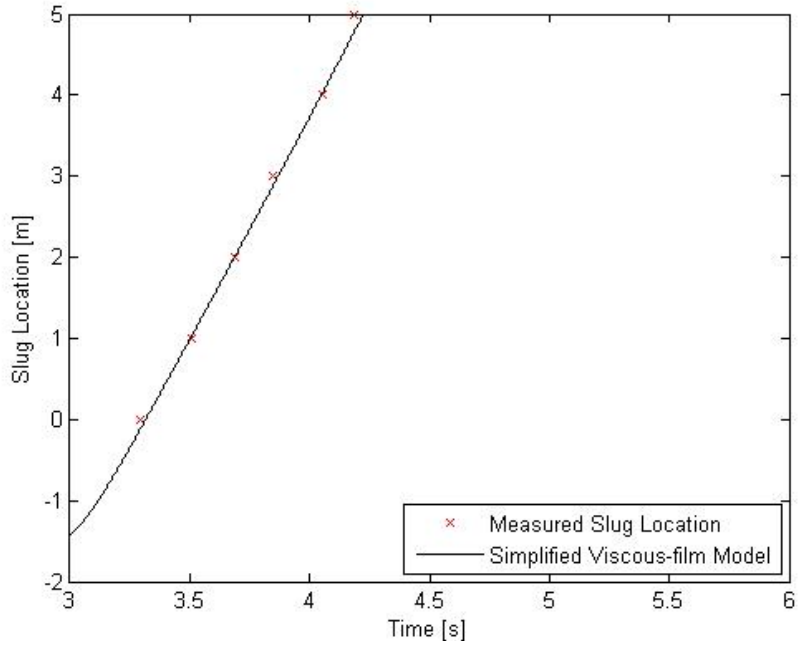

Figure 5.16. Slug Location vs. Time for a 180 kPa Pressure Difference, 115 ml Initial Slug Volume, in 6.35 mm Diameter Tube, R134a Low Side Test Using the Simplified Viscous-Film Model

The time that the slug passes each sensor predicted by the simplified viscous-film model is compared to the experimentally observed slug passage time in Figure 5.17. Figure 5.17 is similar to Figure 5.6 but includes all of the data (including the 6.35 mm diameter tests) and predicts the slug location using approximations outlined in section 5.3. The mean absolute percent deviation is 1.8%, slightly above the 1.7% deviation of the original viscous-film

model. The pressure difference and film thickness approximations made in section 5.3 are reasonable since the percent deviation does not increase significantly.

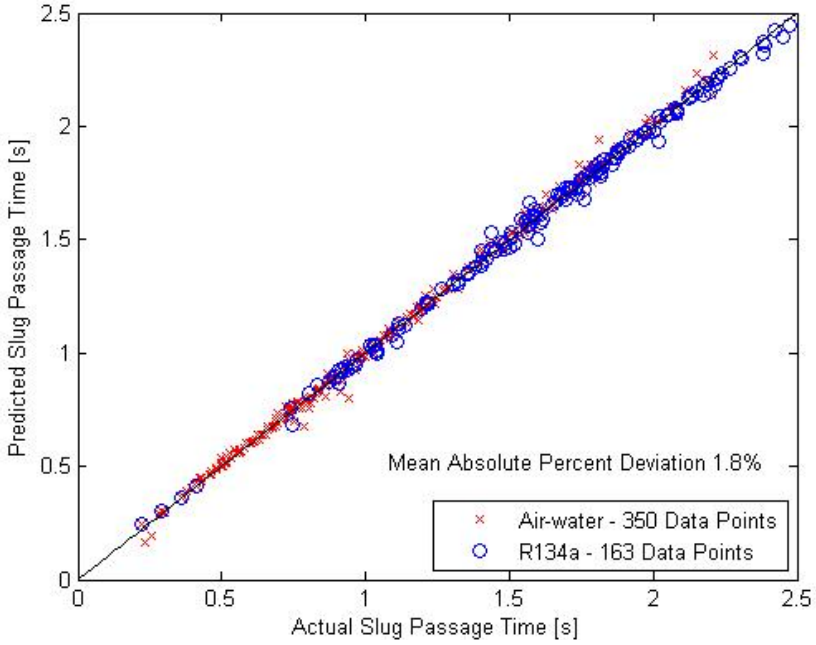

Figure 5.17. Time of Slug Passage Predicted by Simplified Viscous-Film Model vs. Time of Observed Slug Passage for All Experiments

Chapter 6. Concluding Remarks

6.1. Summary of Findings

A test section containing two pressure reservoirs, a liquid trap, a horizontal test section, and flow control valves is developed in order to simulate high side and low side conditions during refrigeration system startup. Experiments consist of accelerating a liquid slug of known volume from an initial rest state in a liquid trap to the low side pressure reservoir. Slug tests included air-water and two-phase R134a, 69-520 kPa applied pressure differences across the slug 40-400 ml initial slug volumes in 6.35, 10.2, and 13.4 mm diameter tubes. The film thickness and time at which the slug front passes is recorded by 11 film thickness sensors for each experiment; the applied pressure difference across the slug is also recorded. Approximate slug velocity, flow morphology, and slug breakdown location are observed through flow visualization video.

Flow visualization images suggest the slug consists of five distinct regions as described in Chapter 4: dense liquid vapor mixture at the slug front; bubble flow following the slug front; complete liquid slug; thick, wavy annular or stratified slug tail; and a thin, uniform annular or stratified film. Annular flow is observed following the slug in air-water tests and stratified flow is observed for R134a tests. Slug breakdown occurs within the 5.0 m test section for initial slug volumes less than 200 ml in air-water tests and for initial slug volumes less than 100 ml for R134a tests in 10.2 and 13.4 mm diameter tubes. R134a slugs breakdown immediately in low-side conditions in the 10.2 and 13.4 mm diameter tubes. Most of the slug acceleration occurs within the first 1.0 m of the test apparatus, before the horizontal test section. Slug acceleration is greater for a larger applied pressure difference, larger pipe diameters, and smaller initial slug volumes.

A simple numerical model, the viscous-film model, which considers rigid body motion, slug mass loss due to film deposition, and viscous pressure drop across the liquid slug is used to predict transient slug motion. The model accurately predicts the slug position in time with a mean absolute percent deviation of 1.7% for all experimental data. Though the film thickness varies significantly along the tube for a variety of initial conditions, the variation is random. The approximation of an axially uniform film thickness for each fluid predicts the slug acceleration and breakdown within 1.8% and 2.3% absolute percent deviation, respectively. Analytical solutions for the pipe length required for slug breakdown are generated for both air-water and R134a as a function of initial volume, pipe diameter, and fluid. An analytical solution for slug location is currently not known, a numerical solutions technique is required. The uncertainty in the slug location using the viscous-film model is ±0.26 m; the uncertainty in the pipe length required for slug breakdown is ±0.12 m.

6.2. Future Work

The present experimental analysis and modeling of slug motion and breakup should be extended to vertical and serpentine pipe orientations, commonly found in air conditioning and refrigeration systems, in the future. This work should include the investigation of the effects of pipe bends, elbows on slug motion and breakup. Inclined pipe effects on slug flow should also be analyzed. Furthermore, slug motion through accumulators, commonly found in air conditioning and refrigeration systems, should be studied.

Development of non-dimensional parameters to predict slug breakdown would improve the utility of the analytical solutions presented in this work. In addition, high speed video should be used in the future to capture the

geometry of the slug tail in order to provide insight in the mechanism of film separation on the tube walls, which may aid in film thickness modeling.

Future work should attempt to more accurately simulate the pressure across a slug provided by a compressor, instead of the step input assumed in the present study. An effort should be made in future studies to determine effective methods to initiate slug breakdown in air conditioning and refrigeration system applications and provide practical design criteria.

Bibliography

Chae, Hee Baik, James W. Schmidt, and Michael R. Moldover. 1990. "Alternative Refrigerants R123a, R134, R141b, R142b, and R152a: Critical Temperature, Refractive Index, Surface Tension, and Estimates of Liquid, Vapor, and Critical Densities." *Journal of Physical Chemistry,* Vol. 94, No. 25, pp. 8840-8845.

Colebrook, C. F. 1939. "Turbulent Flow in Pipes with Particular Reference to the Transition Between the Smooth and Rough Pipe Laws." *Journal of the Institute of Civil Engineers London,* Vol. 11.

Cunliffe, R. S. 1978. "Prediction of Condensate Flow Rates in Large Diameter High Pressure Wet Gas Pipelines." *Australian Petroleum Exploration Association Journal*, Vol. 18, pp. 171-177

De Henau, V. and G. D. Raithby. 1995a. "A Transient Two-Fluid Model for the Simulation of Slug Flow in Pipleines – I. Theory," *International Journal of Multiphase Flow,* Vol. 21, No. 3, pp. 335-349.

De Henau, V. and G. D. Raithby. 1995b. "A Transient Two-Fluid Model for the Simulation of Slug Flow in Pipleines – II. Validation," *International Journal of Multiphase Flow,* Vol. 21, No. 3, pp. 351-363.

Dukler, A. E. and M. G. Hubbard. 1975. "A Model for Gas-Liquid Slug Flow in Horizontal and Near Horizontal Tubes." *Industrial and Engineering Chemistry, Fundamentals,* Vol. 14, No. 4, pp. 337-347.

Grolman, Eric and Jan M. H. Fortuin. 1996. "Transient Gas-Liquid Flow in Upward Sloping Pipes, Approaching the Wavy-to-Slug Flow Transition." *Transactions of the ASME – Journal of Fluids Engineering,* Vol. 118, No. 4, pp. 729-735.

Hurlburt, E. T. and T. A. Newell. 1996. "Optical Measurement of Liquid Film Thickness and Wave Velocity in Liquid Film Flows." *Experiments in Fluids,* Vol. 21, No. 5, pp. 357-362.

Hurlburt, E. T. and T. A. Newell. 1997. "Modeling of the Evaporation and Condensation of Zeotropic Refrigerant Mixtures in Horizontal Annular Flow." *PhD Thesis, University of Illinois, Urbana-Champaign, IL.*

Jassim, E. W. 2006. "Probabilistic Flow Regime Map Modeling of Two-Phase Flow." *PhD Thesis, University of Illinois, Urbana-Champaign, IL.*

Kohda, K., Y. Suzukawa, and H. Furukawa. 1988. "Analysis of Transient Tas-Liquid Two-Phase Flow in Pipelines." *Transactions of the ASME - Journal of Energy Resources Technology,* Vol. 110, No. 2, pp. 93-101.

Kokal, S. L. and J. F. Stanislav. 1989. "An Experimental Study of Two-Phase Flow in Slightly Inclined Pipes – II. Liquid Holdup and Pressure Drop." *Chemical Engineering Science,* Vol. 44, No. 3, pp. 681-693.

Minami, K. and O. Shoham. 1994. "Transient Two-Phase Flow Behavior in Pipelines – Experiment and Modeling." *International Journal of Multiphase Flow,* Vol. 20, No. 4, pp. 739-752.

Richter, S., S. Fleischer, M. Aritomi, and R. Hampel. 2001. "Transient two-phase flow in arbitrary inclined tubes caused by depressurization of liquid with dissolved gasses." *International Journal of Heat and Mass Transfer,* Vol. 44, No. 1, pp. 1-15.

Sakaguchi, Tadashi, Mamoru Ozawa, Hachiro Hamaguchi, Fumitoshi Nishiwaki, and Eiji Fujii. 1987. "Analysis of the Impact Force by a Transient Liquid Slug Flowing Out of a Horizontal Pipe." *Nuclear Engineering and Design,* Vol. 99, No. 1, pp. 63-71.

Sharma, Y., M. W. Scoggins, Jr., O. Shoham, and J. P. Brill. 1986. "Simulation of Transient Two-Phase Flow in Pipelines." *Transactions of the ASME – Journal of Energy Resources Technology*, Vol. 108, No. 3, pp. 202-206.

Taitel, Y., O. Shoham, and J. P. Brill. 1989. "Simplified Transient Solution and Simulation of Two-Phase Flow in Pipelines." *Chemical Engineering Science,* Vol. 44, No. 6, pp. 1353-1359.

Taitel, Y., and D. Barnea. 1997. "Simplified Transient Simulation of Two Phase Flow Using Quasi=Equilibrium Momentum Balances." *International Journal of Multiphase Flow,* Vol. 23, No. 3, pp. 493-501.

Yu, S. C. M., C. P. Tso, and R. Liew. 1996. "Analysis of Thin Film Thickness Determination in Two-Phase Flow Using a Multifiber Optical Sensor." *Applied Mathematical Modeling.* Vol. 20, No. 7, pp. 540-548.

Appendix A. High Side Test Results

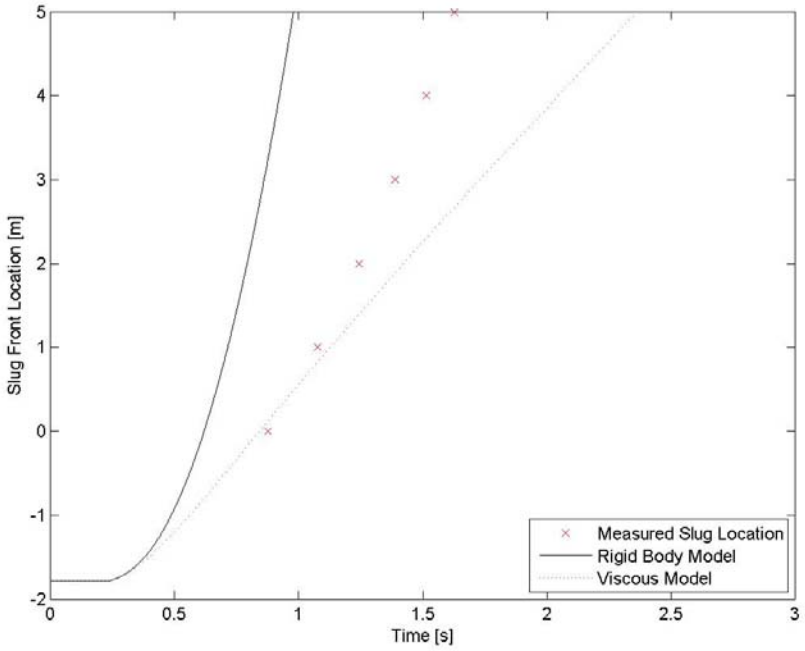

Figure A.1. Model Comparison for a 69 kPa Pressure Difference, 100 ml Initial Slug Volume, in 6.35 mm Diameter Pipe, Air-water High Side Test

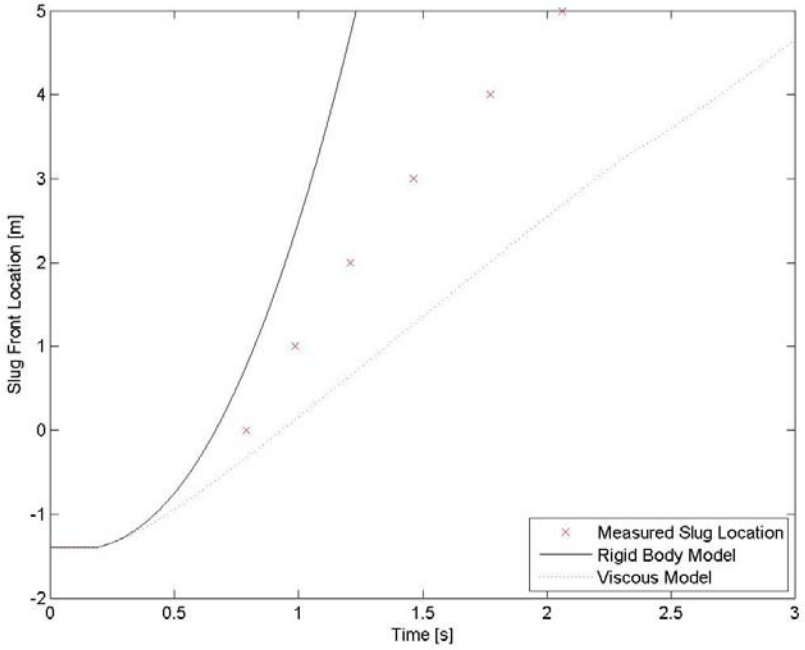

Figure A.2. Model Comparison for a 69 kPa Pressure Difference, 200 ml Initial Slug Volume, in 6.35 mm Diameter Pipe, Air-water High Side Test

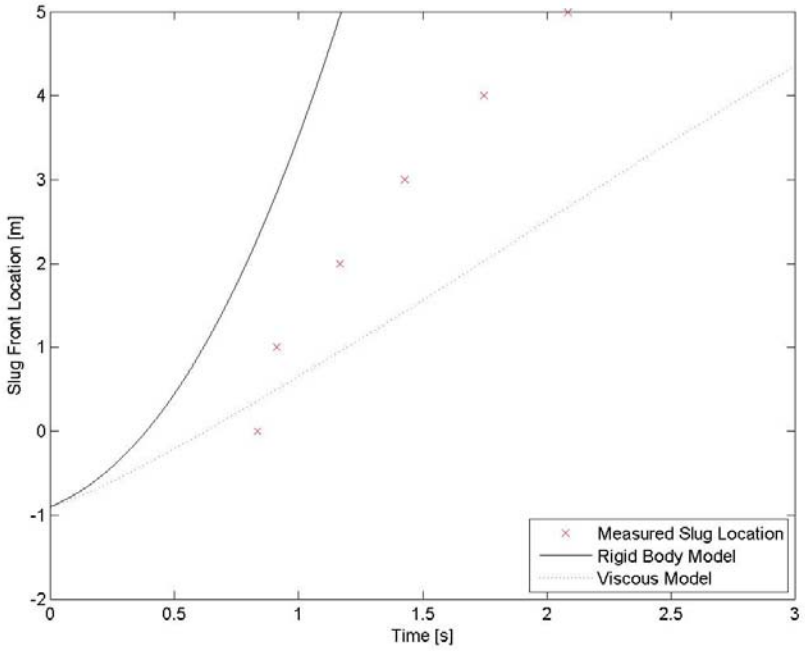

Figure A.3. Model Comparison for a 69 kPa Pressure Difference, 300 ml Initial Slug Volume, in 6.35 mm Diameter Pipe, Air-water High Side Test

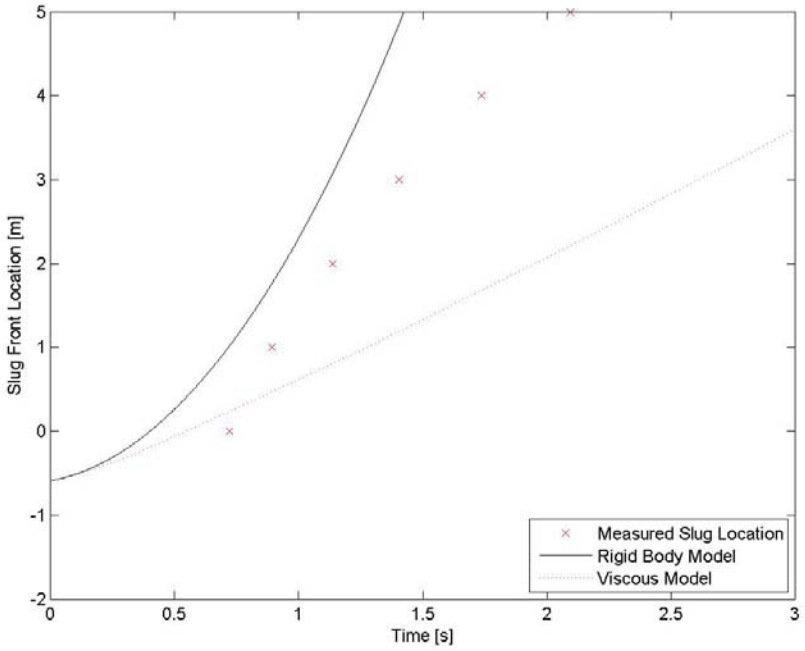

Figure A.4. Model Comparison for a 69 kPa Pressure Difference, 400 ml Initial Slug Volume, in 6.35 mm Diameter Pipe, Air-water High Side Test High Side Test 4

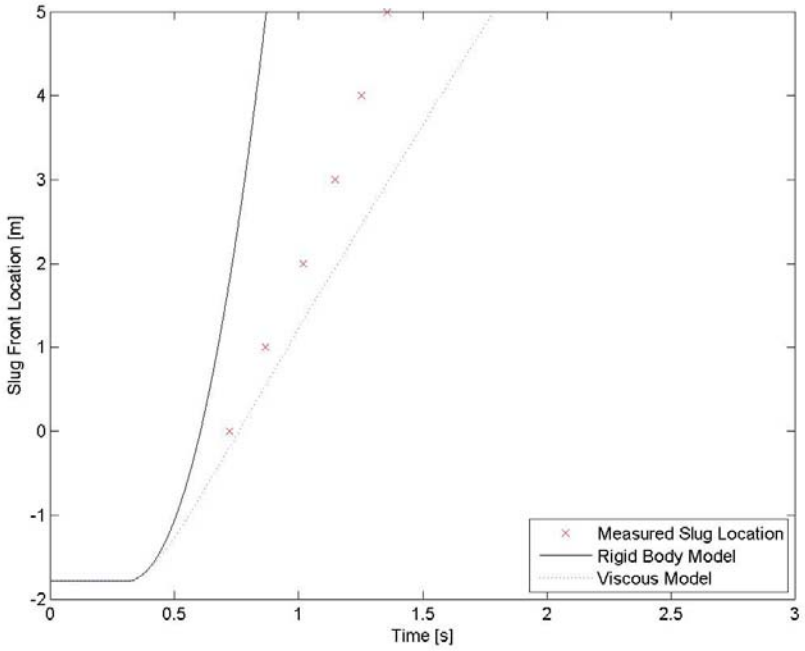

Figure A.5. Model Comparison for a 138 kPa Pressure Difference, 100 ml Initial Slug Volume, in 6.35 mm Diameter Pipe, Air-water High Side Test

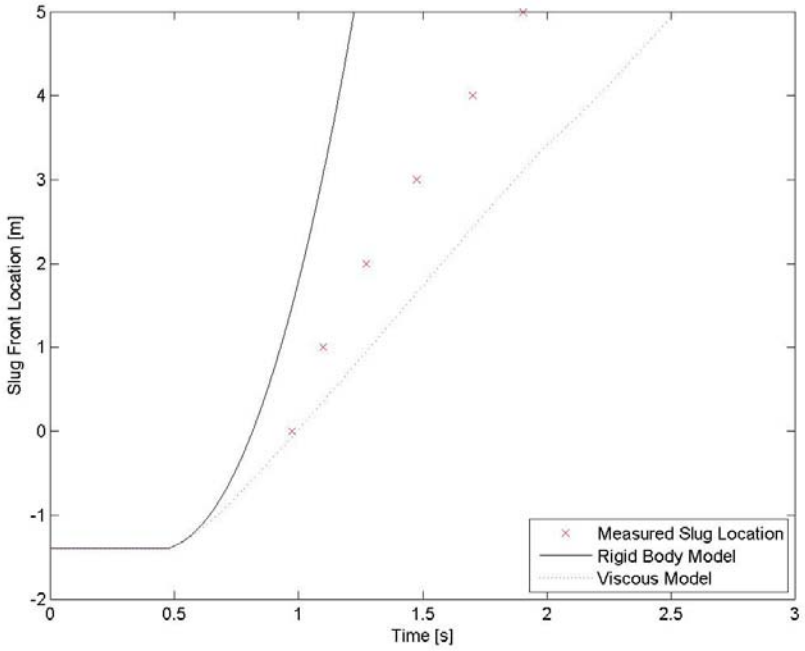

Figure A.6. Model Comparison for a 138 kPa Pressure Difference, 200 ml Initial Slug Volume, in 6.35 mm Diameter Pipe, Air-water High Side Test

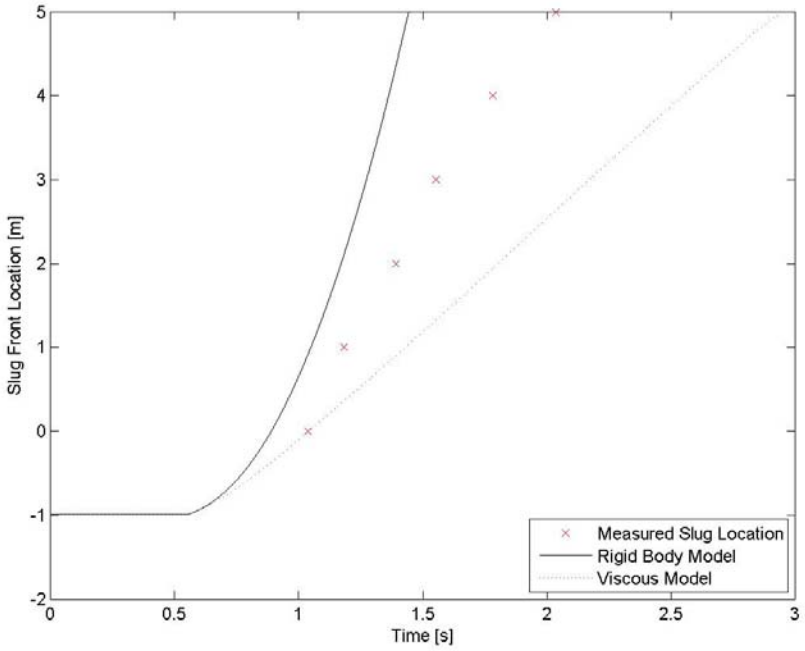

Figure A.7. Model Comparison for a 138 kPa Pressure Difference, 300 ml Initial Slug Volume, in 6.35 mm Diameter Pipe, Air-water High Side Test

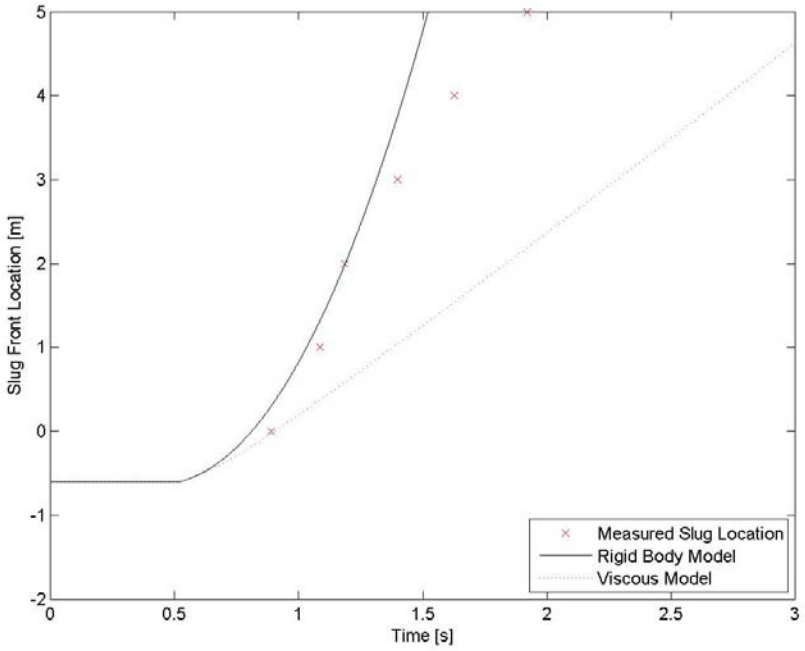

Figure A.8. Model Comparison for a 138 kPa Pressure Difference, 400 ml Initial Slug Volume, in 6.35 mm Diameter Pipe, Air-water High Side Test

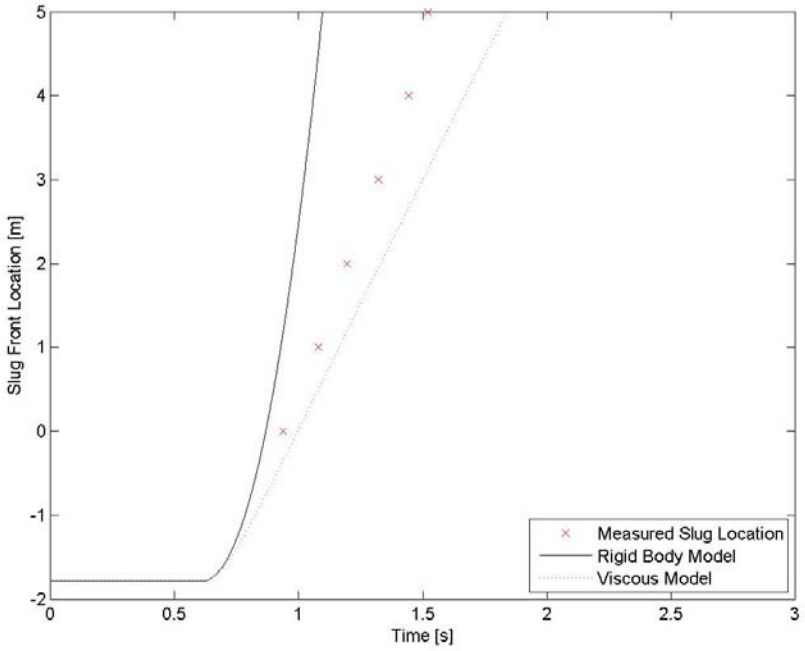

Figure A.9. Model Comparison for a 207 kPa Pressure Difference, 100 ml Initial Slug Volume, in 6.35 mm Diameter Pipe, Air-water High Side Test

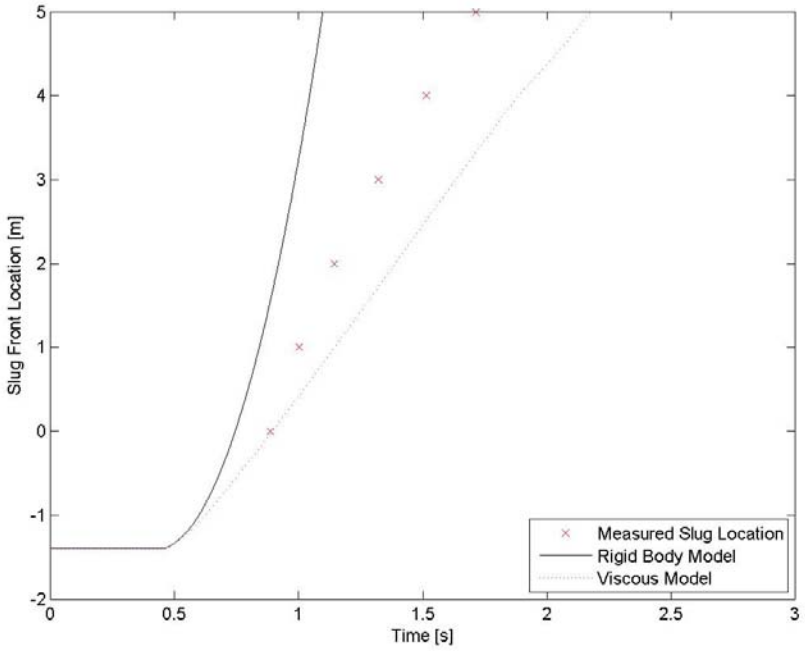

Figure A.10. Model Comparison for a 207 kPa Pressure Difference, 200 ml Initial Slug Volume, in 6.35 mm Diameter Pipe, Air-water High Side Test

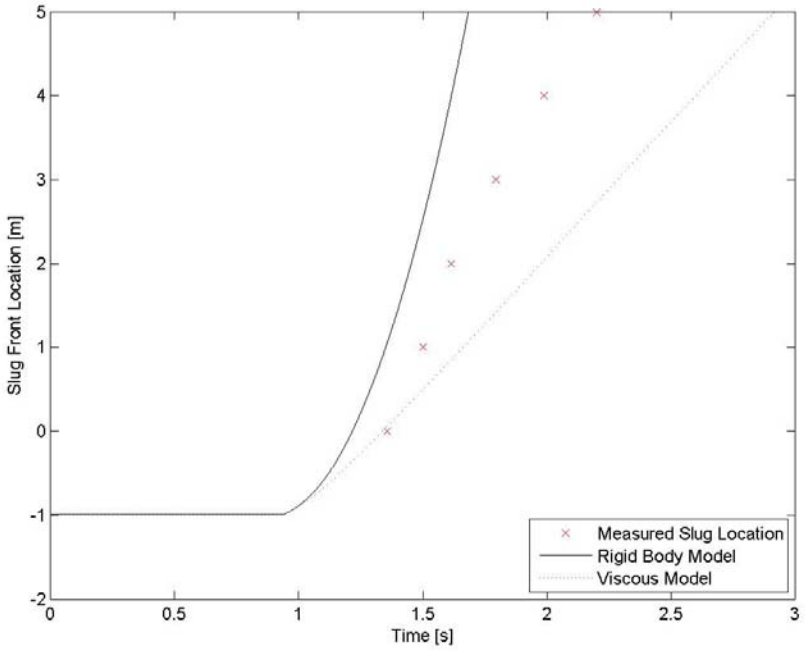

Figure A.11. Model Comparison for a 207 kPa Pressure Difference, 300 ml Initial Slug Volume, in 6.35 mm Diameter Pipe, Air-water High Side Test

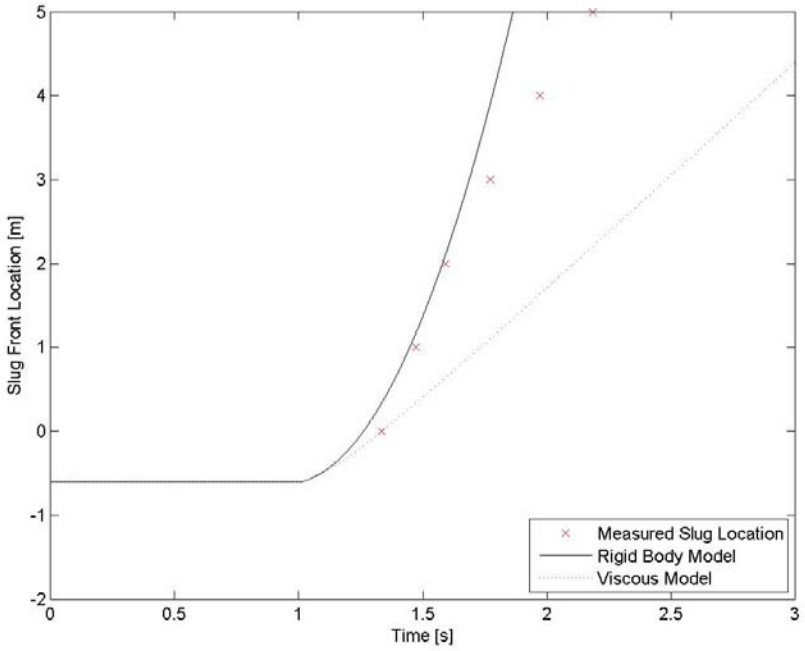

Figure A.12. Model Comparison for a 207 kPa Pressure Difference, 400 ml Initial Slug Volume, in 6.35 mm Diameter Pipe, Air-water High Side Test

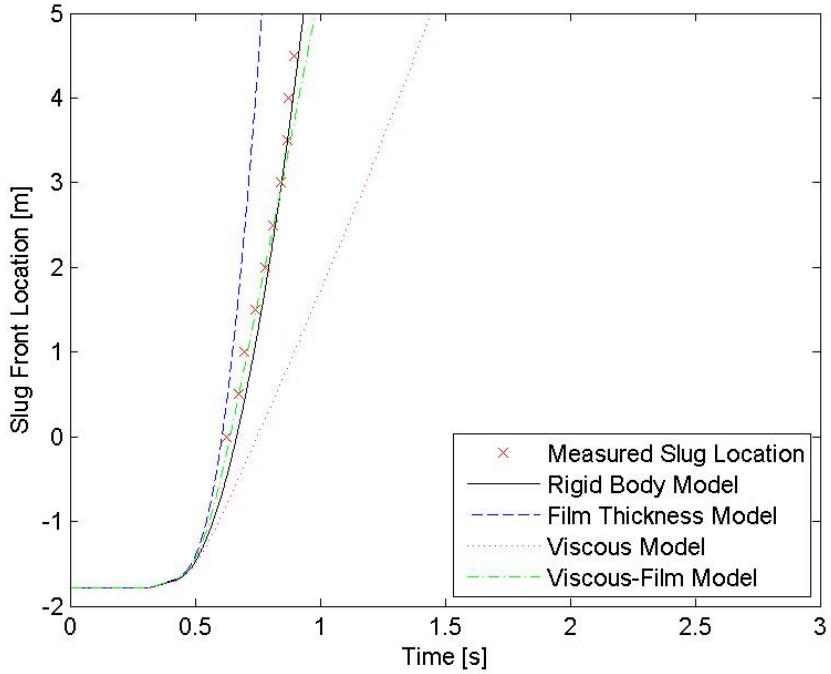

Figure A.13. Model Comparison for a 69 kPa Pressure Difference, 100 ml Initial Slug Volume, in 10.2 mm Diameter Pipe, Air-water High Side Test

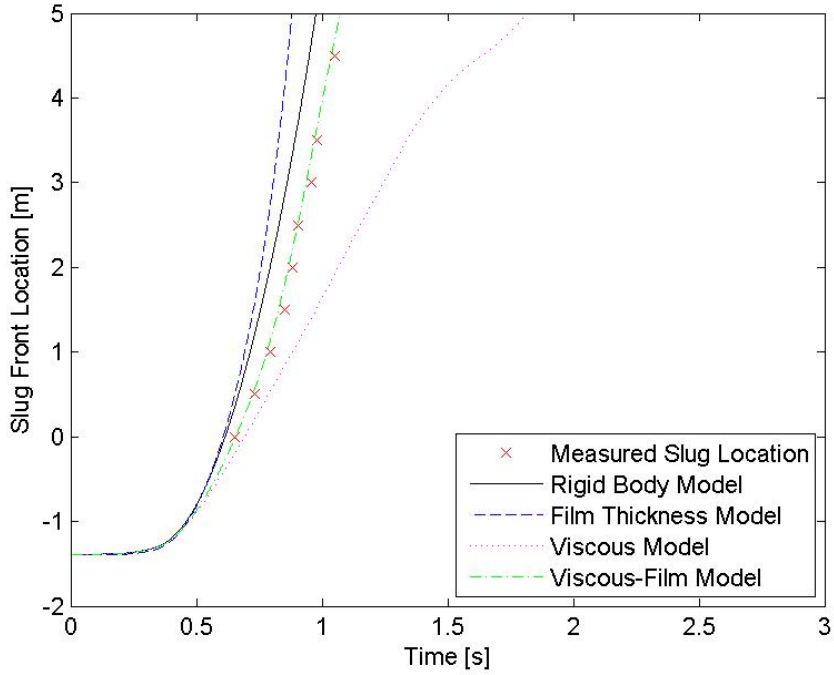

Figure A.14. Model Comparison for a 69 kPa Pressure Difference, 200 ml Initial Slug Volume, in 10.2 mm Diameter Pipe, Air-water High Side Test

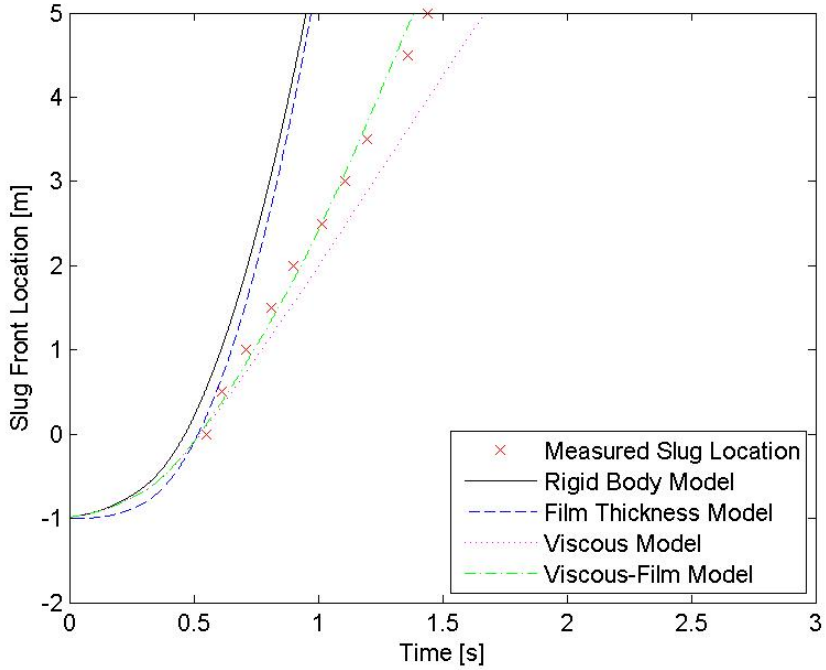

Figure A.15. Model Comparison for a 69 kPa Pressure Difference, 300 ml Initial Slug Volume, in 10.2 mm Diameter Pipe, Air-water High Side Test

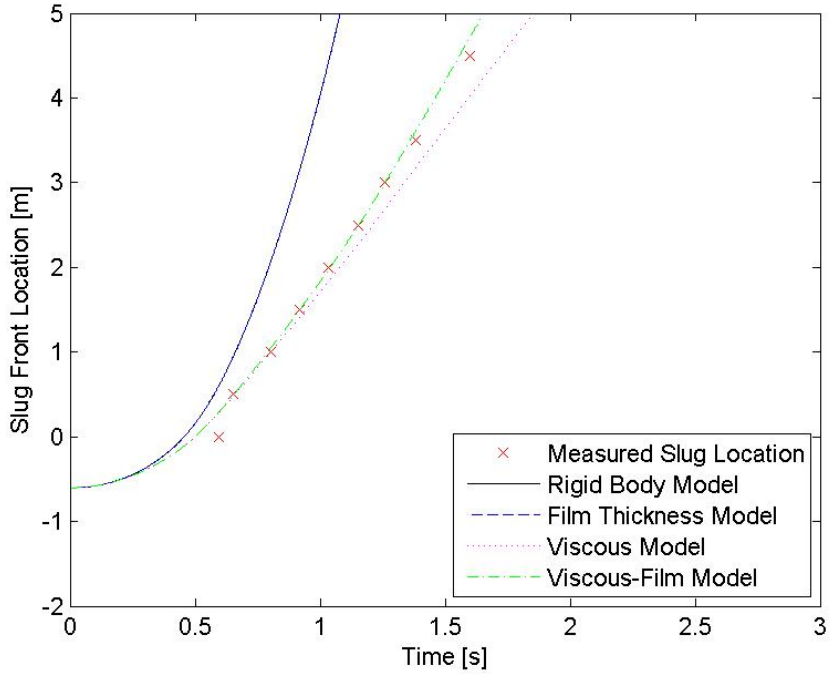

Figure A.16. Model Comparison for a 69 kPa Pressure Difference, 400 ml Initial Slug Volume, in 10.2 mm Diameter Pipe, Air-water High Side Test

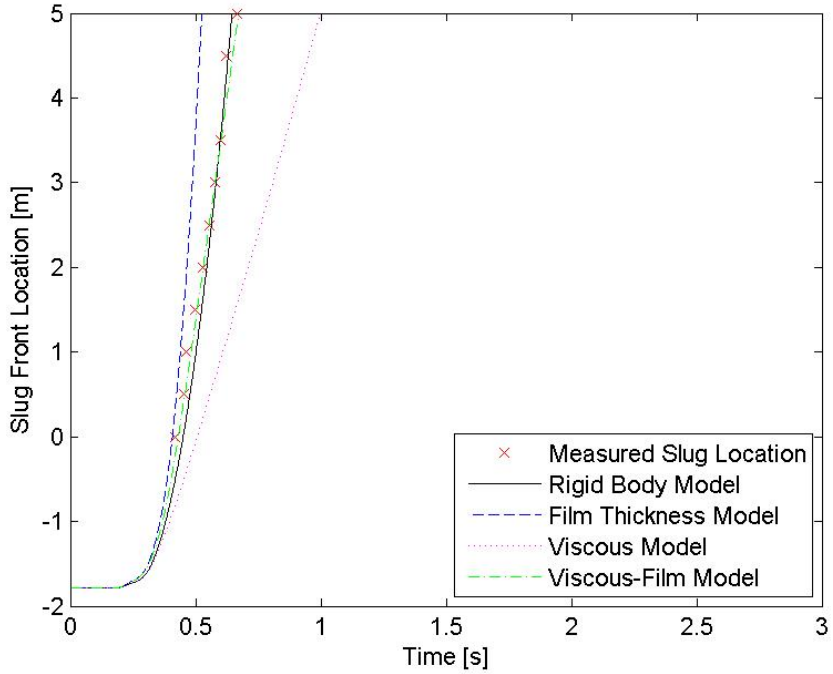

Figure A.17. Model Comparison for a 138 kPa Pressure Difference, 100 ml Initial Slug Volume, in 10.2 mm Diameter Pipe, Air-water High Side Test

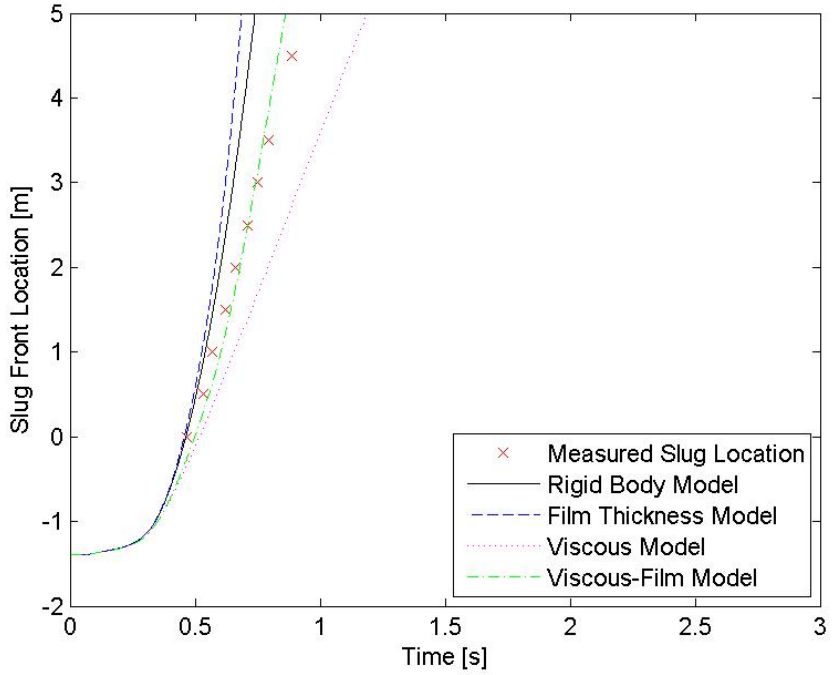

Figure A.18. Model Comparison for a 138 kPa Pressure Difference, 200 ml Initial Slug Volume, in 10.2 mm Diameter Pipe, Air-water High Side Test

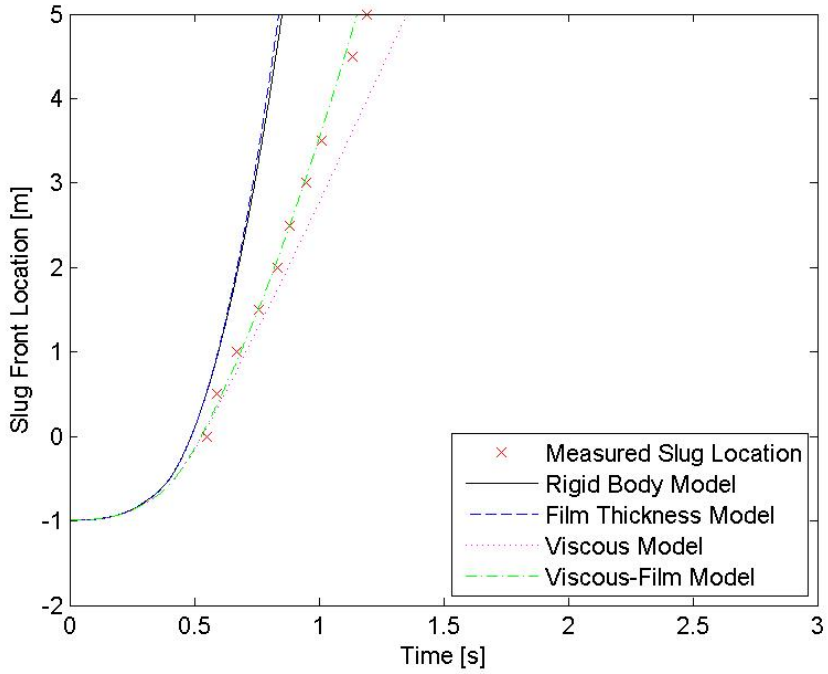

Figure A.19. Model Comparison for a 138 kPa Pressure Difference, 300 ml Initial Slug Volume, in 10.2 mm Diameter Pipe, Air-water High Side Test

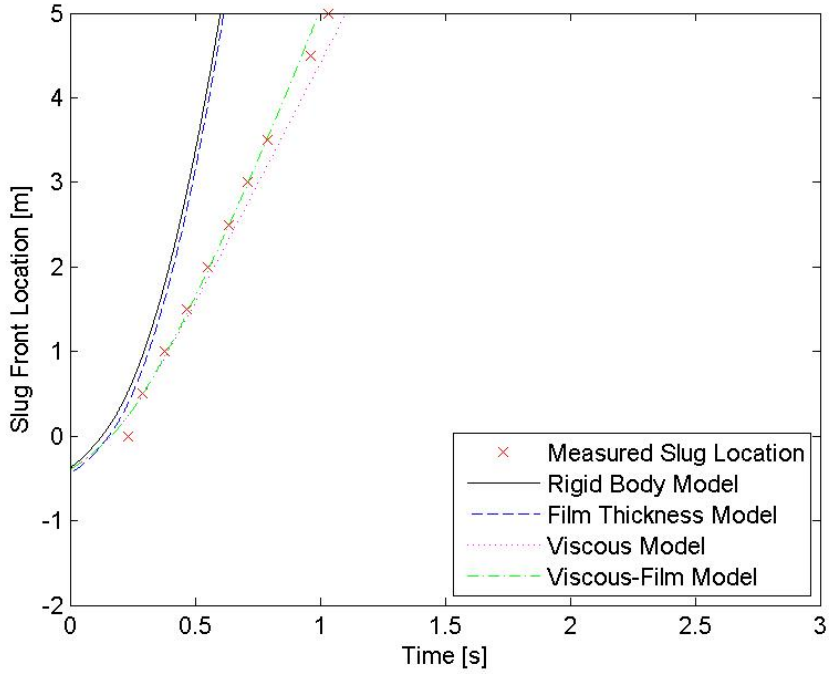

Figure A.20. Model Comparison for a 138 kPa Pressure Difference, 400 ml Initial Slug Volume, in 10.2 mm Diameter Pipe, Air-water High Side Test

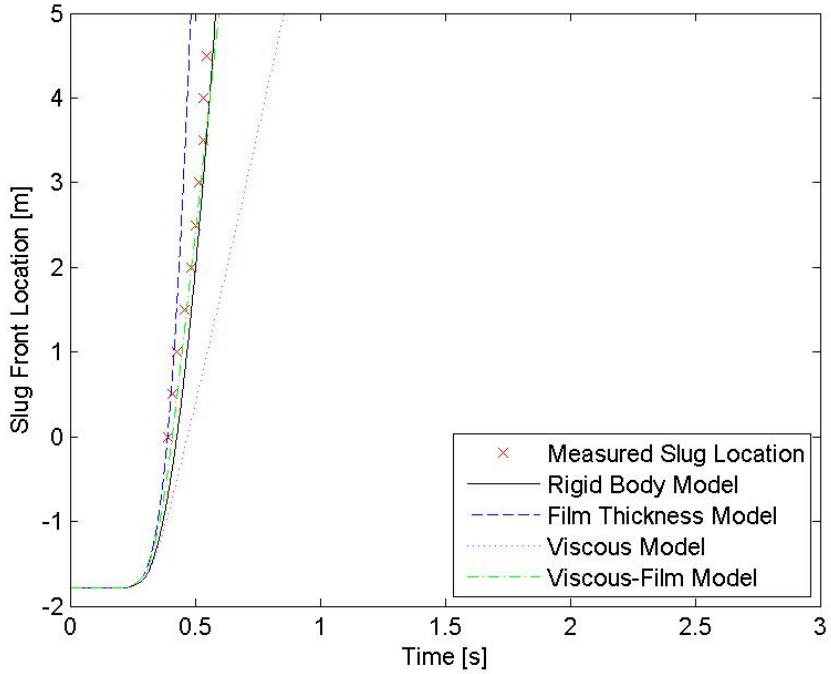

Figure A.21. Model Comparison for a 207 kPa Pressure Difference, 100 ml Initial Slug Volume, in 10.2 mm Diameter Pipe, Air-water High Side Test

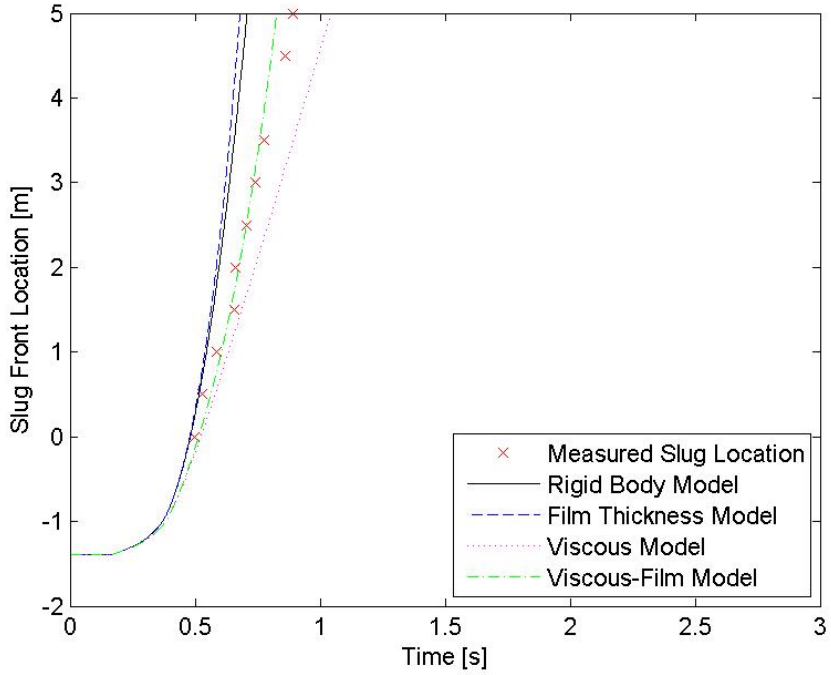

Figure A.22. Model Comparison for a 207 kPa Pressure Difference, 200 ml Initial Slug Volume, in 10.2 mm Diameter Pipe, Air-water High Side Test

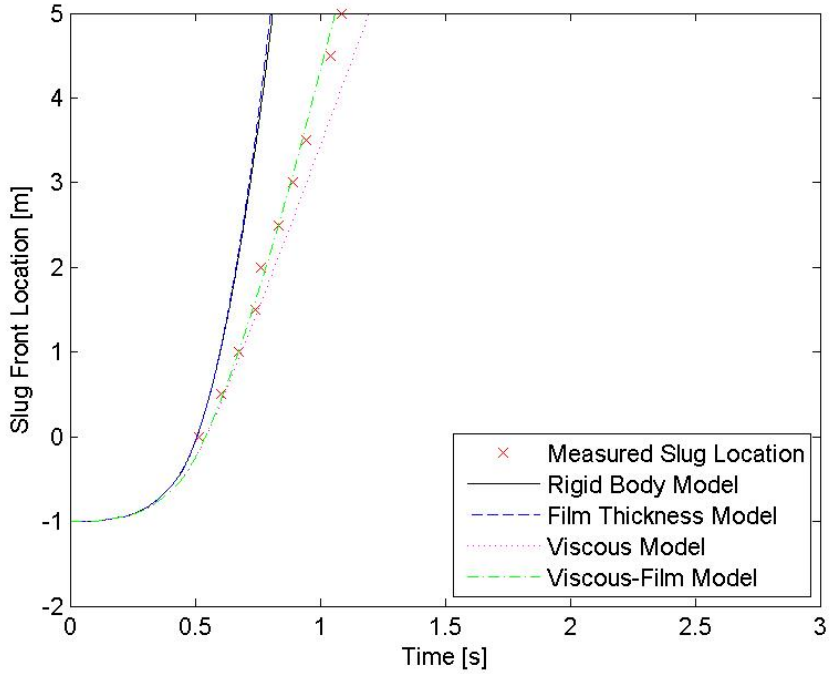

Figure A.23. Model Comparison for a 207 kPa Pressure Difference, 300 ml Initial Slug Volume, in 10.2 mm Diameter Pipe, Air-water High Side Test

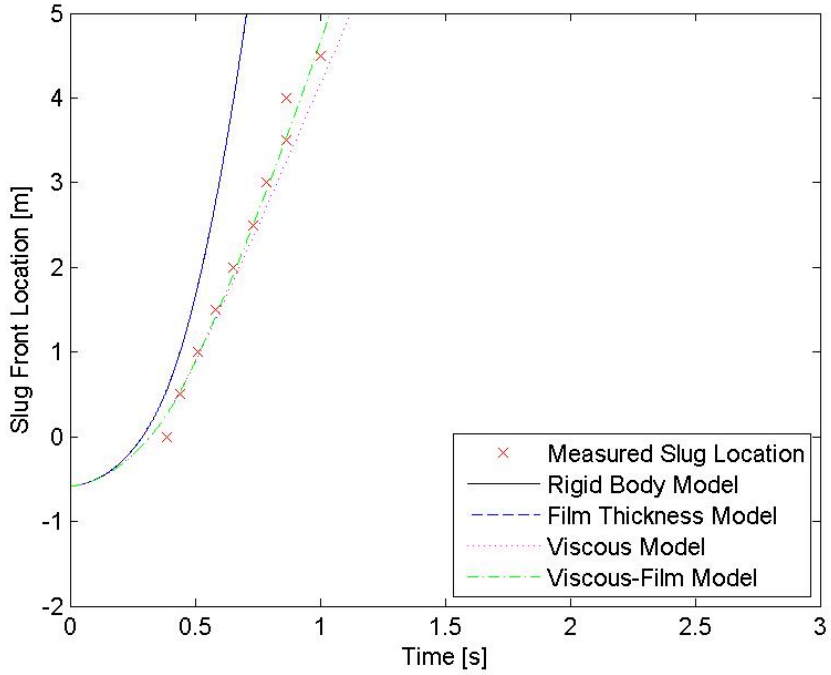

Figure A.24. Model Comparison for a 207 kPa Pressure Difference, 400 ml Initial Slug Volume, in 10.2 mm Diameter Pipe, Air-water High Side Test

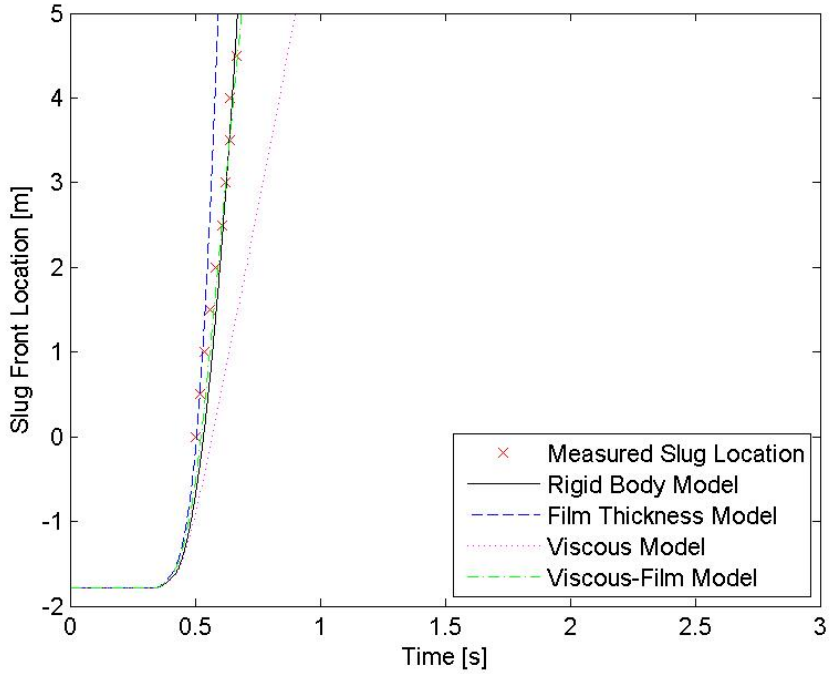

Figure A.25. Model Comparison for a 276 kPa Pressure Difference, 100 ml Initial Slug Volume, in 10.2 mm Diameter Pipe, Air-water High Side Test

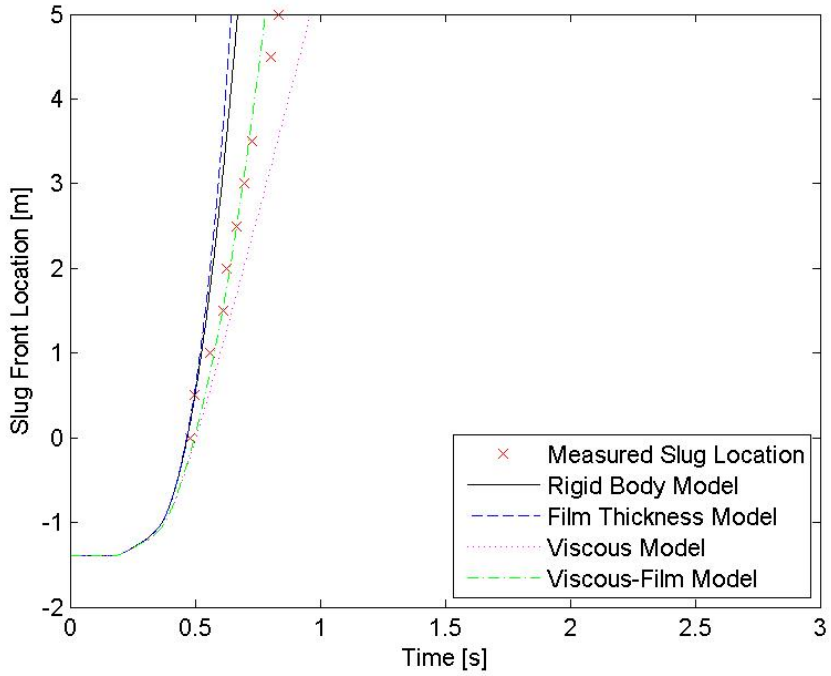

Figure A.26. Model Comparison for a 276 kPa Pressure Difference, 200 ml Initial Slug Volume, in 10.2 mm Diameter Pipe, Air-water High Side Test

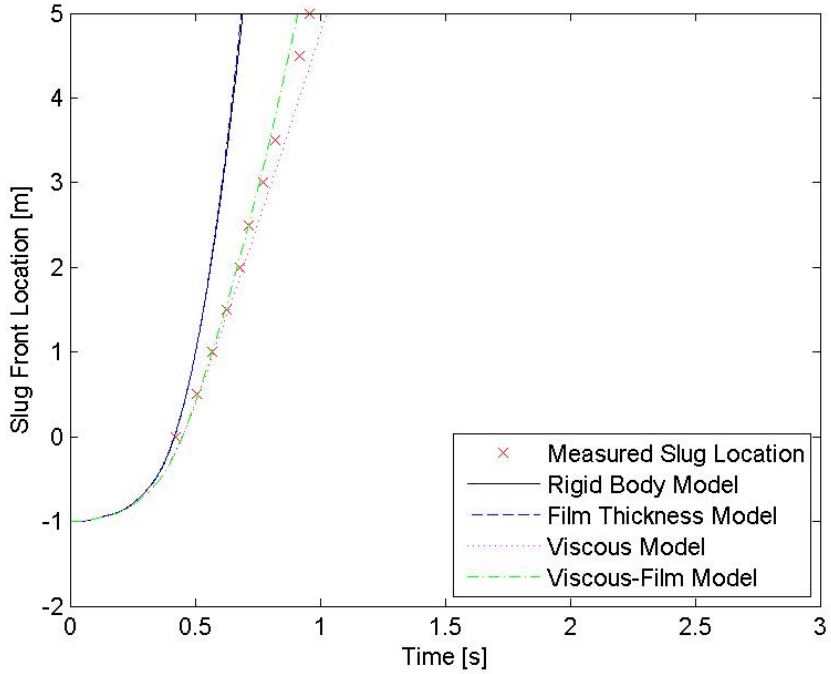

Figure A.27. Model Comparison for a 276 kPa Pressure Difference, 300 ml Initial Slug Volume, in 10.2 mm Diameter Pipe, Air-water High Side Test

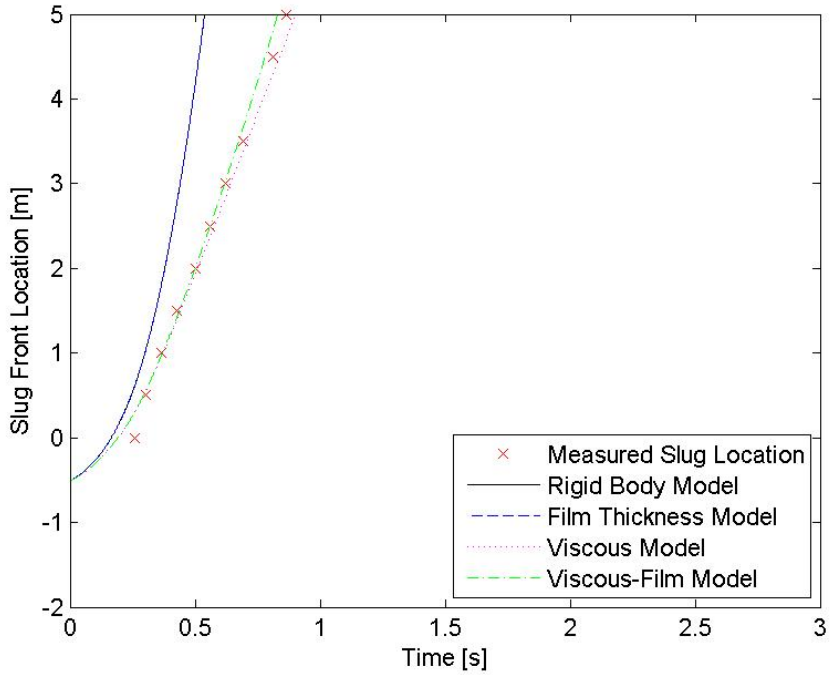

Figure A.28. Model Comparison for a 276 kPa Pressure Difference, 400 ml Initial Slug Volume, in 10.2 mm Diameter Pipe, Air-water High Side Test

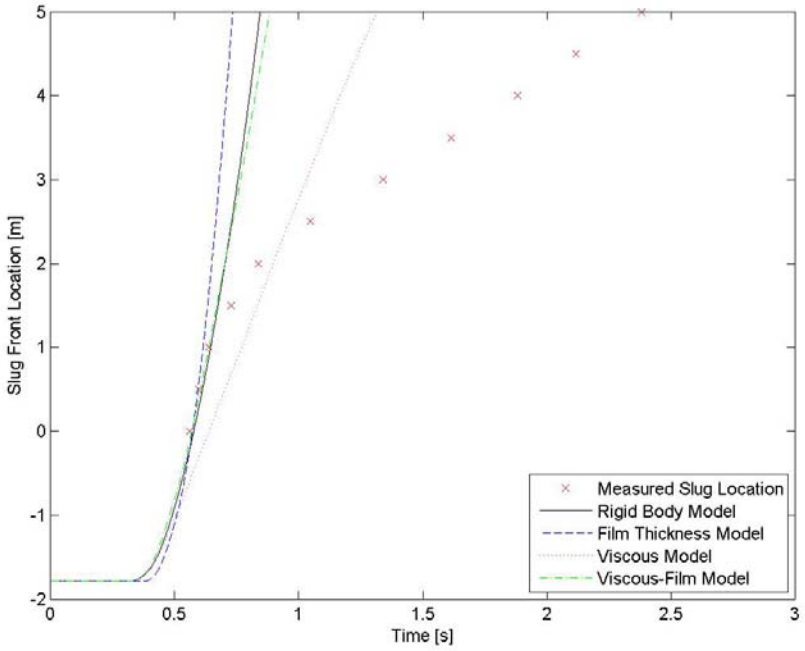

Figure A.29. Model Comparison for a 69 kPa Pressure Difference, 100 ml Initial Slug Volume, in 13.4 mm Diameter Pipe, Air-water High Side Test

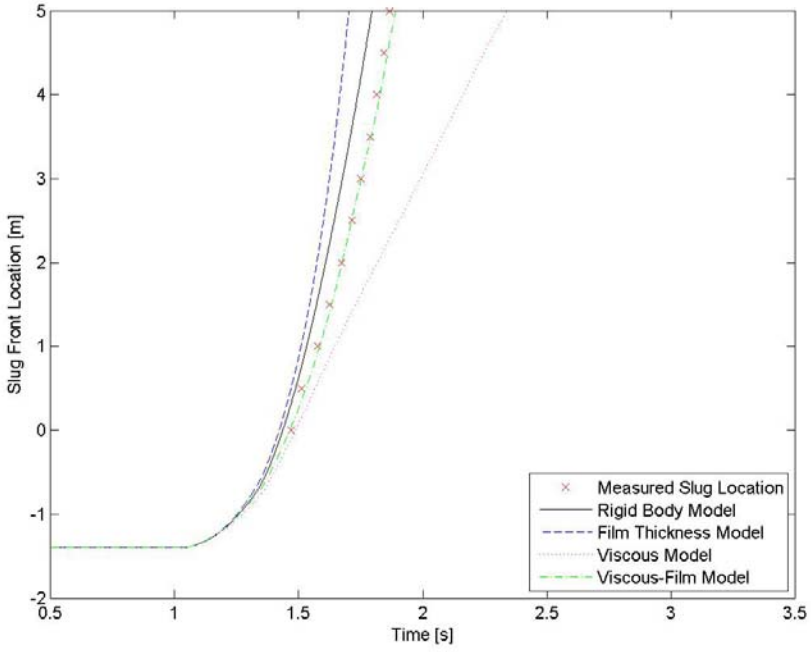

Figure A.30. Model Comparison for a 69 kPa Pressure Difference, 200 ml Initial Slug Volume, in 13.4 mm Diameter Pipe, Air-water High Side Test

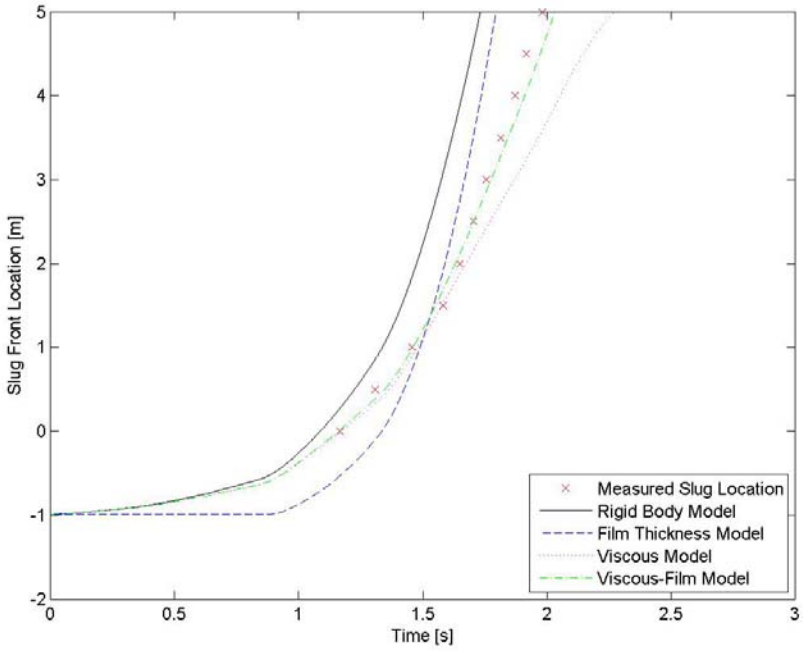

Figure A.31. Model Comparison for a 69 kPa Pressure Difference, 300 ml Initial Slug Volume, in 13.4 mm Diameter Pipe, Air-water High Side Test

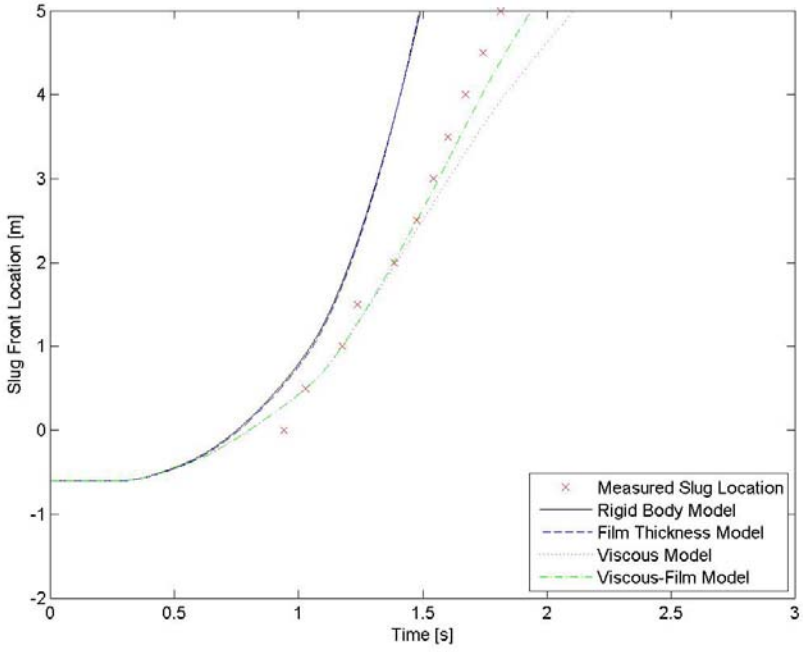

Figure A.32. Model Comparison for a 69 kPa Pressure Difference, 400 ml Initial Slug Volume, in 13.4 mm Diameter Pipe, Air-water High Side Test

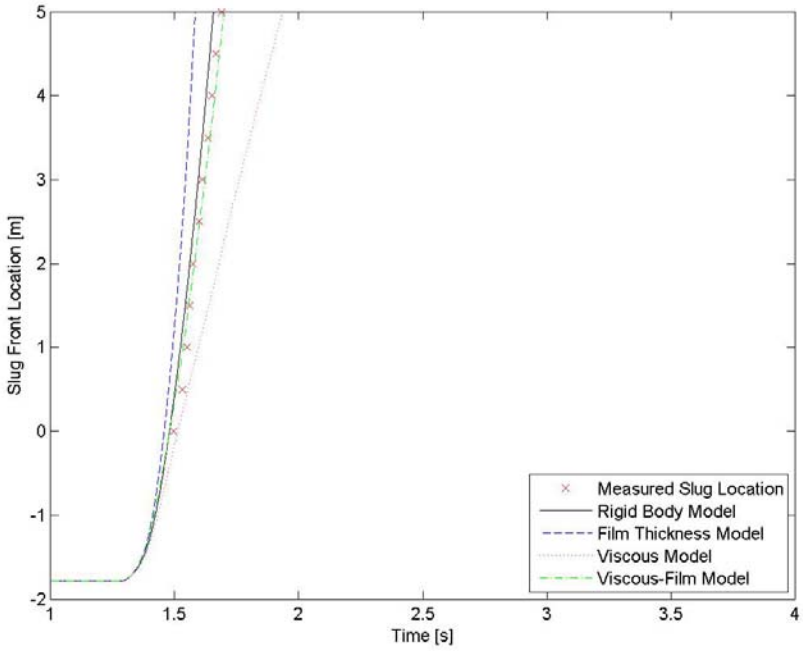

Figure A.33. Model Comparison for a 138 kPa Pressure Difference, 100 ml Initial Slug Volume, in 13.4 mm Diameter Pipe, Air-water High Side Test

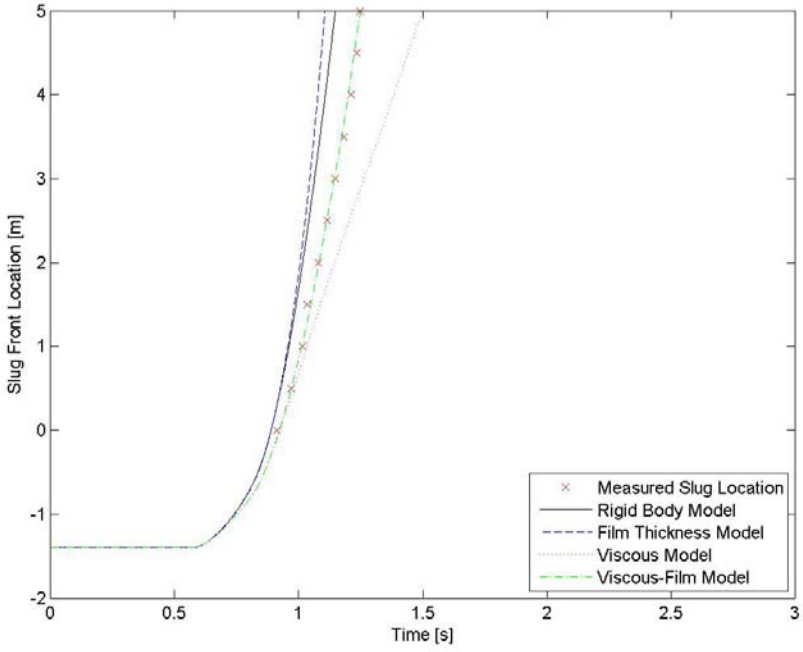

Figure A.34. Model Comparison for a 138 kPa Pressure Difference, 200 ml Initial Slug Volume, in 13.4 mm Diameter Pipe, Air-water High Side Test

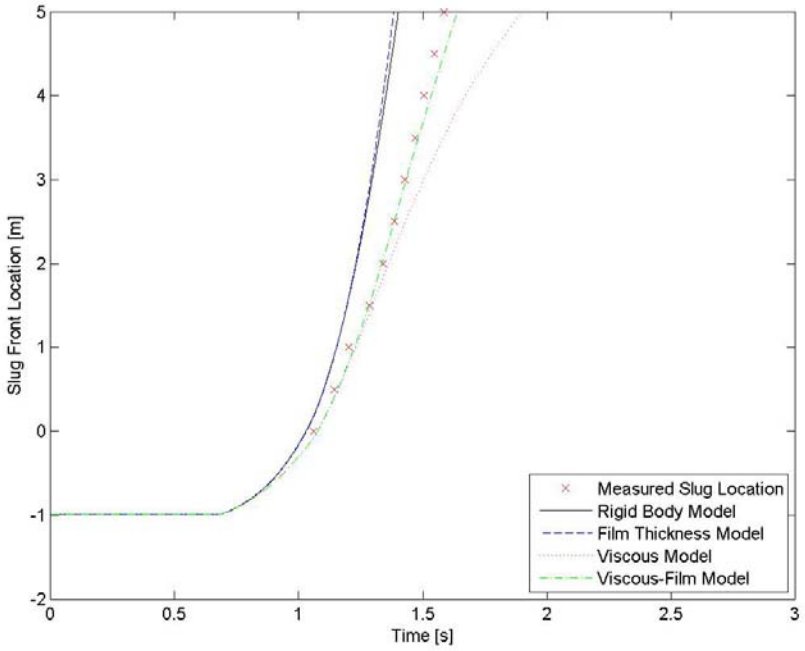

Figure A.35. Model Comparison for a 138 kPa Pressure Difference, 300 ml Initial Slug Volume, in 13.4 mm Diameter Pipe, Air-water High Side Test

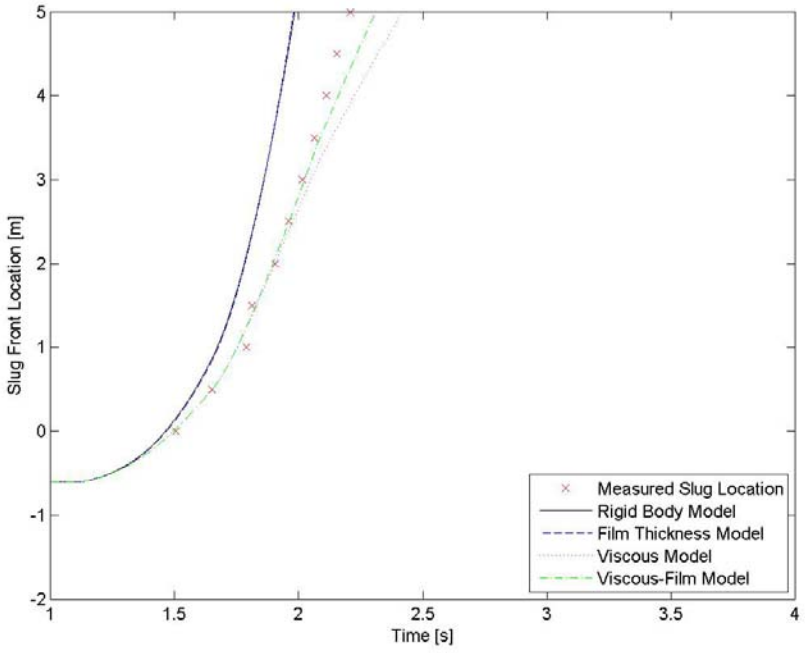

Figure A.36. Model Comparison for a 138 kPa Pressure Difference, 400 ml Initial Slug Volume, in 13.4 mm Diameter Pipe, Air-water High Side Test

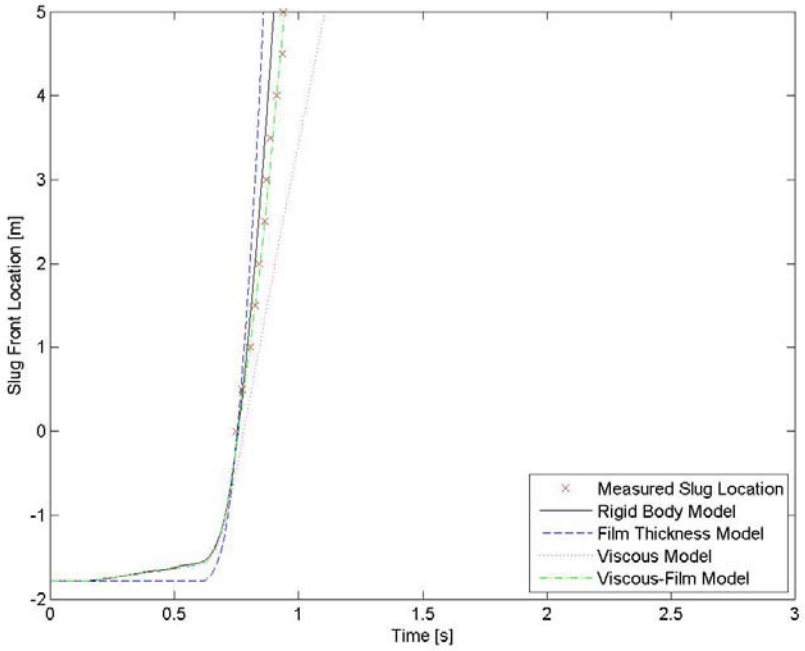

Figure A.37. Model Comparison for a 207 kPa Pressure Difference, 100 ml Initial Slug Volume, in 13.4 mm Diameter Pipe, Air-water High Side Test

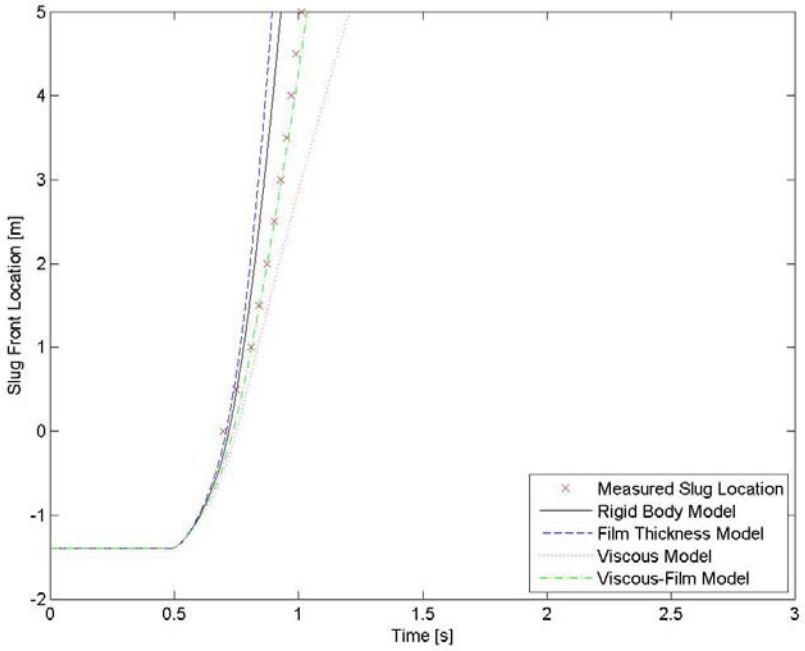

Figure A.38. Model Comparison for a 207 kPa Pressure Difference, 200 ml Initial Slug Volume, in 13.4 mm Diameter Pipe, Air-water High Side Test

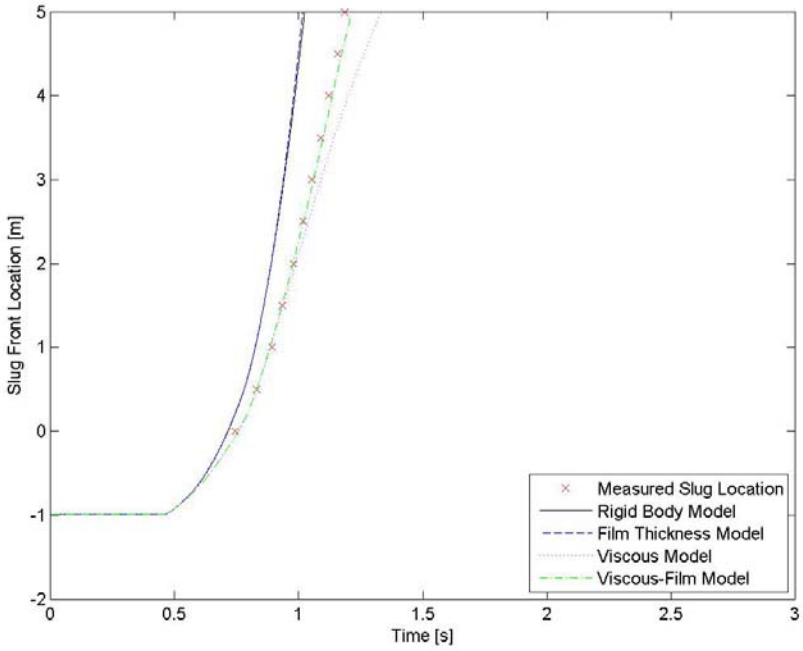

Figure A.39. Model Comparison for a 207 kPa Pressure Difference, 300 ml Initial Slug Volume, in 13.4 mm Diameter Pipe, Air-water High Side Test

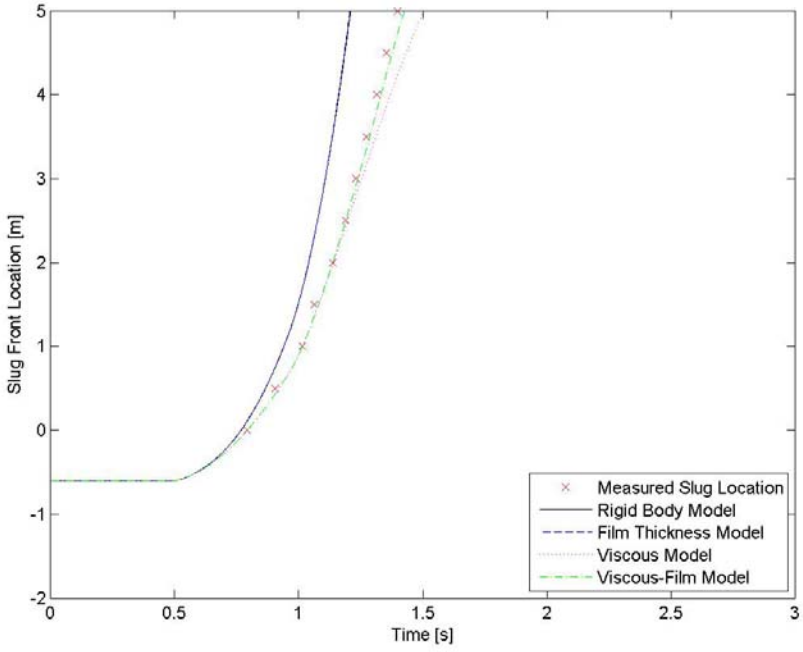

Figure A.40. Model Comparison for a 207 kPa Pressure Difference, 400 ml Initial Slug Volume, in 13.4 mm Diameter Pipe, Air-water High Side Test

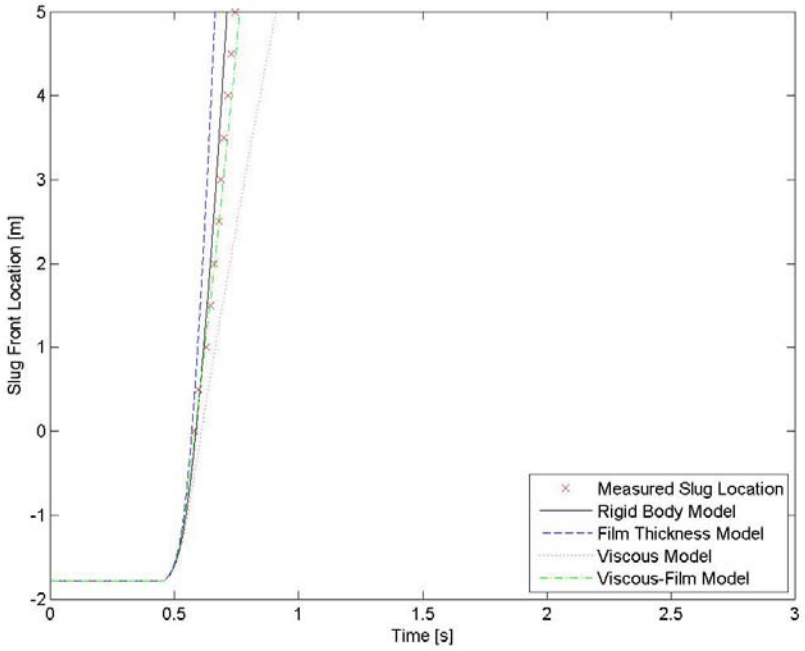

Figure A.41. Model Comparison for a 276 kPa Pressure Difference, 100 ml Initial Slug Volume, in 13.4 mm Diameter Pipe, Air-water High Side Test

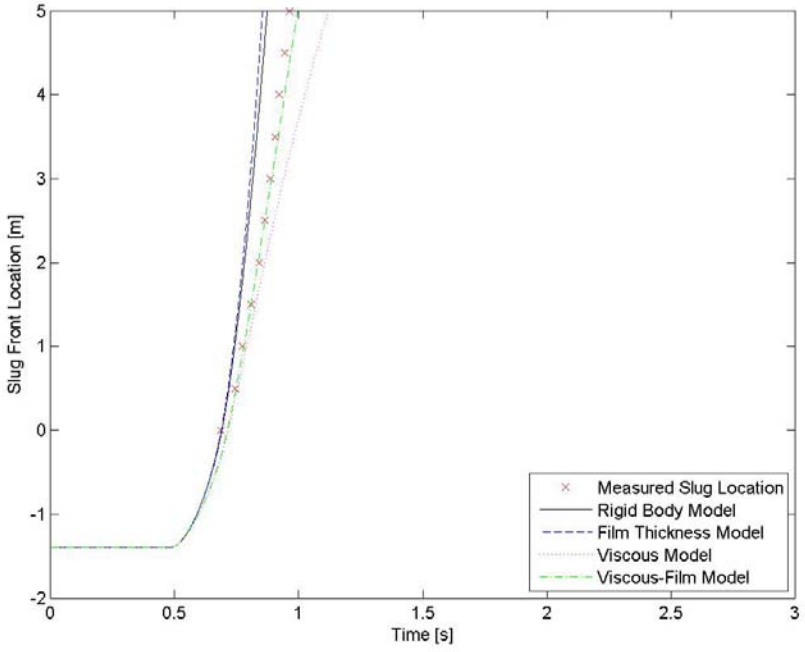

Figure A.42. Model Comparison for a 276 kPa Pressure Difference, 200 ml Initial Slug Volume, in 13.4 mm Diameter Pipe, Air-water High Side Test

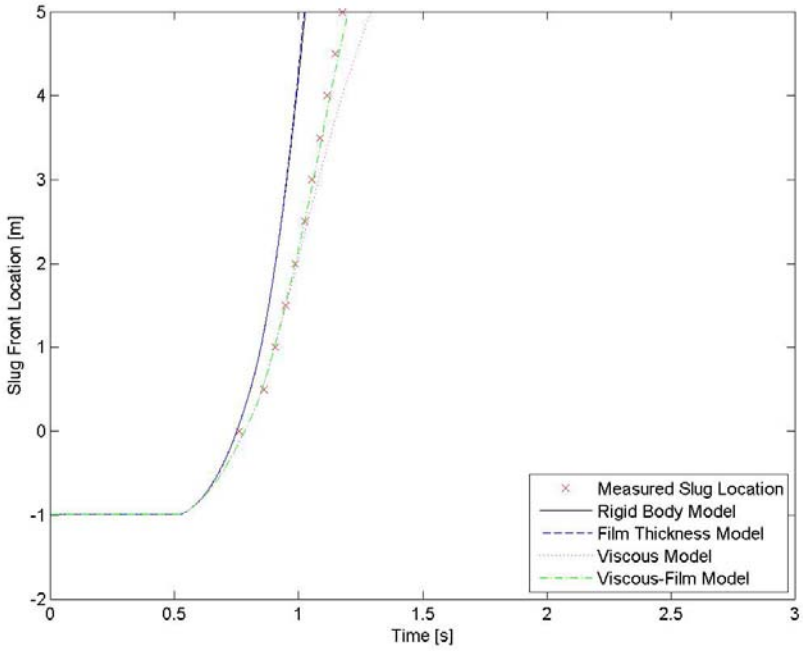

Figure A.43. Model Comparison for a 276 kPa Pressure Difference, 300 ml Initial Slug Volume, in 13.4 mm Diameter Pipe, Air-water High Side Test

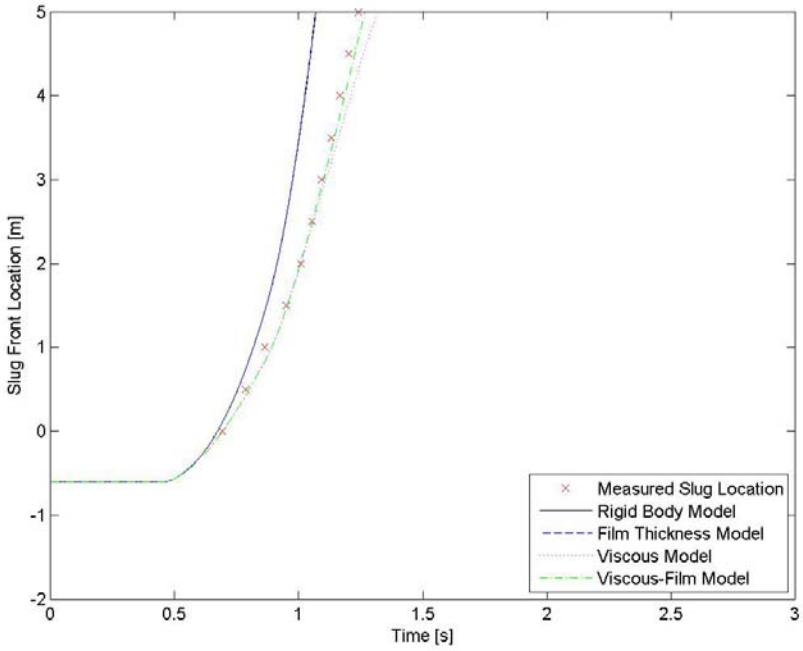

Figure A.44. Model Comparison for a 276 kPa Pressure Difference, 400 ml Initial Slug Volume, in 13.4 mm Diameter Pipe, Air-water High Side Test

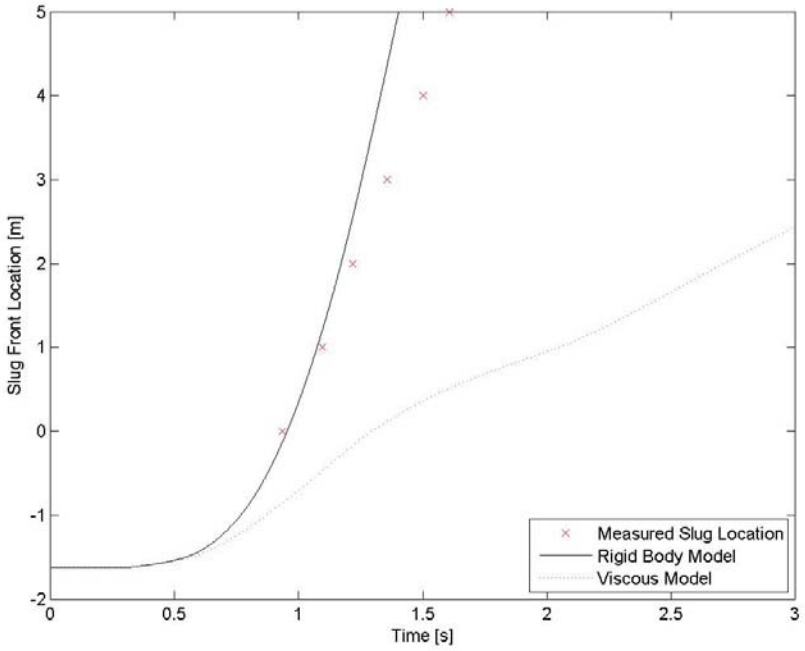

Figure A.45. Model Comparison for a 400 kPa Pressure Difference, 85 ml Initial Slug Volume, in 6.35 mm Diameter Pipe, R134a High Side Test

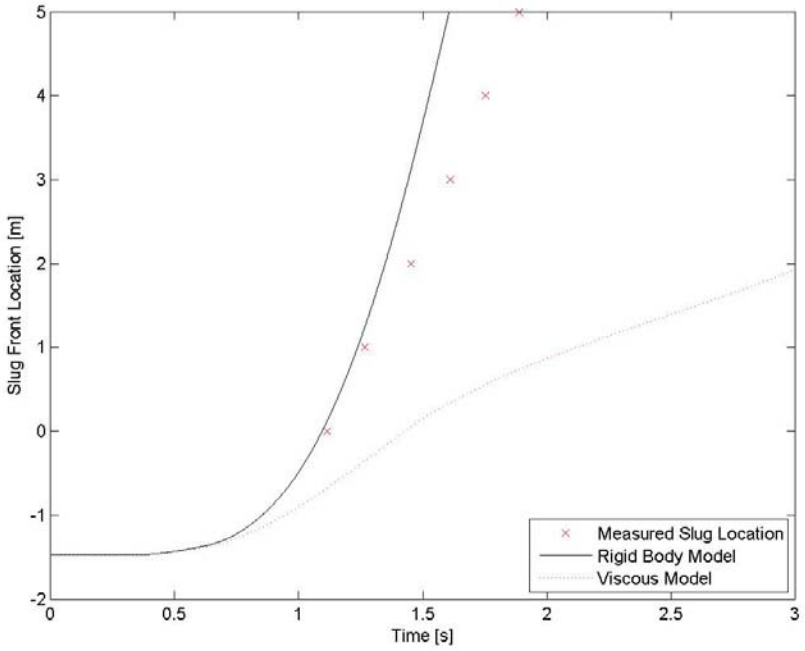

Figure A.46. Model Comparison for a 430 kPa Pressure Difference, 105 ml Initial Slug Volume, in 6.35 mm Diameter Pipe, R134a High Side Test

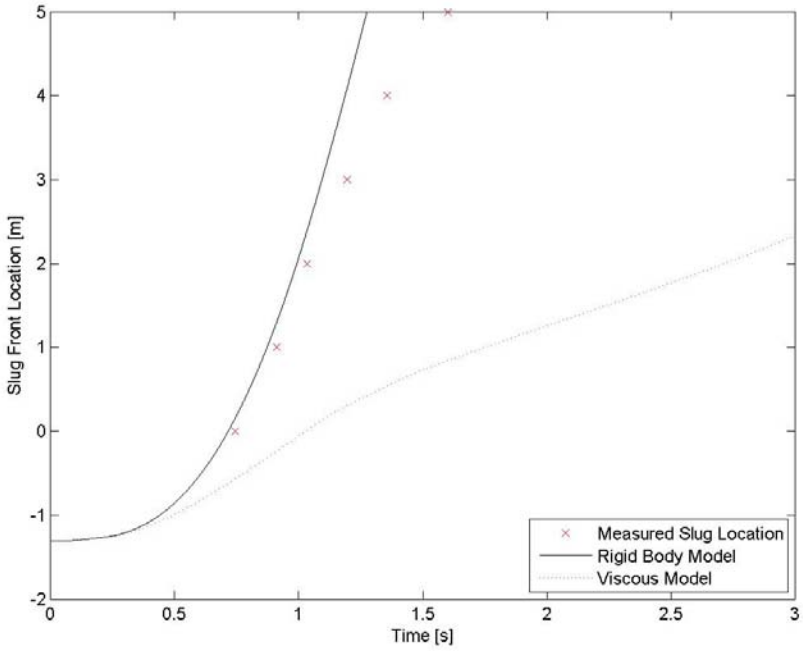

Figure A.47. Model Comparison for a 390 kPa Pressure Difference, 125 ml Initial Slug Volume, in 6.35 mm Diameter Pipe, R134a High Side Test

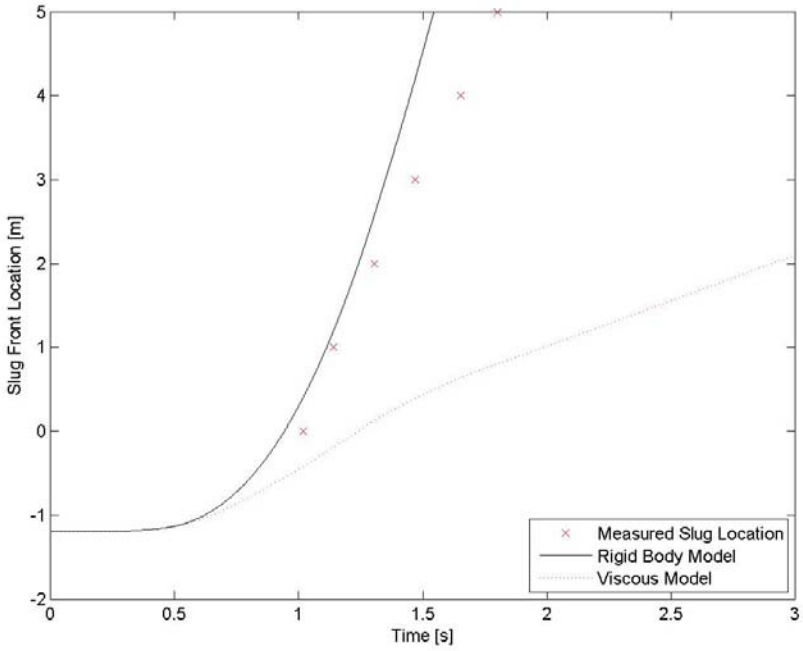

Figure A.48. Model Comparison for a 390 kPa Pressure Difference, 140 ml Initial Slug Volume, in 6.35 mm Diameter Pipe, R134a High Side Test

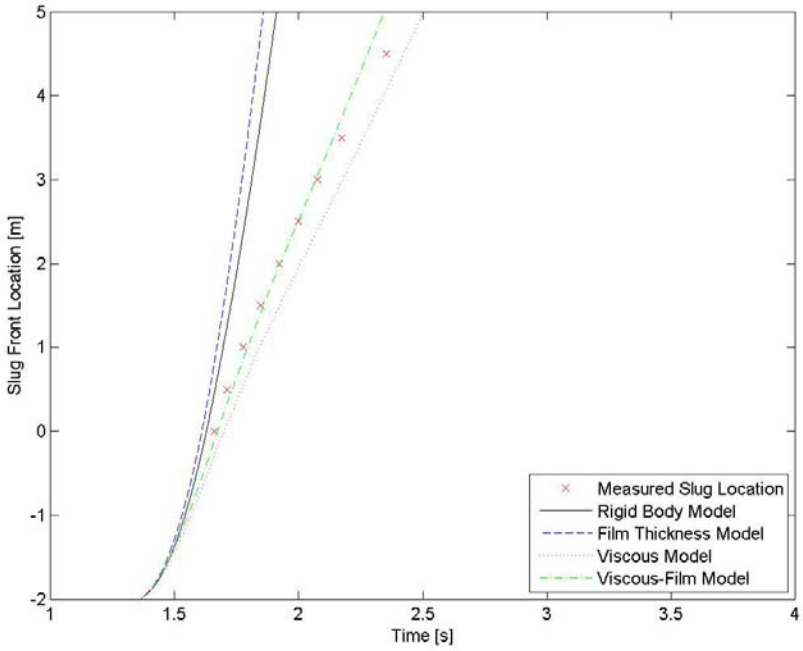

Figure A.49. Model Comparison for a 220 kPa Pressure Difference, 50 ml Initial Slug Volume, in 10.2 mm Diameter Pipe, R134a High Side Test

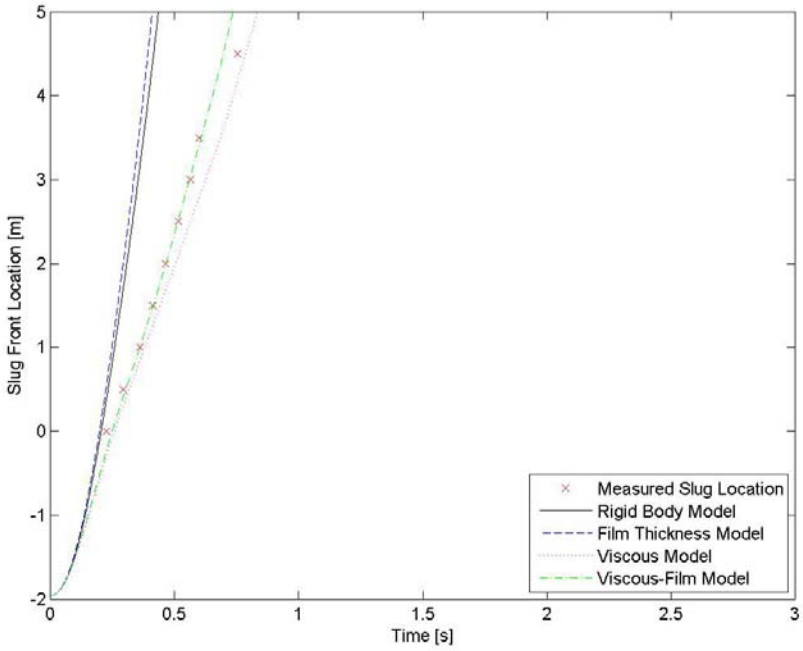

Figure A.50. Model Comparison for a 380 kPa Pressure Difference, 57 ml Initial Slug Volume, in 10.2 mm Diameter Pipe, R134a High Side Test

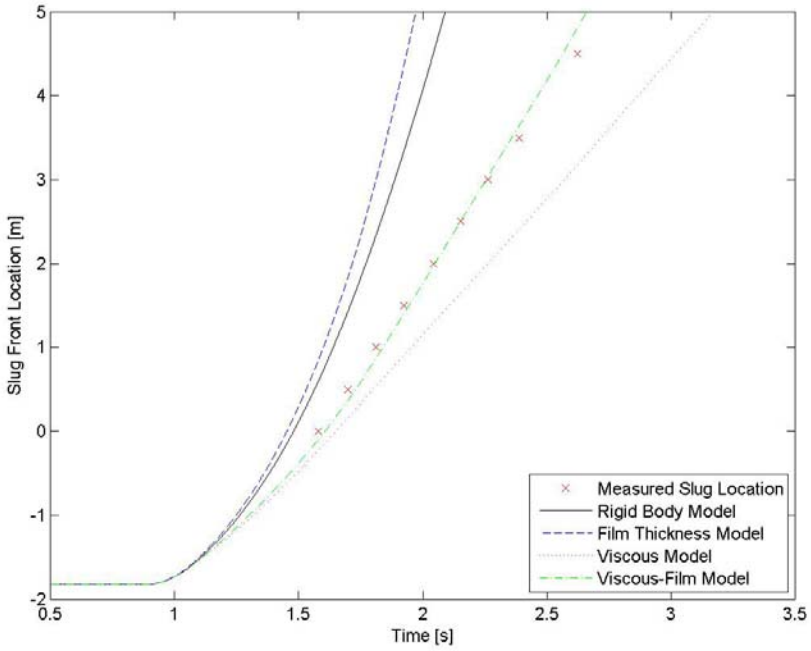

Figure A.51. Model Comparison for a 170 kPa Pressure Difference, 75 ml Initial Slug Volume, in 10.2 mm Diameter Pipe, R134a High Side Test

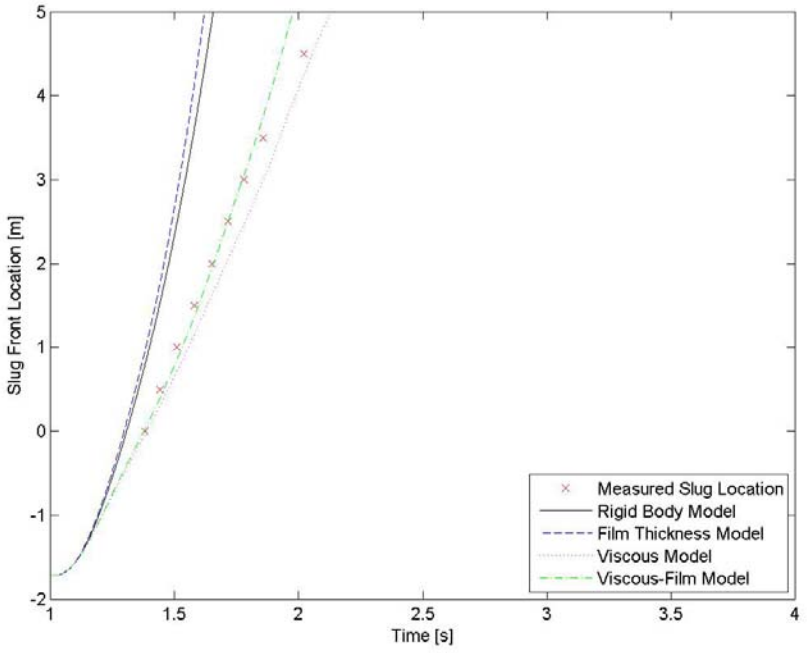

Figure A.52. Model Comparison for a 170 kPa Pressure Difference, 88 ml Initial Slug Volume, in 10.2 mm Diameter Pipe, R134a High Side Test

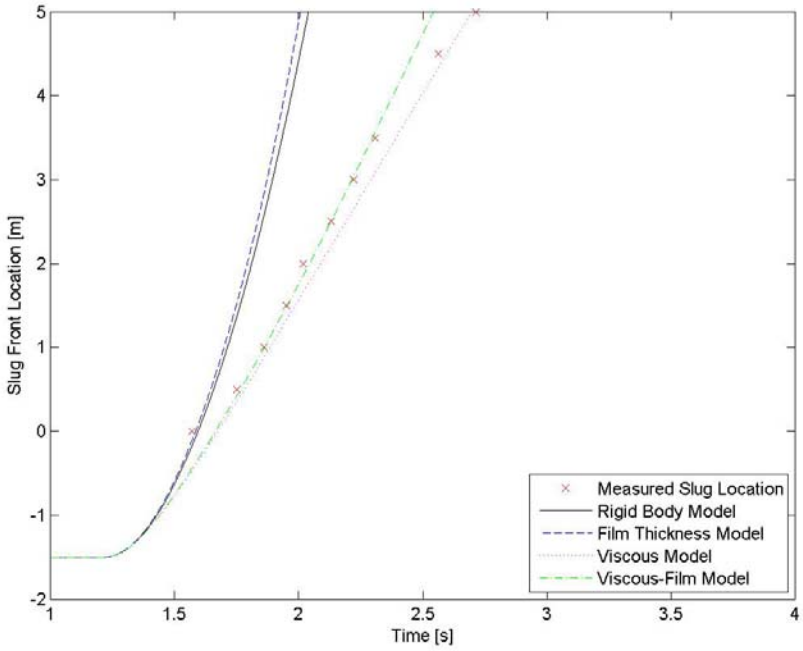

Figure A.53. Model Comparison for a 170 kPa Pressure Difference, 115 ml Initial Slug Volume, in 10.2 mm Diameter Pipe, R134a High Side Test

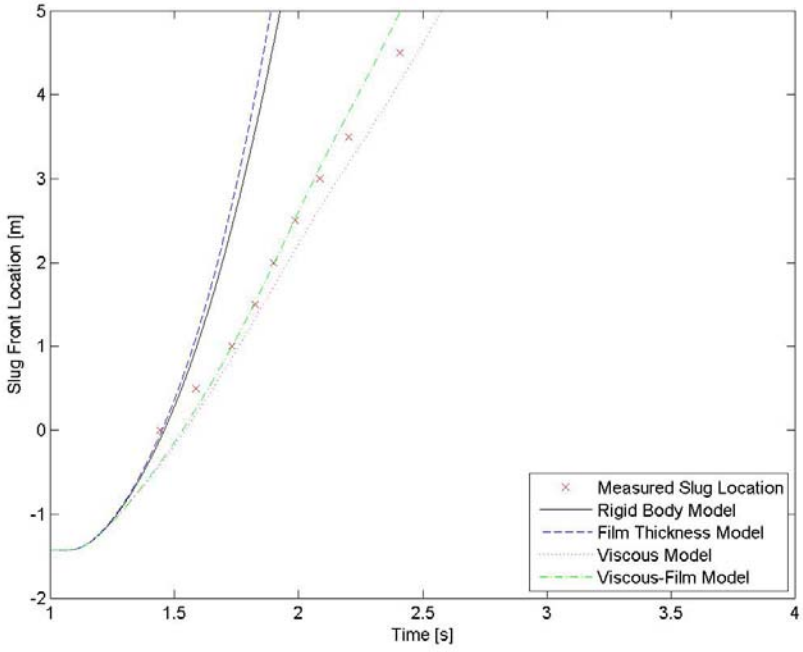

Figure A.54. Model Comparison for a 180 kPa Pressure Difference, 125 ml Initial Slug Volume, in 10.2 mm Diameter Pipe, R134a High Side Test

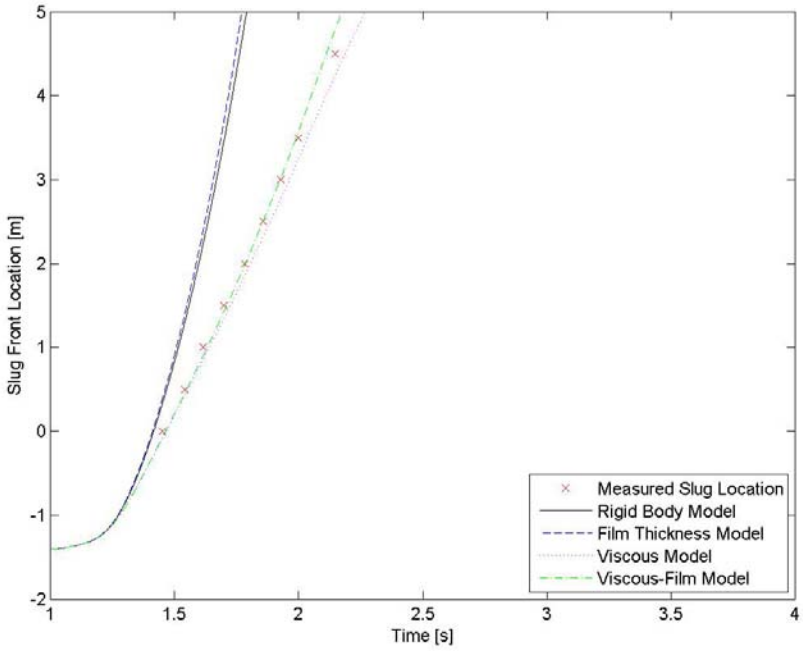

Figure A.55. Model Comparison for a 250 kPa Pressure Difference, 128 ml Initial Slug Volume, in 10.2 mm Diameter Pipe, R134a High Side Test

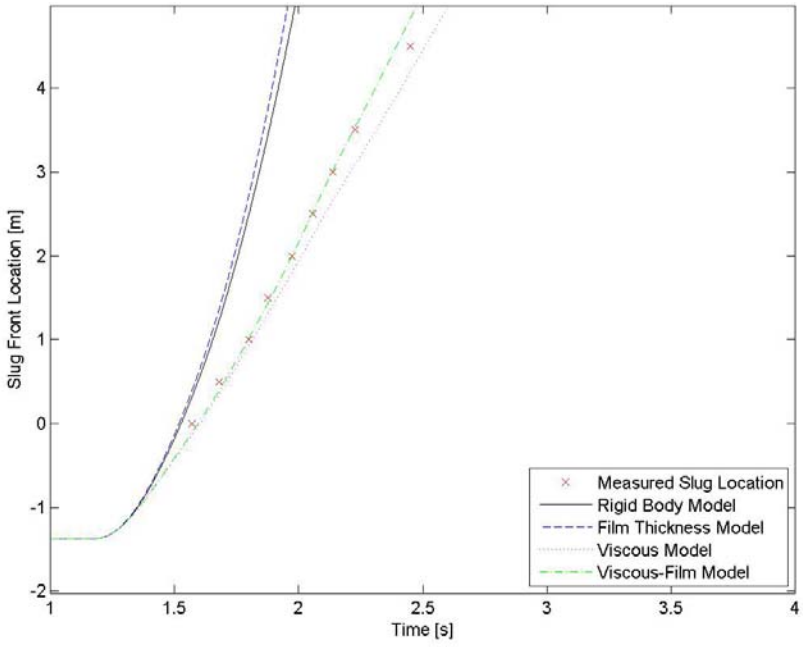

Figure A.56. Model Comparison for a 240 kPa Pressure Difference, 132 ml Initial Slug Volume, in 10.2 mm Diameter Pipe, R134a High Side Test

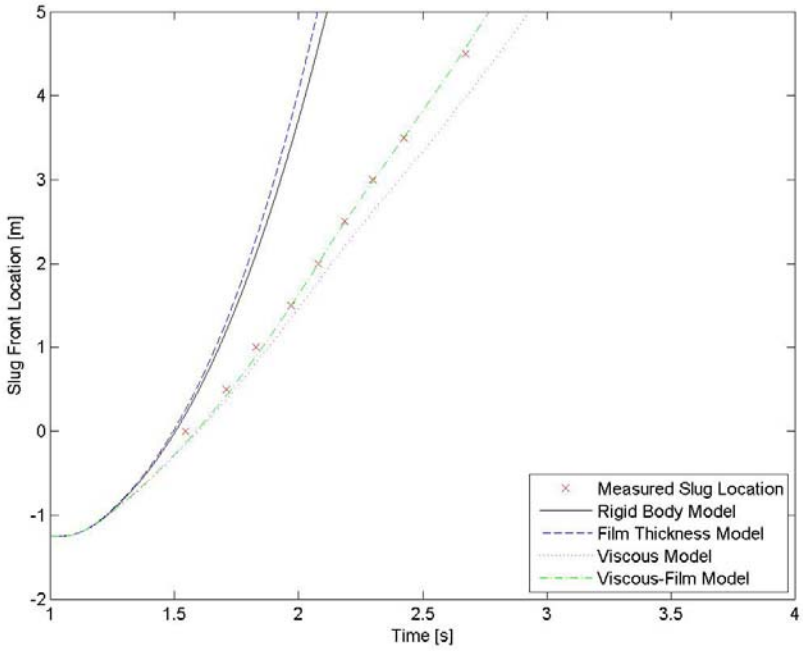

Figure A.57. Model Comparison for a 160 kPa Pressure Difference, 148 ml Initial Slug Volume, in 10.2 mm Diameter Pipe, R134a High Side Test

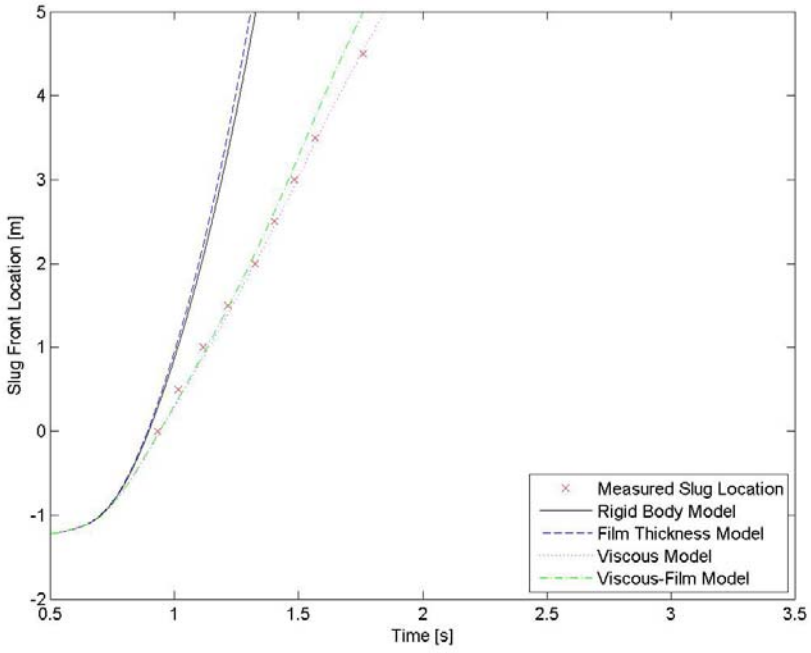

Figure A.58. Model Comparison for a 260 kPa Pressure Difference, 150 ml Initial Slug Volume, in 10.2 mm Diameter Pipe, R134a High Side Test

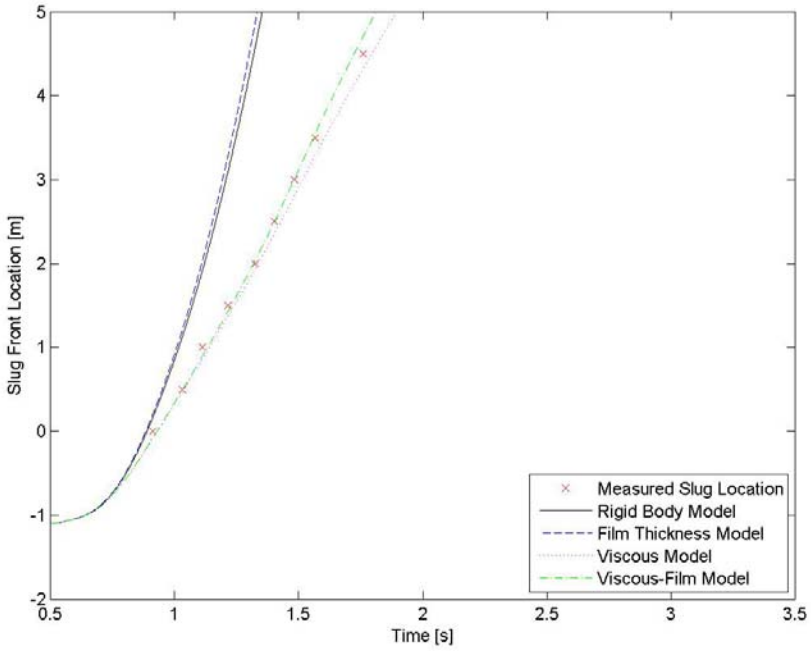

Figure A.59. Model Comparison for a 260 kPa Pressure Difference, 165 ml Initial Slug Volume, in 10.2 mm Diameter Pipe, R134a High Side Test

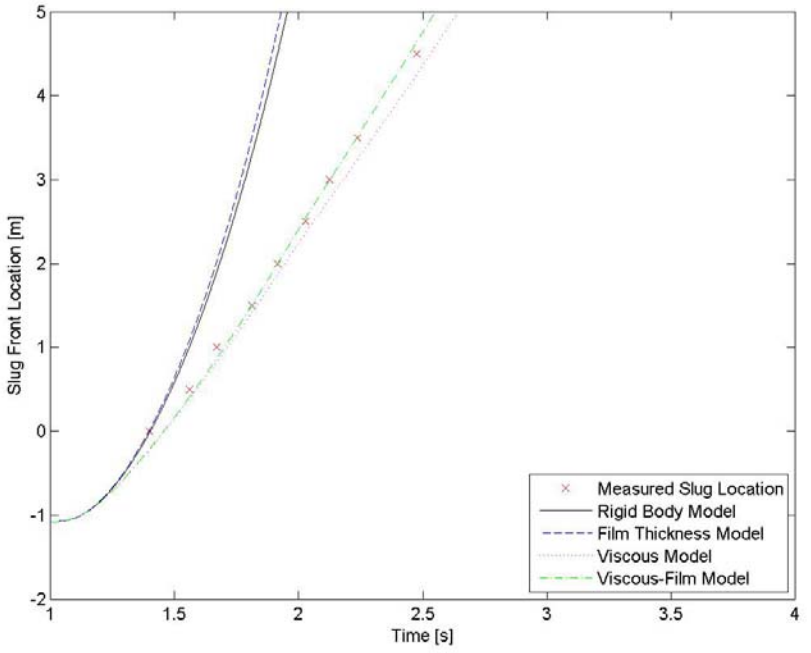

Figure A.60. Model Comparison for a 180 kPa Pressure Difference, 170 ml Initial Slug Volume, in 10.2 mm Diameter Pipe, R134a High Side Test

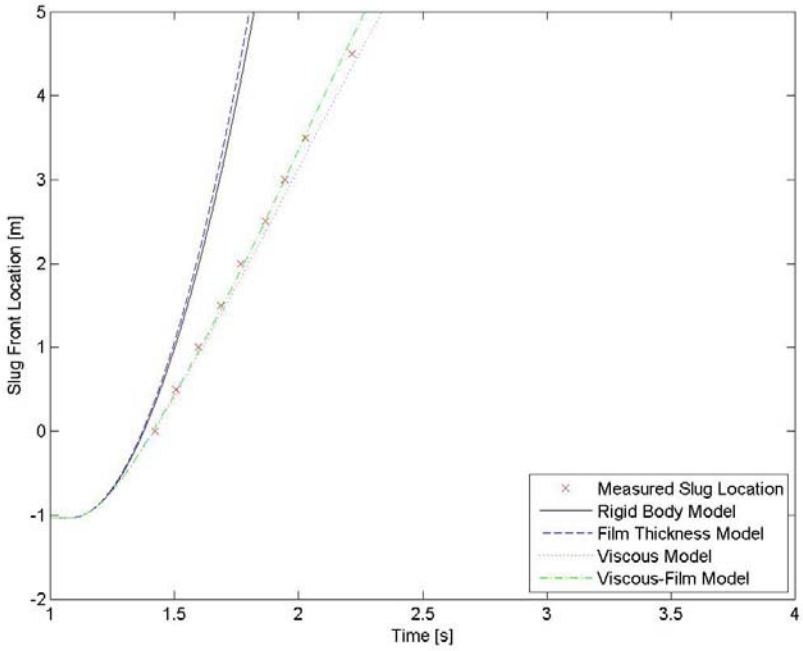

Figure A.61. Model Comparison for a 240 kPa Pressure Difference, 175 ml Initial Slug Volume, in 10.2 mm Diameter Pipe, R134a High Side Test

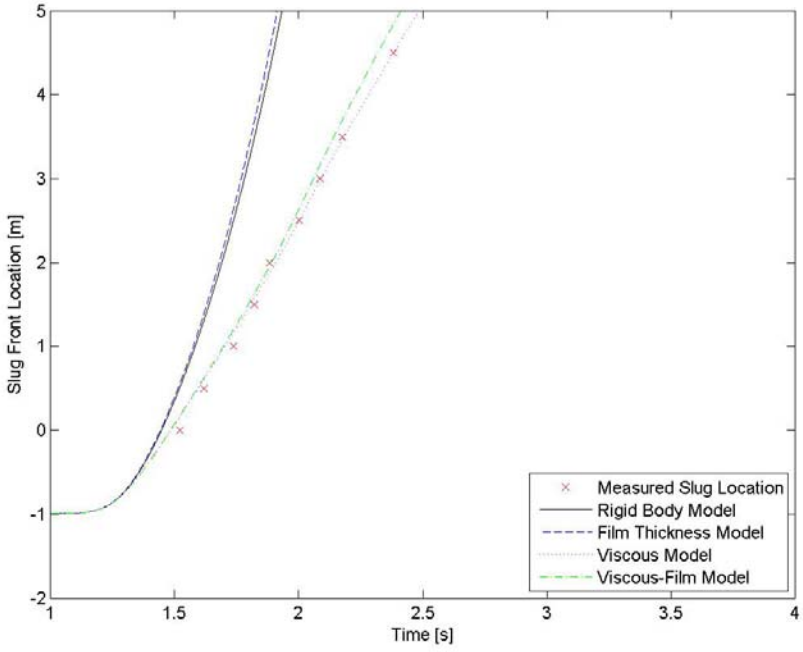

Figure A.62. Model Comparison for a 240 kPa Pressure Difference, 180 ml Initial Slug Volume, in 10.2 mm Diameter Pipe, R134a High Side Test

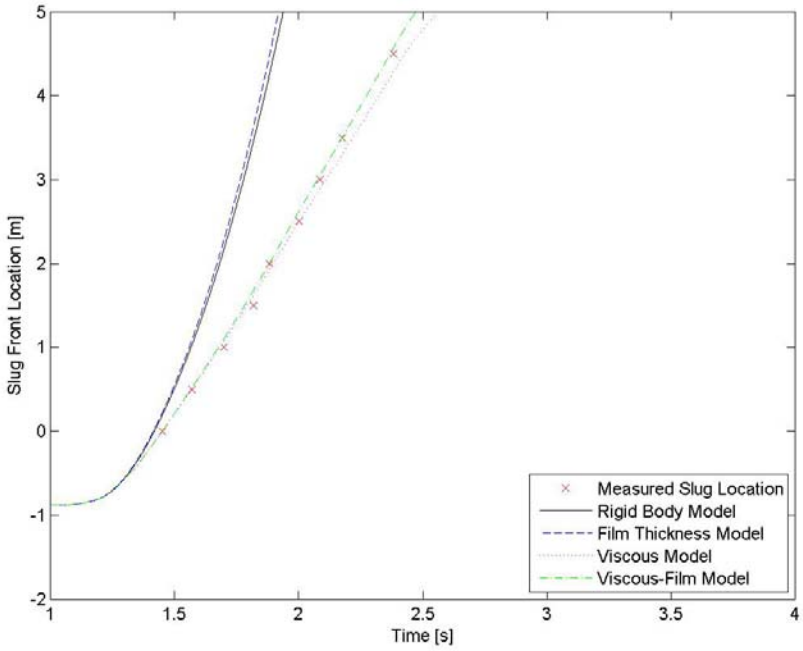

Figure A.63. Model Comparison for a 240 kPa Pressure Difference, 195 ml Initial Slug Volume, in 10.2 mm Diameter Pipe, R134a High Side Test

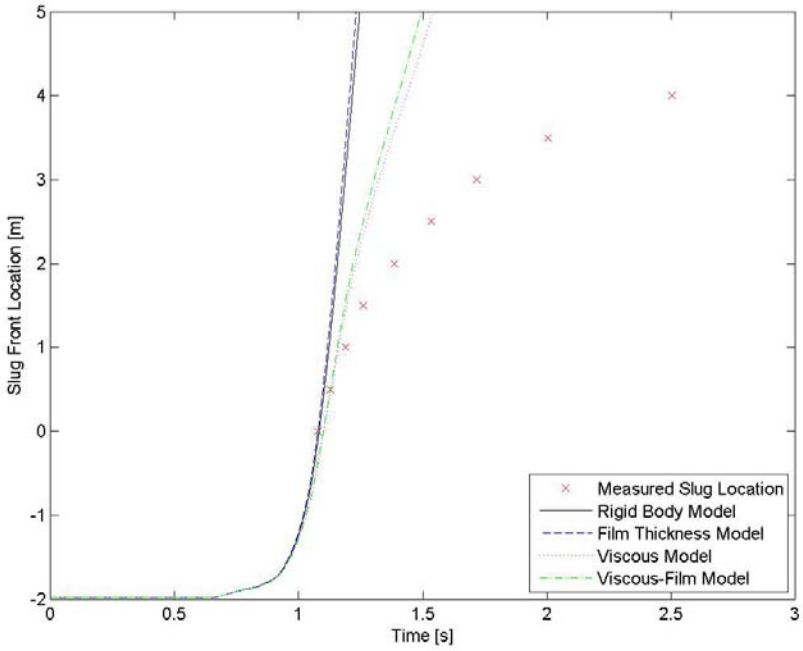

Figure A.64. Model Comparison for a 380 kPa Pressure Difference, 40 ml Initial Slug Volume, in 13.4 mm Diameter Pipe, R134a High Side Test

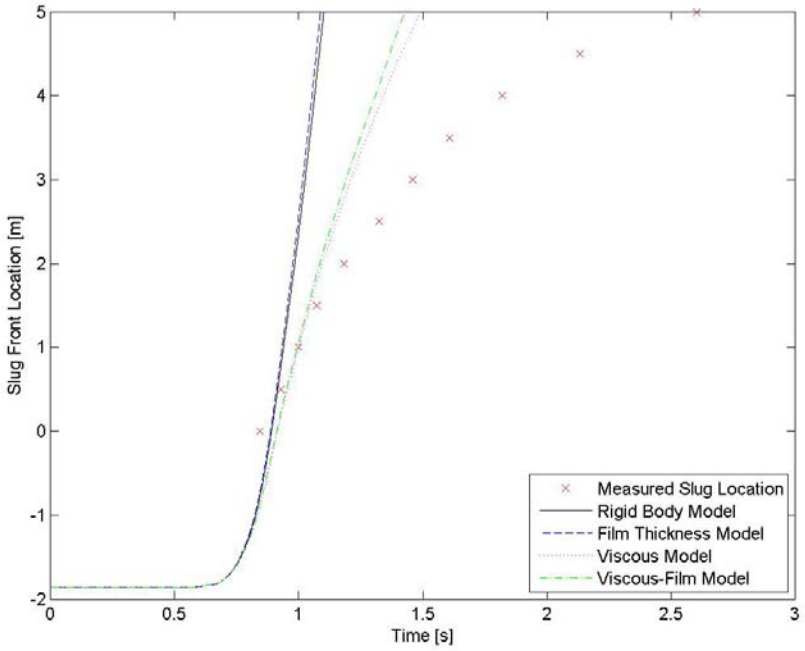

Figure A.65. Model Comparison for a 400 kPa Pressure Difference, 60 ml Initial Slug Volume, in 13.4 mm Diameter Pipe, R134a High Side Test

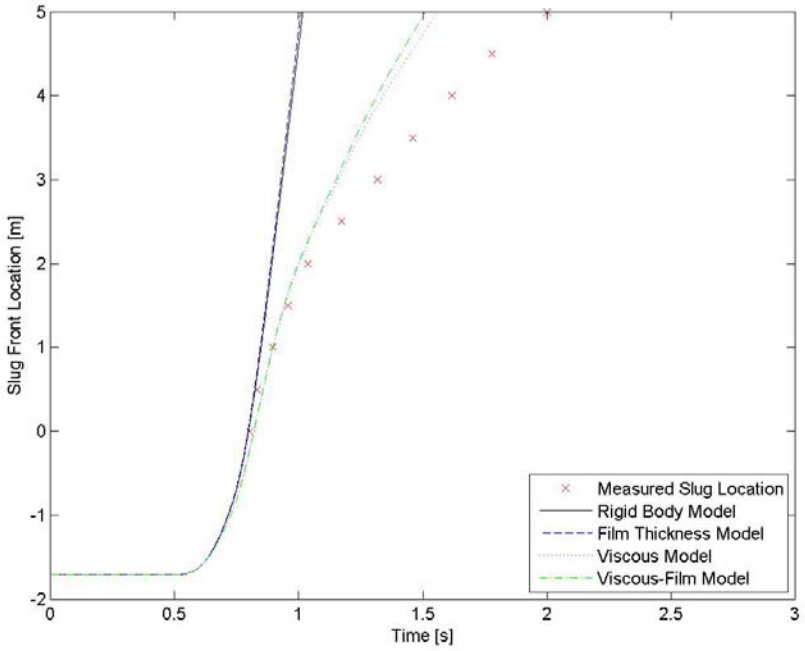

Figure A.66. Model Comparison for a 400 kPa Pressure Difference, 75 ml Initial Slug Volume, in 13.4 mm Diameter Pipe, R134a High Side Test

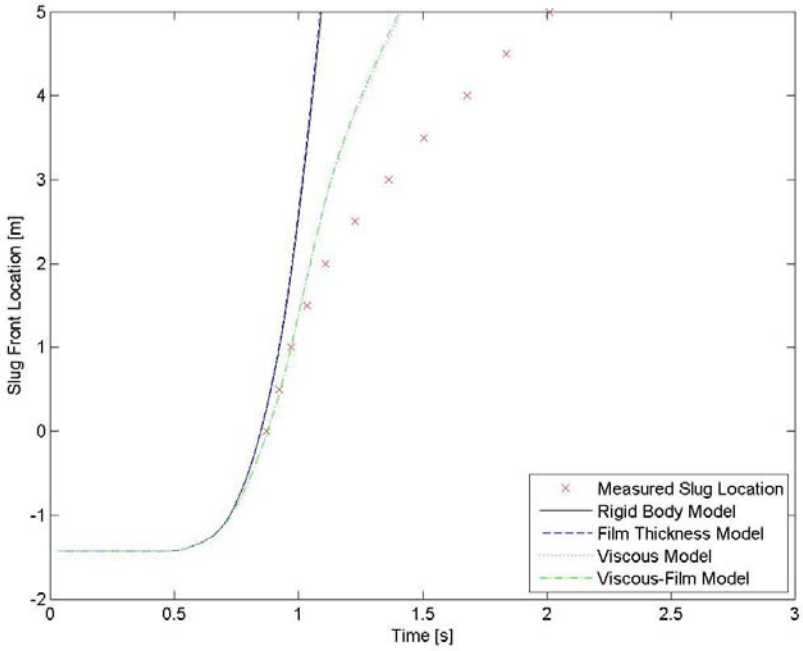

Figure A.67. Model Comparison for a 450 kPa Pressure Difference, 110 ml Initial Slug Volume, in 13.4 mm Diameter Pipe, R134a High Side Test

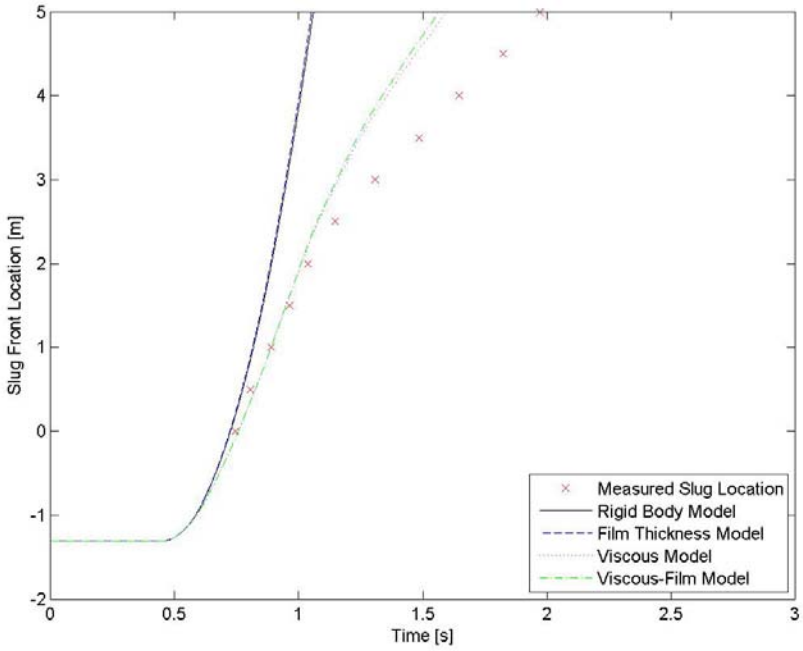

Figure A.68. Model Comparison for a 310 kPa Pressure Difference, 125 ml Initial Slug Volume, in 13.4 mm Diameter Pipe, R134a High Side Test

Appendix B. Low Side Test Results

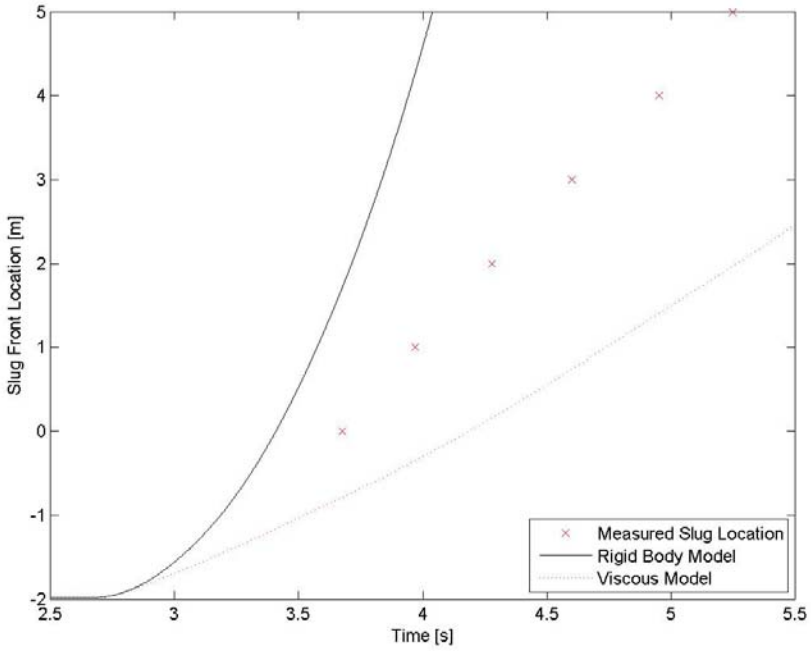

Figure B.1. Model Comparison for a 160 kPa Pressure Difference, 40 ml Initial Slug Volume, in 6.35 mm Diameter Pipe, R134a Low Side Test

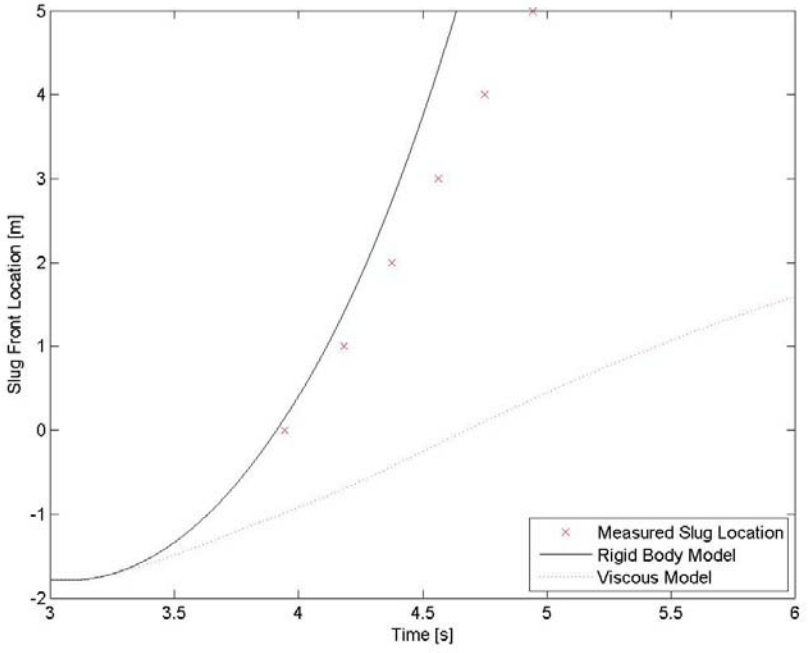

Figure B.2. Model Comparison for a 140 kPa Pressure Difference, 65 ml Initial Slug Volume, in 6.35 mm Diameter Pipe, R134a Low Side Test

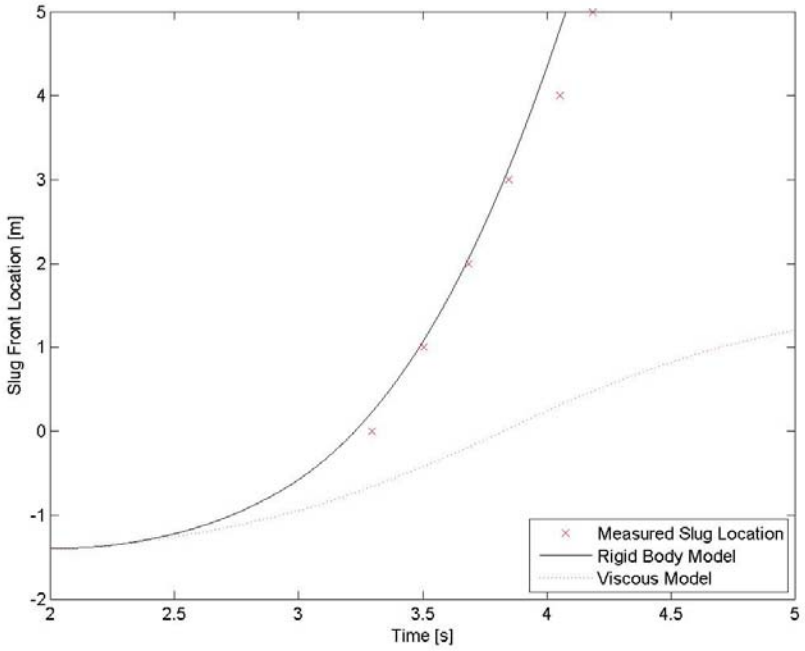

Figure B.3. Model Comparison for a 180 kPa Pressure Difference, 115 ml Initial Slug Volume, in 6.35 mm Diameter Pipe, R134a Low Side Test

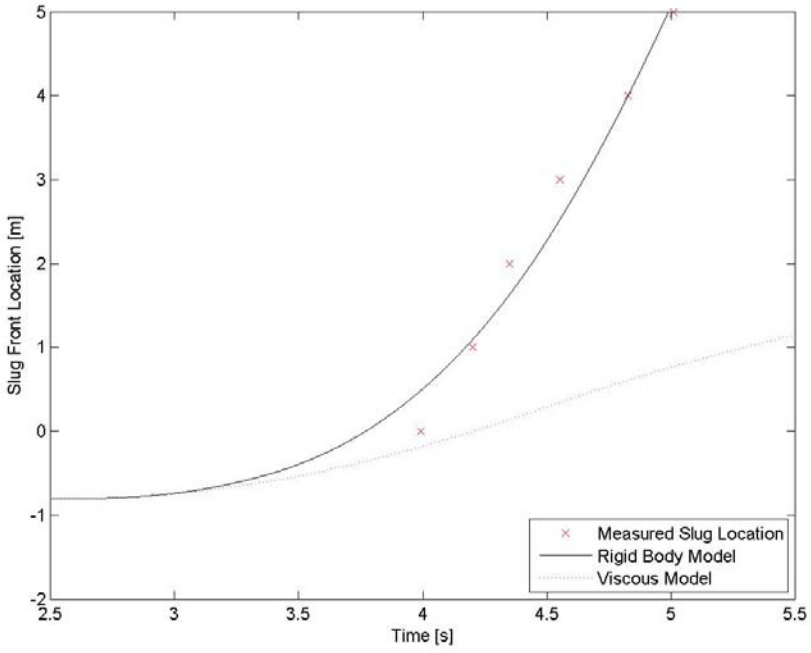

Figure B.4. Model Comparison for a 180 kPa Pressure Difference, 190 ml Initial Slug Volume, in 6.35 mm Diameter Pipe, R134a Low Side Test

Appendix C. Matlab Program

Main Program

```
%Program: main.m
    %This program calculates slug motion and breakdown for multiple test
    %conditions specified by the user through an input file.

%Clear all existing variables
clear all, clc
%Load the following inputs: pipe diameter, applied pressure difference,
%fluid, pipe orientation, high side pressure, and slug volume.  Inputs are
%arrays of equal size.  The same index of each input variable completely
%defines the testing conditions.
    %Pipe diameter: 'dia' - the diameter of the pipe in [mm]
    %Applied pressure difference: 'dp' - the value of the applied pressure
    %   difference across the slug in [kPa]
    %Fluid: 'fluid' - '1' for air-water and '2' for R134a
    %Pipe orientation: 'orient' - '1' for horizontal, '2' for vertical
    %   down, '3' for serpentine down
    %High side pressure: 'p_hi' - the value of the high side test pressure
    %   in [kPa]
    %Slug Volume: 'vol' - the value of the initial slug volume in [ml]
load inputs;
%Allows the user to modify the test conditions that the program calculates
%slug motion for
disp('Modify the inputs "dia","dp","fluid","orient","p_hi", and "vol".')
disp('Note: "dia" should be in [mm], "dp" and "p_hi" should be in [kPa], and
"vol" should be in [ml]')
disp('Note: Enter "1" for air-water or "2" for R134a in the "fluid" array')
disp('Note: Enter "1" for horizontal, "2" for vertical downward, or "3" for
serpentine pipe orientation in the "orient" array')
disp('Variables in the same index of the arrays specify the test conditions
for one calculation.')
disp('Type "return" once finished changing the arrays to run the program.')
%keyboard
%Type 'return' to return to and run the program

%Determine the number of test conditions to be analyzed
s=size(dp);
%Size and set loop variables
loc_term=zeros(s(1),1); loc_breakup=loc_term; breakup=loc_term;
t_break=loc_term;
acc_p=zeros(6000,s(1)); vel_p=acc_p; loc_p=acc_p; vol_p=acc_p; f_p=acc_p;
dp_p=acc_p;
%Set the current figure and release any data already plotted
figure(1), hold off
%Loop to calculate slug motion for each test and store in loop variables
for k=[1:1:s(1)];
    %Run 'setup' function to set up independent variables from inputs and
calculate
    %slug motion.

[dp_p(:,k),acc_p(:,k),vel_p(:,k),loc_p(:,k),t_p,breakup(k,1),loc_breakup(k,1)
```

```
,vol_p(:,k),t_break(k,1)]=setup(dia(k,1),dp(k,1),fluid(k,1),orient(k,1),p_hi(
k,1),vol(k,1));
    %Plot slug locaiton vs time until slug breakdown for each test

plot(t_break(k,1),loc_breakup(k,1),'bo',t_p(1:t_break(k,1)*1000+1),loc_p(1:t_
break(k,1)*1000+1,k),'k-',t_p((t_break(k,1)*1000+1):(6000-
t_break(k,1)*1000+1)),loc_p((t_break(k,1)*1000+1):(6000-
t_break(k,1)*1000+1),k),'k--')
    %Plot the slug motion for each input on the same graph
    hold on
end
%Clear unwanted variables (looping variables)
clear s k

%Show title, axes labels, and legend
title('Slug Motion')
xlabel('Time [s]')
ylabel('Slug Location [m]')
legend('Slug Breakdown','Simplified Viscous-film Model',4)
```

Setup Function

```
%Function: 'setup.m'
    %This function formats the inputs into usable variables for calulation
    %of slug motion and calls on the 'moiton.m' funtion to calulate the
    %slug motion.

function
[dp_p,acc_p,vel_p,loc_p,t_p,breakup,loc_breakup,vol_p,t_break]=setup(dia,dp,f
luid,orient,p_hi,vol);
%Inputs:
    %'dia' - pipe diameter provided through index of 'input.m' called in
'summary.m' program
    %'dp' - applied pressure difference provided through index of
    %   'input.m' called in 'summary.m' program
    %'fluid' - value indicating fluid provided through index of 'input.m'
    %   called in 'summary.m' program
    %'orient' - value indicating pipe orientation provided through index of
    %   'input.m' called in 'summary.m' program
    %'p_hi' - high side pressure provided through index of 'input.m'
    %   called in 'summary.m' program
    %'vol' - initial slug volume provided through index of 'input.m'
    %   called in 'summary.m' program
%Outputs:
    %'dp_p' - applied pressure difference across slug using simplified
    %   vicous-film model from 'motion.m' funciton
    %'acc_p' - slug acceleration calculated using simplified visoucs-film
    %   model from 'motion.m' funciton
    %'vel_p' - slug velocity calculated using simplified visoucs-film
    %   model from 'motion.m' funciton
    %'loc_p' - slug location calculated using simplified visoucs-film
    %   model from 'motion.m' funciton
    %'t_p' - time
    %'breakup' - '1' if slug breakdown occurs, '2' if not from 'motion.m'
    %   funciton
```

```
    %loc_breakup - value of location of slug at breakdown, 'NaN' if
    %   breakdown does not occur from 'motion.m' funciton
    %'vol_p' - slug volume calulated using simplified viscous-film model
    %   from 'motion.m' funciton
    %'t_break' - time at which slug breakdown occurs (rounded to nearest
    %   0.001 [s]


%Creates step profile for the pressure difference from the pressure input
%of the current test.  Step occurs at 0.005 [s]
dp=[zeros(5,1);dp*ones(9995,1)]; %[kPa]
%Converts pipe diameter into [m]
dia=dia/1000; %[m]
%Converts inital volume from [ml] to [m^3]
vol=vol*10^(-6); %[m^3]
%Converts 'fluid' input into a string containing the fluid name and
%determines the average of the high and low side pressure across the slug
%to evaluate constant density and viscosity
if fluid==1;
    fluid='airwa';
    %Water density and viscosity do not vary significantly over the test
    %pressures, so the average pressure is not needed.
    p_ave=0;
elseif fluid==2;
    fluid=='r134a';
    %Low side pressure is calculated from high side pressure and pressure
    %difference
    p_lo=p_hi-dp(5);
    p_ave=(p_hi+p_lo)/2;
    %Clear unused variables
    clear p_hi p_lo
end
%Converts 'orient' input into string indicating the orientation
if orient==1;
    orient='h';
elseif orient==2;
    orient='v';
elseif orient==3;
    orient='s';
end

%Calls 'motion.m' function to caluclate slug motion
[dp_p,acc_p,vel_p,loc_p,breakup,loc_breakup,vol_p]=motion(dp,vol,dia,fluid,p_
ave,orient);
%Time for test is stepped from 0.000 to 5.999 [s] in 0.001 [s] increments
t_p=[0:.001:5.999]';

%Determine the slug breakdown time from interpolation and round to the
%nearest 0.001 [s]
t_break=round(interp1(loc_p(6:6000),t_p(6:6000),loc_breakup)*1000)/1000;
```

Motion Function

```
%Function: 'motion.m'
    %This function calulates the slug motion according to the viscous-film
    %model and delivers outputs to the 'setup.m' function.
```

```
function
[dp_a,acc,vel,loc,breakup,loc_breakup,Vol_slug]=motion(dp,vol,dia,fluid,p_ave
,orient);
%Inputs:
    %'dp' - step pressure difference profile in [kPa] from 'setup.m'
    %'vol' - initial slug volume in [m^3] from 'setup.m'
    %'dia' - pipe diameter in [m] from 'setup.m'
    %'fluid' - string indicating fluid from 'setup.m'
    %'p_ave' - average high side-low side pressure from 'setup.m'
    %'orient' - string indicating pipe orientation from 'setup.m'
%Outputs:
    %'dp_a' - applied pressure difference across slug using simplified
    %   vicous-film model
    %'acc' - slug acceleration calculated using simplified visoucs-film
    %   model
    %'vel' - slug velocity calculated using simplified visoucs-film
    %   model
    %'loc' - slug location calculated using simplified visoucs-film
    %   model
    %'breakup' - '1' if slug breakdown occurs, '2' if not
    %'loc_breakup' - value of location of slug at breakdown, 'NaN' if
    %   breakdown does not occur
    %'Vol_slug' - slug volume calulated using simplified viscous-film model


%Load lookup tables for R134a properties
    %Friction factor as a funciton of saturaiton pressure over test
    %pressure range from EES
    load f_table
    %Density and viscosity as a function of saturation pressure over test
    %pressure range from EES
    load dens_table

%Determine fluid properties (density and viscosity)
%Air-water propterties at STP
if fluid=='airwa'
    dens = 998; %[kg/m^3]
    vis=1.004*10^(-6); %[m^2/s]
    L_B=.117; %Slug breakdown length [m]
    hf_ave=1.2; %Average maximum film thickness [mm]
    %Annular film for air-water
    A_S=pi/4*(dia-2*hf_ave*10^(-3))^2; %[m^2]
%R134a properties interpolated from loaded tables at p_ave from 'setup.m'
%function
else
    dens=interp1(dens_lookup(:,1),dens_lookup(:,2),p_ave);
    vis=interp1(dens_lookup(:,1),dens_lookup(:,3),p_ave)/dens;
    L_B=.153; %Slug breakdown length [m]
    hf_ave=1.5; %Average maximum film thickness [mm]
    %Stratified film for R134a
    A_S=1/4*dia^2*(pi-(acos(1-2*hf_ave*10^(-3)/dia)-(1-2*hf_ave*10^(-
3)/dia)*sin(acos(1-2*hf_ave*10^(-3)/dia))));
end

g=9.81; %Gravity [m/s^2]

%Size and set loop variables
```

```
A=zeros(6000,1);
acc=A; dp_act=A; f=A; l_slug=A; loc=A;
Re_D=A; vel=A; visc_dp=A; V_F=A; Vol_slug=A;
clear A;
count=1;
%Breakdown occurs if 'breakup' counter is equal to 2
breakup=1;
%Calculate motion for 6 seconds
for m=[1:1:6000];
    %While dp==0
    if m<6;
        vel(m)=0; %[m/s]
        loc(m)=0; %[m]
        Re_D(m)=0; %[ ]
        L_S(m)=vol/(pi/4*(dia)^2); %[m]
    %After step increase in dp at 0.005 [s]
    else
        vel(m)=vel(m-1)+.001*(acc(m-1)+acc(m-2))/2;
        loc(m)=loc(m-1)+.001*vel(m);
        %Reynolds Number based on diameter for liquid only
        Re_D(m)=vel(m)*dia/vis;
        %Slug length
        L_S(m)=Vol_slug(m-1)/(pi/4*(dia)^2);
    end
    %Calculate friction factor from Reynolds Number - Critical Reynolds
Number=2300
    %Prevent divide by zero
    if Re_D(m)==0;
        f(m)=0;
    %Maximum Reynolds Number in loaded table is 10^7
    elseif Re_D(m)>10^7
        f(m)=.0081;
    %Laminar pipe flow
    elseif Re_D(m)<2300;
        f(m)=64/Re_D(m);
    %Tubulent pipe flow - table created using Colebrook formula
    else
        f(m)=interp1(f_lookup(:,1),f_lookup(:,2),Re_D(m));
    end
    %Viscous pressure drop
    visc_dp(m)=f(m)*(L_S(m)/dia)*(vel(m)^2/2)*dens/1000;
    %Applied pressure difference
    dp_a(m)=dp(m)-visc_dp(m);
    %Film volume
    V_F(m)=(pi*(dia/2)^2-A_S)*loc(m); %[m^3]
    %Slug volume
    Vol_slug(m)=vol-V_F(m); %[m^3]
    %Breakdown occurs when the slug length is less than the breakdown
    %length.
    if (L_S(m)<L_B | breakup==2);
        %The volume of the liquid mass is assumed to stay approximately
        %constant after breakdown.
        Vol_slug(m)=L_B*pi*(dia/2);
        %For the first iteration where breakdown occurs
        if breakup==1;
            %Modify the counter
            breakup=2;
```

```
            %Breakdown location is equal to the location at this iteration.
            loc_breakup=loc(m);
        end
    end
    %Test section oriented vertically downward
    if orient=='v'
        %Slug acceleration
        acc(m)=1000*dp_a(m)*A_S/(dens*Vol_slug(m))+g; %[m/s^2]
    %Test section orieinted horizontally
    elseif orient=='h'
        acc(m)=1000*dp_a(m)*A_S/(dens*Vol_slug(m));
    end
end
%If slug breakdown does not occur, the breakdown location does not exist
if breakup==1;
    loc_breakup=NaN;
end
```